CHEMICAL ENGINEERING SCIENCE
GENIE CHIMIQUE

VOL. 11 1959 No. 4

Conserved-property diagrams for rate-process calculations—Part II

New diagrams and constructions

D. B. SPALDING
Imperial College, London, S.W.7

(*Received 2 January* 1959)

Abstract—It is shown that the three types of diagrams discussed in Part I are members of a larger family, the defining feature of which is that they are homographically related, i.e. transformable into each other by central projection.

The rules of homographic transformation are outlined, and then used: (1) for the derivation of general rate-process constructions, (2) for the establishment of new types of diagram, the H_2O–air system serving as an example, (3) for the development of a new, entirely graphical, construction procedure for determining the number of transfer units of exchange equipment.

A new diagram is presented which is suitable for problems arising in drying practice, heating and ventilating and cooling-tower design. An example of the latter is worked out.

Résumé—L'auteur a montré que les trois types de diagrammes étudiés dans la part I, font partie d'une famille à caractère homographique c'est-à-dire transformable les uns dans les autres par une projection centrale.

Les règles de la transformation homographique sont esquissées et ensuite utilisées: (1) pour l'établissement des constructions des processus généraux de vitesse.

(2) pour l'établissement de nouveaux types de diagrammes, le système H_2O–air servant d'exemple.

(3) pour le développement d'un nouveau procédé entièrement graphique de construction pour la détermination du nombre des unités de transfert d'un appareil d'échange.

Un nouveau diagramme est présenté qui est approprié pour les problèmes se présentant dans la practique du séchage, du chauffage, et de la ventilation et pour le calcul des tours de refroidissement. Un exemple de ce dernier est étudié.

Zusammenfassung—Die drei im Teil I diskutierten Diagrammtypen sind Glieder einer grösseren Schar von Diagrammen. Das definierende Kriterium ist die homographische Verwandtschaft, d.h. die gegenseitige Transformierbarkeit durch Zentralprojektion.

Die Regeln der nomographischen Transformation werden mitgeteilt und auf folgende Fälle angewandt.

1. Auf die Ableitung allgemeiner Konstruktionen für Übertragungsvorgänge.
2. Auf die Herstellung neuer Diagrammtypen, für die das System Wasser–Luft als Beispiel dient.
3. Auf die Entwicklung einer neuen, rein graphischen Konstruktion zur Bestimmung der Anzahl der Übertragungseinheiten eines Austauschers.

Ferner wird ein neues Diagramm mitgeteilt, das besonders für Probleme der Trocknung, Heizung und Lüftung und Kühlturm-Berechnung geeignet ist. Für die letztere wird ein Beispiel ausgeführt.

1. Generalized Conserved-Property Charts

1.1 *The Choice of Mass Unit*

We have seen, in Part I, [1] that graphical rate-process constructions can be carried out on the $H - M$ chart just as well as on the $h - m$ chart; only their interpretations need modification. Now the $H - M$ formulation is characterized by measuring quantity in terms of a unit (e.g. the lb mole) which varies according to the composition of the mixture: the unit is 18 lb_m for pure H_2O, 29 lb_m for pure air, and has intermediate values for intermediate mixtures (see equation 6 of Part I). Why should these units be chosen?

Examination of the arguments (not given here) which lead to the construction of a chart on the "mole-of-mixture" basis, and to the formulae relating its co-ordinates to h and m, shows that at no point is any knowledge required of the actual relative masses of the molecules in question; even if matter were continuous (i.e. did not consist of molecules), the charts and constructions would remain valid.

This recognition leads to an important conclusion: we may choose *any* size of mass unit whatever for each of the two components. Is there advantage in so doing? Fig. 11, to be discussed later, shows a chart for H_2O - air in which the H_2O mass unit has been taken as 1 lb_m and the air mass unit as 25 lb_m (only the ratio of the units is important, so one of them can conveniently be taken as unity). A glance at this new chart shows that the important region covering gas-phase mixtures between 32°F and 212°F has been greatly enlarged; graphical constructions for these mixtures are thus easier to make. So the freedom to choose the mass-unit ratio makes it possible to "blow-up" particular regions, while still retaining the whole range of mixture compositions (pure air to pure H_2O) on the chart.

"Molecular weight" of water on the Mollier ($I - x$) chart

It is interesting to note that Mollier has implicitly made extreme use of this freedom in in constructing the $I - x$ chart: he has made the "molecular weight" of water, μ_{H_2O}, tend to infinity. For in this case, equation (5) of Part I, for example, takes the form (with μ_{H_2O} in the place of 18, and 1 in the place of 29):

$$M \cdot \mu_{H_2O} = m/(1 - m) \qquad (1)$$

Comparison of (1) above with (5) of Part I shows that $M \cdot \mu_{H_2O}$ is the same as x. So the $I - x$ chart is really an $H - M$ chart, but with $\mu_{air} = 1$, μ_{H_2O} = very large. (The appearance of μ_{H_2O} on the left-hand side of (1) is insignificant, for we are always free to introduce a constant multiplier when choosing a scale to which to plot the diagram). This choice of mass unit happens so to cramp the region of moderate H_2O contents that the part of the diagram dealing with large H_2O contents has in practice to be discarded.

Further generalization

Although the free choice of mass unit already provides possibilities of chart design which will not be quickly exhausted, an even wider range is possible. These are revealed by considering the charts from the point of view of projective geometry. We first state the features of this branch of mathematics which will be used below.

1.2. *Some Facts about Projective Geometry*

(i) Projective geometry concerns the relations between a diagram drawn on one plane and its shadow on a second plane when illuminated by a point source of light. The process of forming the second diagram from the first is known as *central projection.*

(ii) If the co-ordinates of a point on the first plane are (h, m) in a rectangular system, and the co-ordinates of the corresponding point on the second plane are (η, ξ) in a second rectangular system, the co-ordinates are related by

$$\xi = \frac{a_1 m + b_1 h + c_1}{pm + qh + r}; \quad \eta = \frac{a_2 m + b_2 h + c_2}{pm + qh + r} \qquad (2)$$

where a_1, b_1, c_1, a_2, b_2, c_2, p, q, r depend only on the relative positions of the two planes and the light source (vertex of projection), and on the chosen co-ordinate axes, and so are valid for all parts of corresponding points on the two planes. Note that the denominators of the two expressions are identical.

If (2) is treated as representing an analytical operation, it is known as *homographic transformation.*

(iii) In a homographic transformation, a point in the $h - m$ plane corresponds to just one point in the $\eta - \xi$ plane, and vice versa. Similarly, there is a one-to-one correspondence between straight lines on the two planes.

(iv) If four points A, B, C, D lie on a straight line (not necessarily in the order stated), the product of the length ratios

$$\frac{\overline{AB}\,.\,\overline{CD}}{\overline{AD}\,.\,\overline{CB}}$$

is known as the *cross-ratio* of the *range* of points A, B, C, D.

(v) If the straight line A, B, C, D is transformed into the line straight A′, B′, C′, D′ homographically, i.e. by central projection, the cross-ratios of the two corresponding ranges are equal.

(vi) If a range of points A, B . . . . P, Q . . . . on a straight line l is in homographic relation to a range of points A, B′, ... P′, Q′ . . . . on a second straight line l', then the intersection of the lines PQ′ and P′Q lies on a fixed straight line which passes through the point of intersection, A, of l and l' (Fig. 1).

(vii) If two planes $h - m$ and $\eta - \xi$ are in homographic relation, in general one of the straight lines on the $h - m$ plane does not appear on the $\eta - \xi$ plane: it "vanishes" or "goes to infinity." This is the line $pm + qh + r = 0$.

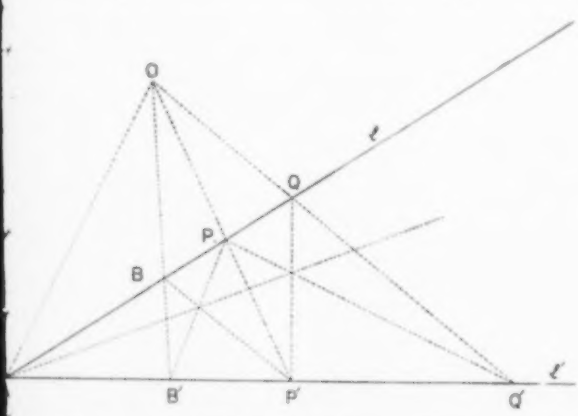

FIG. 1. Illustrating that the intersection of PQ′ and P′Q lies on a fixed straight line.

Similarly one of the ines on the $\eta - \xi$ plane corresponds to the line at infinity on the $h - m$ plane.

(viii) Conics (ellipses, parabolae, hyperbolae) on the $h - m$ plane project into conics on the $\xi - \eta$ plane and vice versa.

(ix) Any conic can be projected into a circle having the projection of any given point (not on the conic) as its centre.

Of these statements, the most important for the present purposes are (ii), (v) and (vii). All the statements are used explicitly or implicitly, in the following pages.

1.3 *Application of Projective Geometry to the Conserved-Property Charts*

Relevance to the $h - m$, $H - M$, and $I - x$ charts for H_2O – air

Comparison of equations (4), (5), (10) and (11) of Part I, for example, with the general homographic transformation (2) above, shows that the $h - m$, $H - M$ and $I - x$ charts are in homographic relation to each other, with M and x as particular forms of ξ and H and I as particular forms of η.

The transformations relating the three charts are not of the most general form since only the horizontal co-ordinate appears in the denominator of the equations. It is for this reason that lines of constant composition remain vertical in each of the charts. The transformations are further restricted in that $M = 0$ and $x = 0$ when $m = 0$.

In the transformation between the $h - m$ and $H - M$ planes, only the vertical co-ordinate appears in the numerator of the transforming relation (10) of Part I; so the line corresponding to $h = 0$ is horizontal in both charts. In the transformation from h to I on the other hand, the horizontal co-ordinate m does appear in the numerator (equation 11 of Part I); so the line $h = 0$ (or $i = 0$) becomes a sloping line on the $I - x$ chart. This has already been commented on above.

The line $m = 1$ (pure H_2O) on the $h - m$ chart is the line at infinity on the $I - x$ chart. In the transformation from the $h - m$ to the $H - M$ plane, it is the line $(18/29) + [1 - (18/29)] \times m = 0$ which vanishes; since this does not

correspond to a realistic composition (for m cannot in practice be negative), no physically interesting mixtures are lost.

In general, the line which goes to infinity in a transformation to the $H-M$ plane is that corresponding to mixtures of infinite " molecular weight " μ.

The possibility of other enthalpy-composition charts

The chief way in which the construction of enthalpy-composition charts can be generalized, in addition to the free choice of μ already mentioned, lies in introducing the vertical co-ordinate h into the denominator of the transforming relations. This results in lines of constant composition ceasing to be vertical, or even parallel; the region of realistic mixtures maps, in general, on to a triangular area. Interpretation in terms of the choice of mass unit becomes more difficult: enthalpy is now being treated in some respects as equivalent to mass.

There are nine constants in the general transformation (2) [corresponding to the six degrees of freedom in choosing the position of the second plane relative to the first plus the three degrees of freedom in choosing the position of the vertex of projection (light-source)]. However, only four of these are of great interest; the other five merely govern the horizontal and vertical positions, the horizontal and vertical scales and the orientation of the axes of the graph paper on which the transformed chart is being drawn. Of the four interesting constants, the two in the denominator of the expressions for η and ξ determine which line on the $h-m$ chart will be projected to infinity; the two remaining ones determine the slopes of the projections on the plane of the $m=0$ and $h=0$ lines.

Summarizing, the enthalpy-composition chart for mixtures of a given pair of substances at a given pressure can be drawn in a four-fold infinity of ways, mere scale changes being left out of account. This allowance should be sufficient for most purposes !*

Diagrams for ternary mixtures

Diagrams showing the phase boundaries and mixed-phase isotherms of ternary mixtures are similar in many respects to enthalpy-composition diagrams for binary mixtures: the mass or mole fraction of the third component takes the place of enthalpy. The chemical engineering literature abounds in triangular diagrams (in which the quantity unit is that of the three-component mixture), and rectangular (" solvent-free basis ") diagrams (in which the quantity unit is that of only two of three components).

It should be clear, without detailed discussion, that the triangular diagrams and the solvent-free ones are homographically related, that great freedom of choice exists in the mass units used, that the triangular diagrams do not have to be equilateral triangles, and so on. Ternary-mixture diagrams do not exhibit any special features therefore.

The Lever Rule in terms of cross-ratios

The foundation of the usefulness of conserved-property charts is the Lever Rule, equation (1) of Part I. It will now be shown how this can be expressed as a cross-ratio; the result will then be used to provide simple proofs of some of the rate-process formulae.

Consider the $h-m$ chart of Fig. 2(a). The points X and Z represent systems which are mixed to form a new system Y; F is the intersection of X, Y, Z with the line $m=0$. From equation (12) of Part 1, and consideration of Fig. 2(a), we can write:

$$\frac{w_Z}{w_X} = \frac{XY}{YZ} = -\frac{XY \cdot ZF}{XF \cdot ZY} \cdot \frac{m_X}{m_Z}$$

i.e.

$$\frac{w_Z}{w_X} \cdot \frac{m_Z}{m_X} = -\frac{XY \cdot ZF}{XF \cdot ZY} \tag{3}$$

Now the expression on the right-hand side of this equation is the cross-ratio of the range of points X, Y, Z, F. So, since cross-ratios are invariant under homographic transformation,

*Since writing the present pair of papers, the author has obtained the book by Busemann referred to in Part I. This work shows clearly that Busemann recognized the projective nature of the connexion between the various types of diagram, although he did not exploit his recognition in the manner of the present work. Busemann's publication appears to have been undeservedly neglected.

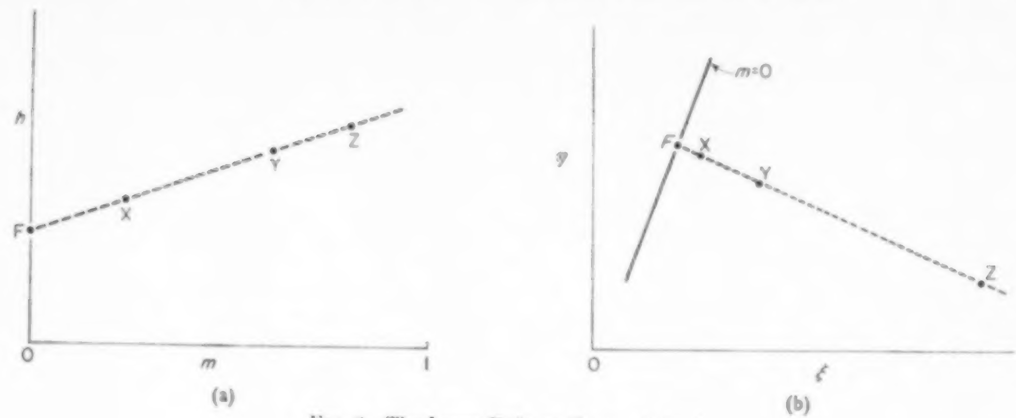

Fig. 2. The Lever Rule on the $\eta - \xi$ chart

(a) $\dfrac{\overline{XY}}{\overline{YZ}} = \dfrac{w_Z}{w_X}$ (b) $\dfrac{\overline{XY}}{\overline{YZ}} = \dfrac{w_Z}{w_X} \cdot \dfrac{m_Z}{m_X} \cdot \dfrac{(\xi_Z - \xi_F)}{\xi_Z - \xi_F}$

the expression may be evaluated on the $\eta - \xi$ chart (Fig. 2b) formed from the $h - m$ chart by central projection. Now on the $\eta - \xi$ chart, the ratio $\overline{ZF}/\overline{XF}$ is equal to $(\xi_Z - \xi_F)/(\xi_X - \xi_F)$. Equation (3) therefore can be written:

$$\left(\frac{\overline{XY}}{\overline{YZ}}\right)_{\eta-\xi} = \frac{w_Z}{w_X} \cdot \frac{m_Z}{m_X} \cdot \frac{(\xi_X - \xi_F)}{(\xi_Z - \xi_F)} \tag{4}$$

in which the suffix $\eta - \xi$ signifies evaluation on the $\eta - \xi$ chart.

If now we restrict attention to transformations of the $H - M$ variety (which includes $I - x$) in which the horizontal co-ordinate ξ (i.e. M) is equal to zero whenever $m = 0$, equation (4) reduces to equation (13) of Part I.

Rate-process constructions in terms of cross-ratios

The constructions involved in heat and mass transfer rate calculations require the evaluation of length ratios for which one point, for example H in the ratio $\overline{AG}/\overline{HA}$, lies on the line $m = 1$. We will now see how $\overline{AG}/\overline{HA}$ on an $H - M$ chart is related to that for the corresponding $h - m$ chart.

Appropriate substitutions in (3) and (4), (M for ξ, H for η, $M_F = 0$, G for X, H for Y, A for Z, $m_H = M_H = 1$), lead to

$$\left(\frac{\overline{AG}}{\overline{HA}}\right)_{h-m} = \left(\frac{\overline{AG}}{\overline{HA}}\right)_{H-M} \cdot \frac{M_G}{m_G} \tag{5}$$

which, taking account of (6) of Part I, proves the validity of the procedure described under Section 2.4 (b) (iii) of Part I.

In calculating the change of gas state resulting from a contact between gas and liquid, it was shown above that the increment in the number of gas-side mass transfer units was equal to the quantity $\overline{G_2G_1} \,.\, \overline{TJ}/\overline{G_2J} \,.\, \overline{TG_1}$, (equation 21, Fig. 5 of Part I). This quantity may now be recognized as a cross-ratio: it therefore does not matter on which diagram the lengths are evaluated. This was why the same procedure could be used on the $H - M$ chart as on the $h - m$ chart.

1.4 *Some* $\eta - \xi$ *Charts for* H_2O *– Air Mixtures Diagram with horizontal parallel gas-phase isotherms*

The specific heats at constant pressure of steam and air at moderate temperatures are in the ratio 0·445 : 0·24. As a consequence of this, and of the choice of enthalpy base for the $h - m$ chart, all the gas-phase isotherms converge on the point (m^*, h^*) where $m^* = -1{\cdot}17$ and $h^* = -1260$ B.t.u/lb_m.

In order to obtain a diagram with parallel gas-phase isotherms, we project the line $m = m^*$ to infinity. This is effected by the transformation:

*The symbols H and M are used instead of η and ξ wherever the constant-composition lines are vertical and the whole range of compositions appear in a finite horizontal range.

$$M\dagger = \frac{2{\cdot}17\, m}{m + 1{\cdot}17} \tag{6}$$

In order to correspond with (6), and in addition to cause the gas-phase isotherms to be horizontal, the following transformation of the vertical co-ordinate can be used:

$$H = \frac{2{\cdot}17\,(h - mh_{fg})}{m + 1{\cdot}17} \tag{7}$$

The corresponding diagram is shown in Fig. 3. It has the advantage that the gas-phase part of the diagram is particularly easy to draw. Physically interpreted, the diagram may be thought of as employing mass units of 1·85 lb_m of air and 1 lb_m of H_2O.

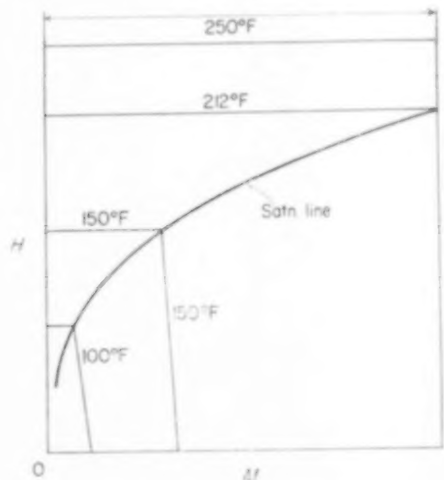

Fig. 3. $H - M$ chart for H_2O – air at 1 atm pressure: parallel gas-phase isotherms.

Diagram using mass of H_2O *as basis*

The inability of the $I - x$ diagram to represent very moist mixtures has been noted. If condensation of steam containing small quantities of air is to be studied, it may be preferable to project the $m = 0$ line to infinity. The corresponding transformation of the horizontal co-ordinate is:

$$\xi = (1 - m)/m \tag{8}$$

A suitable transformation for the vertical co-ordinate is

$$\eta = h/m \tag{9}$$

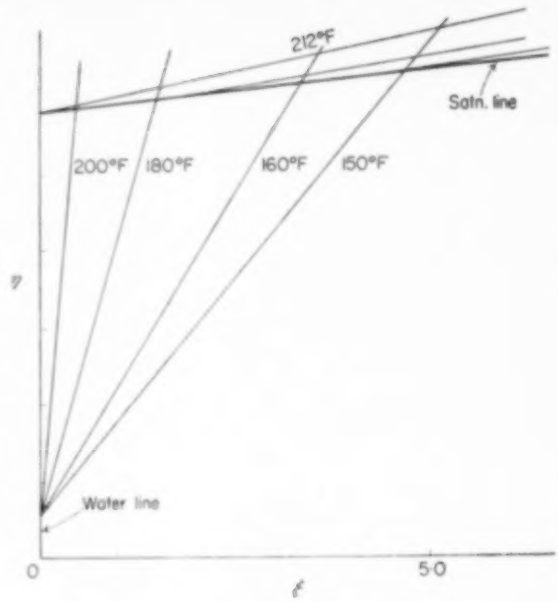

Fig. 4. Enthalpy-composition chart for H_2O – air at 1 atm pressure: "mass-of-H_2O" basis.

This makes the intersections of the isotherms with the $\xi = 0$ line identical with those on the $m = 1$ line.

The resulting diagram is shown in Fig. 4. Of course only a limited range of ξ can be used; the range 0 to 5·0 has been chosen in the example. The diagram may be interpreted as employing a mass unit for air which is very much larger than that for H_2O.

N.B. The focus of the gas-phase isotherms (ξ^*, η^*) is now at ($-$ 2·17/1·17, 1260/1·17); plotting this point assists in drawing the diagram).

A triangular diagram

To underline the fact that enthalpy-composition and ternary-mixture diagrams are all members of the same family, a transformation will be introduced which maps the $h - m$ plane for H_2O–air on a triangular area, which may be equilateral. A transformation giving an isosceles triangle is:

$$\xi = \frac{m + \frac{1}{2}\, h/h_{fg}}{1 + h/h_{fg}}; \quad \eta = \frac{h/h_{fg}}{1 + h/h_{fg}} \tag{10}$$

h_{fg} can be taken as 1076 B.t.u/lb_m H_2O.

FIG. 5. A triangular enthalpy-composition diagram for H_2O – air at 1 atm pressure.

Fig. 5 shows the resulting diagram ; the vertical and horizontal scales have been chosen to make the vertex angle of the triangle 60°. Since points of infinite enthalpy appear on the diagram (at the vertex), such charts may be useful when very large temperature differences have to be dealt with, for example those obtaining when a body travelling at high Mach Number is cooled by water flowing on its surface. Note that the focus of the gas-phase isotherms is at $\xi^* = -7{\cdot}39$, $\eta^* = -6{\cdot}86$. This is far off the diagram ; so the gas-phase isotherms are nearly parallel.

Other diagrams

As will by now be apparent, the number of conserved property diagrams which can be drawn is inexhaustible : one must choose the diagram which has the most convenient shape for the particular computational problem which has arisen. The following suggestions may be worth making here however.

Mixtures with large moisture contents do not have to be represented on diagrams such as that of Fig. 4 ; this diagram, like the $I - x$ one, has the disadvantage of lacking one boundary. Instead it may be preferable to use an $H - M$ transformation employing, in effect, a very small mass unit for air compared with that for H_2O. This has the effect of stretching the part of the $h - m$ diagram near $m = 1$ and contracting the part near $m = 0$.

If a suitably small mass-unit ratio is chosen, it is possible to exhibit, as an area of finite size, the region of air-in-water solutions. The diagram can then be used for solving problems connected with de-aerating plant, and the like.

The plotting of the saturated-gas line is the most tedious part of the construction of an enthalpy-composition chart. Yet if the interesting part of this line can be approximated on the $h - m$ plane by a part of a conic, projective geometry shows that it is possible to find a homographic

transformation which projects this conic into a circle with any desired point as centre, so permitting the saturation line to be drawn with compasses.

Further possibilities lie in the Principle of Duality [2]: this should permit the devising of diagrams embodying the thermodynamic properties of a mixture system, amenable to constructions such as those of the present paper, in which the isotherms are represented by points rather than lines. Whether the resulting simplification can counter-balance the unfamiliarity of such a representation can only be decided by further study.

It is troublesome to have to plot a new diagram for each pair of substances. It therefore seems desirable to study whether, by suitable choice of reduced co-ordinates, the equilibrium diagrams for various pairs of substances can be made to correspond closely. The new freedom of choice of co-ordinate presented by projective geometry may make this possible.

2. Rate-Process Constructions on the General Conserved-Property Chart

The constructions will now be given which permit heat and mass transfer rates to be calculated with the aid of $\eta - \xi$ charts. These may be regarded as generalizations of those in Section 2.4 of Part I. The H_2O – air system will continue to be used as an example, but no restriction of generality is implied thereby except, where straightness of gas-phase isotherms is assumed, to ideal mixtures.

Thereafter, new constructions will be presented which permit graphical determination of the size of equipment needed to perform a given transfer operation.

2.1 *Determination of the Interface States* L *and* S (Fig. 6)

The problem and notation are as for Section 2.4 above. The procedure is:

(i) Locate O on the pure-H_2O line corresponding to water at t_O.

(ii) Locate H on the pure-H_2O line corresponding to water at t_H, which is given by

$$t_H - t_O = \frac{t_G - t_O}{1 + [\sigma/(\sigma - 1)] \, . \, [U/g\,c]} \tag{11}$$

(iii) Draw the line HG and find A on it such that

$$\frac{\mathrm{AG}}{\mathrm{HA}} = \left[\frac{U}{g\,c_f} \cdot \sigma + \frac{c}{c_f}(\sigma - 1)\right] \cdot \frac{(\xi_G - \xi_F)}{m_G(\xi_H - \xi_F)} \tag{12}$$

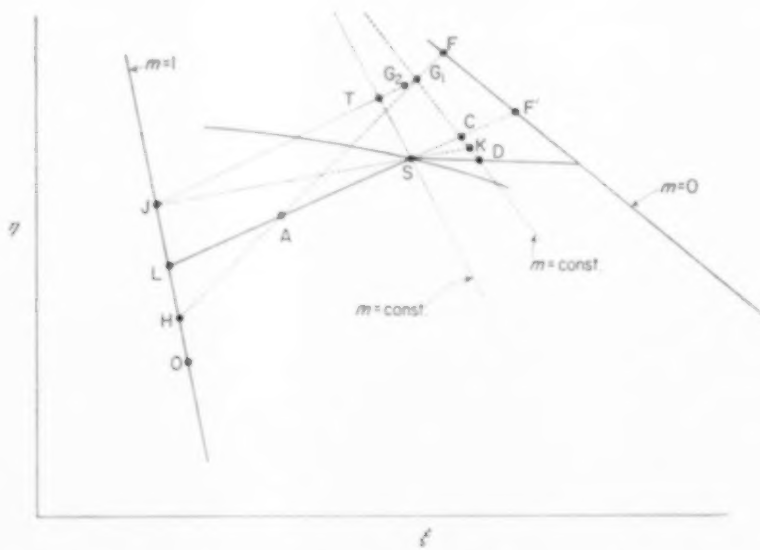

Fig. 6. Rate-process and gas-state change construction.

where F lies on $\overline{HG}$ and on the pure-air ($m = 0$) line.

(iv) Locate L and S which lie at the extremities of the mixed-phase isotherm through A. L lies on the pure-H_2O line; S lies on the saturation line.

2.2 *Determination of Transfer Rates* (Fig. 6)
Construction

(i) Locate D on the gas-phase isotherm through G such that $m_D = m_G$.

N.B. Lines of constant m are conveniently drawn on the chart. Of course, when ξ depends only on m these lines are vertical; in triangular diagrams like Fig. 5, they all pass through the vertex of the triangle.

(ii) Produce $\overline{LS}$ to cut $\overline{DG}$ at C. Plot K at the intersection of $\overline{DG}$ and the gas-phase isotherm t_K, where

$$\frac{t_K - t_S}{t_G - t_S} = \sigma \qquad (13)$$

Transfer rates

The mass transfer rate is given by

$$\frac{\overline{CS}}{\overline{SL}} = \frac{\dot{m}'' \sigma}{g} \cdot \frac{(\xi_C - \xi_{F'})}{m_C (\xi_L - \xi_{F'})} \qquad (14)$$

where F′ lies on CL and on the pure air line ($m = 0$).

The heat transfer rate to the reservoir is given by

$$h_K - h_C = \frac{\dot{q}''_f \cdot \sigma}{g} \qquad (15)$$

The heat transfer rate from the gas to the liquid surface is given by

$$h_G - h_D = \frac{\dot{q}''_g}{g} \qquad (16)$$

N.B. For the last two evaluations, it is convenient to have lines of constant h drawn on the chart.

2.3 *Change of Gas Condition* (Fig. 6)

Construction

(i) Produce $\overline{KS}$ to cut the pure-H_2O line at J.

(ii) Locate T where $\overline{G_1J}$ cuts the constant-composition line through S.

N.B. G is now called G_1; it represents gas approaching the contact surface.

(iii) Find G_2 on $\overline{G_1J}$ such that

$$\frac{\overline{G_2G_1} \cdot TJ}{G_2J \cdot TG_1} = \delta N_{m,g} \qquad (17)$$

Comments

Sometimes it is preferable to fix G_2, arbitrarily, at, say, some fraction of the distance from G_1 to T. Then evaluation of the expression on the left-hand side of (17) gives the necessary contact area in terms of number of gas-side mass transfer units. Bošnjaković [3], for example, in his constructions carried out on the $I - x$ chart, suggests making $\overline{G_1G_2}/\overline{G_1T} = 1/2$ for rough calculations.

Equation (17) is, in essence, a finite-difference approximation to a differential equation. It is therefore only strictly valid when $\delta N_{m,g}$ is infinitesimal. Except in very rare circumstances however the finite-difference form has to be used in order to permit integration, i.e. determination of the number of transfer units of the equipment. Then the usual compromise between truncation and rounding-off errors has to be made in choosing the size of step.

2.4 *Determining Corresponding Gas and Liquid States in Transfer Equipment*

So far we have considered heat and mass transfer at an infinitesimal element of the contact surface. In plant such as cooling-towers or packed distillation-columns, both gas and liquid states vary with position; the corresponding interface states vary also. We now turn to the graphical procedures for determining these sets of states.

Part of the technique for doing so is well known: it involves the use of the so-called polar diagram [4, 5, 6]. For adiabatic parallel-flow or counter-flow plant, this diagram consists of a pencil of lines radiating from a single point on a conserved-property diagram, the position of which is fixed by the states of the ingoing fluid streams and the ratio of their mass flow rates. The importance of the polar diagram lies in the fact that the state-points for the liquid and gas streams, at any level of the equipment, lie on one of these lines. The validity of the construction derives from the laws of conservation of mass and energy.

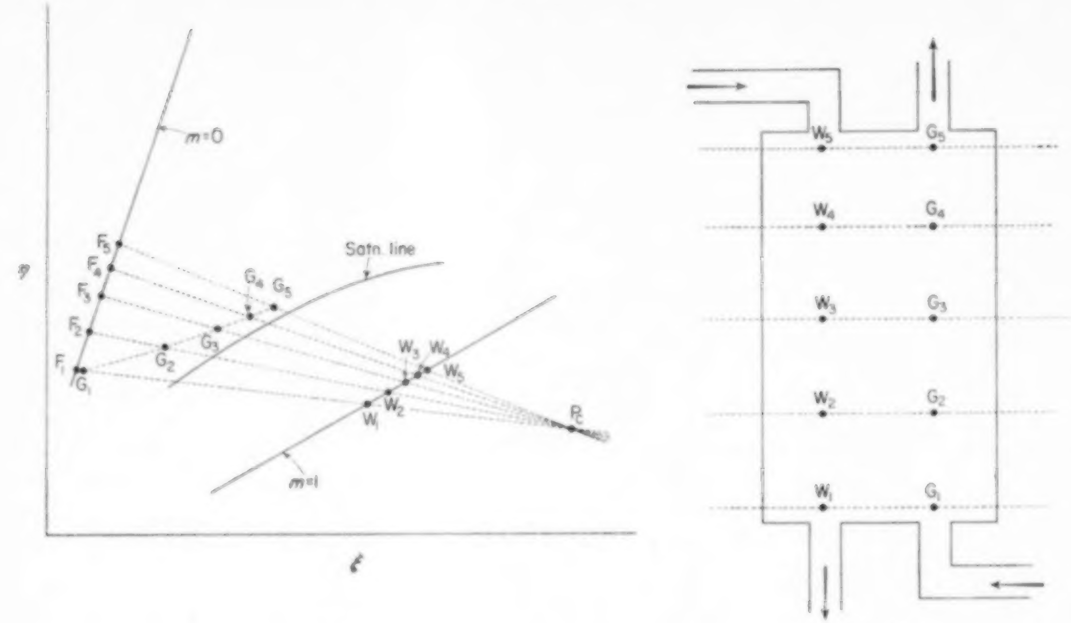

(a) (b)

FIG. 7. Polar diagram

(a) for adiabatic equipment (b) for counter-flow equipment

Fig. 7(a) shows such a polar diagram for the adiabatic counter-flow plant shown in Fig. 7(b). G represents the gas-stream and W the liquid. $\overline{G_1W_1}$, $\overline{G_2W_2}$ etc. all pass through the "counter-flow pole," P_c, which represents the state of a single stream from which the pairs of liquid and gas streams could be derived.

The position of P_c is such that

$$\frac{\overline{P_cW_n}}{\overline{P_cG_n}} = \frac{\dot{m}_{G_n}}{\dot{m}_{W_n}} \cdot \frac{m_{G_n}}{1} \cdot \frac{(\xi_{W_n} - \xi_{F_n})}{(\xi_{G_n} - \xi_{F_n})} \qquad (18)$$

where the subscript n denotes the tower section in question, $\dot{m}_G$ and $\dot{m}_W$ denote respectively the mass flow rates of the gas and liquid streams, and F_n is the intersection of the line $P_cW_nG_n$ with the pure-air line.

Normally the pole P_c is determined from (18) through specification of the liquid and gas states at one end of the plant, say, W_1 and G_1, and of their mass flow rate ratio there. Then the rays P_cW_2, P_cW_4, etc. are drawn.

In order to locate the points G_2, G_3, etc., it is common to *assume* that they lie on the saturation line; they are then completely fixed by the rays through P_c. In a rigorous calculation, however, it is necessary to apply the construction for the direction of change of the gas state several times in succession, starting at G_1 and finishing (in the example shown) at G_5. The result is an "operating line" for the gas in the equipment, i.e. a curve which gives the gas-state for any water state.

The analysis of the equipment thus proceeds in three stages:

(i) P_c is fixed. Then conservation principles ensure that the G-states lie on the appropriate $\overline{P_cW}$ lines.

(ii) Rate-process considerations, giving the direction of movement of G, combine with (i) to allow the position of the G's to be fixed.

(iii) Further rate-process considerations lead to determination of the number of transfer units of the equipment.

Sufficient attention has already been given to stages (i) and (ii). We now turn to stage (iii).

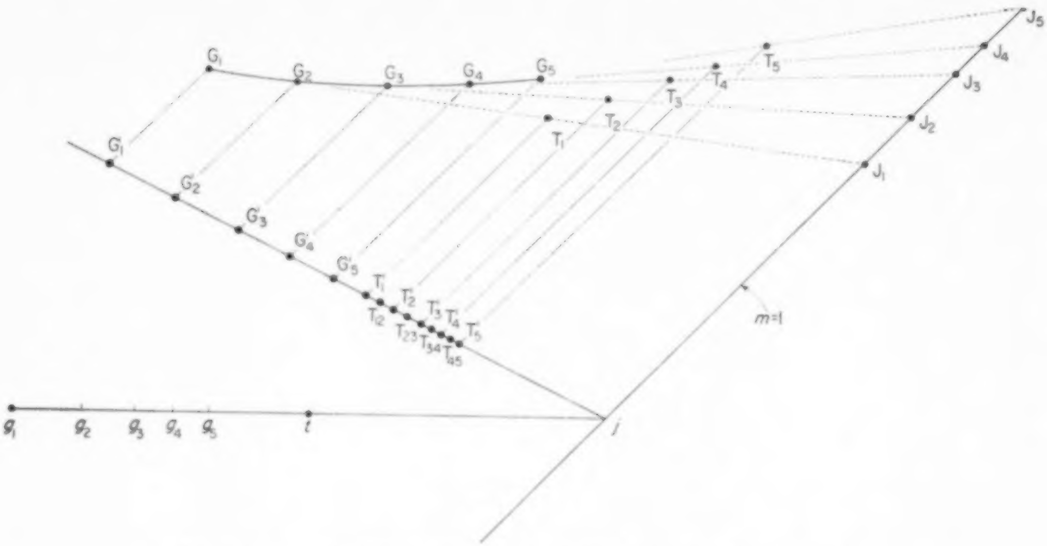

FIG. 8. Determination of number of gas-side mass transfer units, $N_{m,g'}$.
$N_{m,g'} = \ln[\frac{1}{2}(1 + \overline{g_1t}/\overline{g_2t})]$

VOL. 11 1959/60

2.5 *Determining the Equipment Size* (N.T.U.)
The problem

The column height of the transfer process shown in Fig. 7(a) can be obtained simply by evaluating the expression (17) for each of the stages shown. This procedure is straightforward but involves the measuring of lengths and calculation of ratios. It would be more convenient if a purely graphical integration procedure could be devised, so that the only numerical step occurs at the very end.

Graphical integration procedure

The recommended procedure will first be described. Then its validity will be demonstrated, and other possibilities discussed.

Fig. 8 shows a part of the construction for five gas states. $G_1, G_2 \ldots\ldots G_n \ldots$ represent successive gas states, and the corresponding points $T_1, T_2 \ldots\ldots T_n \ldots$ and $J_1, J_2 \ldots\ldots\ldots J_n \ldots$ are those featuring in the rate-process construction and in equation (17). The steps are as follows:

(i) Draw any line cutting the pure-H_2O line at j.

(ii) Draw parallels to the pure-H_2O line through the G's and T's, to intersect the line just drawn in $G_1', G_2' \ldots G_n' \ldots\ldots$ and $T_1', T_2' \ldots\ldots T_n' \ldots\ldots$

(iii) Plot T_{12}' at the mid-point of $T_1'T_2'$; plot T_{23}' at the mid-point of $T_2'T_3$; etc.

(iv) Draw a second line through the point j. Choose any point, g_1, on it. Plot t at the mid-point of g_1 j.

(v) Project the range of points G_1', G_2', T_{12}', j into the range of points g_1, g_2, t, j. This fixes the point g_2.

(N.B. Two methods of projection can be used. The simpler is shown in Fig. 9 (a): $g_1 G_1'$ and t T_{12}' are produced to cut at R; RG_2' is produced to cut g_1 j at g_2.

This construction is inconvenient when $g_1 G_1'$ and t T_{12}' are nearly parallel; for then R may lie out of reach. An alternative construction, which does not suffer from this defect, is shown in Fig. 9 (b): G_1' t and $g_1 T_{12}'$ are drawn intersecting at N; $g_1 G_2'$ is drawn, intersecting jN at Q: G_1' Q is drawn to cut g_1 j at g_2)

(vi) Project the range of points G_2', G_3', T_{23}', j into the range g_2, g_3, t, j. This fixes the point g_3.

(vii) Find any other g_n by successive applications of the same procedure.

(viii) Measure the ratio of lengths $\overline{g_1t}/\overline{g_nt}$.

(ix) Evaluate the number of gas-side mass

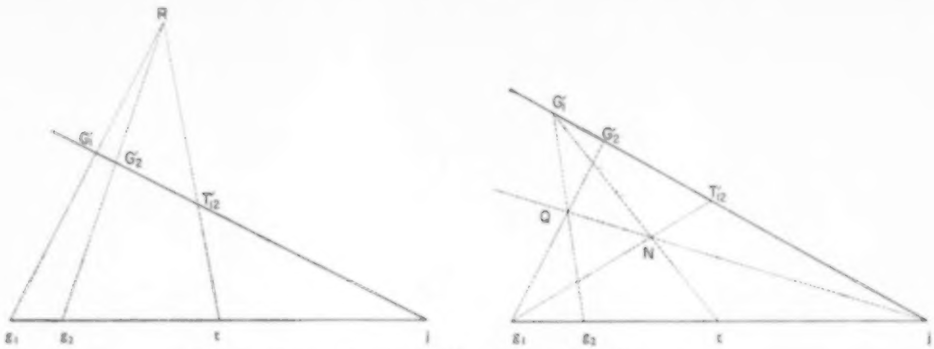

FIG 9. Two methods of determining the position of g_2.

transfer units necessary between level 1 and level n from

$$N_{m,g} = \ln\left\{\tfrac{1}{2}\left(1 + \overline{g_1 t}/\overline{g_n t}\right)\right\} \tag{19}$$

(NB. The last two steps are avoided if the g – points have been drawn on a suitably marked scale provided on the diagram. Only one such scale is needed, since we are otherwise free to choose the point j anywhere on the pure – H_2O line).

Validity of the construction

The range of points G_1', G_2', T_1', j is obtained from the range G_1, G_2, T_1, J_1 by central projection (the vertex of projection happens to be at infinity in the recommended procedure, but it need not be); therefore the cross-ratios of these ranges are equal. The same is true of the other pairs of ranges. From (17) therefore, the number of gas-side mass transfer units $N_{m,g}$ is given by

$$N_{m,g} = \sum \frac{\overline{G'_{n+1}\,G'_n}}{\overline{G'_{n+1}\,j}} \cdot \frac{\overline{T'\,j}}{\overline{T'\,G'_n}} \tag{20}$$

The suffix for T in this equation could be either n or n + 1; for the equation is only strictly valid when the difference between the n th and (n + 1) th states is very small. With steps of finite size, it seems wisest to use the T corresponding to the mid-point of the interval, namely $T_{n,n+1}$.

The range of points g_1, g_2, t, j is derived from the range G_1, G_2', T_{12}', j by central projection. Their cross-ratios are therefore equal. The same is true of the other pairs of ranges. From (20), therefore,

$$N_{m,g} = \sum \frac{\overline{g_{n+1}\,g_n}}{\overline{g_{n+1}\,j}} \cdot \frac{\overline{t\,j}}{\overline{t\,g_n}} \tag{21}$$

Now for a very large number of intervals, (21) can be written

$$N_{m,g} = -\int_{g_1}^{g_n} \frac{(\xi_j - \xi_t)}{(\xi_j - \xi_g)\,(\xi_g - \xi_t)} \cdot d\,\xi_g \tag{22}$$

This integral can be evaluated analytically, since ξ_j and ξ_t are constants (the construction has been specially designed to fix these points). We obtain

$$N_{m,g} = \ln\left[\frac{(\xi_j - \xi_{gn})}{(\xi_{gn} - \xi_t)} \cdot \frac{(\xi_{g1} - \xi_t)}{(\xi_j - \xi_{g1})}\right] \tag{23}$$

For the particular case in which t is midway between g_1 and j, as above, this reduces to equation (19).

It is therefore clear that the recommended procedure gives a finite-difference approximation to the solution of a differential equation: it gives an exact solution, if drawing errors are neglected, when the size of step is small.

Comments on the procedure

Many variants of the construction can be be devised. For example, t need not be at the mid-point of g_1 j, though this arrangement gives the greatest accuracy if g_1 j is finite. $N_{m,g}$ can be read from the scale with still higher accuracy if j is projected to infinity, though this slightly complicates the construction. The first projection (G_n to G_n') need not be a parallel one; any point on the pure-H_2O line can be taken as vertex. If all the T's lie approximately on a straight line, there is advantage in making the vertex just mentioned lie on this line also. Many other

possibilities will occur to anyone performing such constructions.

The time taken to carry out an integration, once the G's and T's have been determined, does not exceed more than a few minutes in most practical problems (up to, say, ten steps). The mental effort, after some practice, is also small.

The accuracy of the result falls off as $N_{m,g}$ increases and will often be unacceptably low for $N_{m,g}$ greater than 3. Equipment involving large numbers of transfer units is probably best calculated in two or more parts, the total size being calculated by adding the N_m's of the parts.

An example of the use of the recommended procedure is given below in connexion with a cooling-tower.

3. A Useful Chart for H_2O – Air Mixtures

3.1 *Description of the Chart*

For many of the problems arising in heating and ventilating, industrial drying, and cooling-tower design, the " mass-of-mixture " basis yields enthalpy-composition charts on which the state-points of interest are restricted to an inconveniently small area. The chart shown in Fig. 10 is designed to avoid this difficulty.

The transformation

The chart is of the $H - M$ variety, i.e. lines of constant composition remain vertical, and the horizontal range is from 0 to 1. The co-ordinate transformations are

$$M \equiv \frac{m}{(1/25) + (24/25)\, m} \tag{24}$$

$$H \equiv \frac{h}{(1/25) + (24/25)\, m} \tag{25}$$

The numbers appearing in the denominator are chosen so as to make the gas-phase isotherm approximately horizontal at the atmospheric boiling-point (212°F). It will be noted that,

$$\text{close to } m = 1 \ : \ M \simeq m \, ; \quad H \simeq h \tag{26}$$

$$\text{close to } m = 0 \ : \ M \simeq 25\, m \, ; \ H \simeq 25\, h \tag{27}$$

So a 25-fold enlargement of the air side of the diagram has been effected, when compared with the $h - m$ chart, while the H_2O side of the diagram is unaffected.

The mass basis

The transformations (24) and (25) permit interpretation as involving the use of 1 lb_m as the mass unit for H_2O but 25 lb_m as the mass unit for air. The effective " molecular weight " is thus

$$\mu = 1 \bigg/ \left(\frac{1}{25} + \frac{24}{25}\, m\right) \tag{28}$$

For the sake of simplicity of speech, μ lb_m of mixture is called 1 "lb nol" on the ordinate scale.

Scales of μ, and of m, are provided at the base of the diagram. M (and m) happen to increase from right to left on Fig. 10, to accord with the practice of [7] and [8]; this fact is without other significance.

Saturation lines

Provided that air and steam obey the Gibbs–Dalton laws, and that, like water, their enthalpies depend on temperature alone, which may be assumed for practical purposes, the positions of the gas-phase isotherms are independent of pressure. It is convenient therefore to make a single chart valid for several pressures by drawing several saturation lines. Those for 0·05, 0·1, 0·2, 0·4, 0·6, 1·0, 2·0, 5·0 and 10·0 atmospheres are drawn on Fig. 10.

To use the chart for mixtures at a particular pressure, the appropriate saturation line is chosen. The branches of the gas-phase isotherms to the left of their intersection with the saturation line are now ignored. In their place are drawn mixed-phase isotherms ; these are straight lines, terminating at one end on the temperature scale marked on the water line ($M = 1$), and at the other end at the appropriate intersection of the gas-phase isotherm and the saturation line.

The saturation line for 1 atm (14·696 lb/in²) total pressure is distinguished by hatching. If its shape is compared with that on an $h - m$ chart (Fig. 2a of Part I), it will be seen to be more curved ; a point of any given temperature is displaced towards the line $m = 1$.

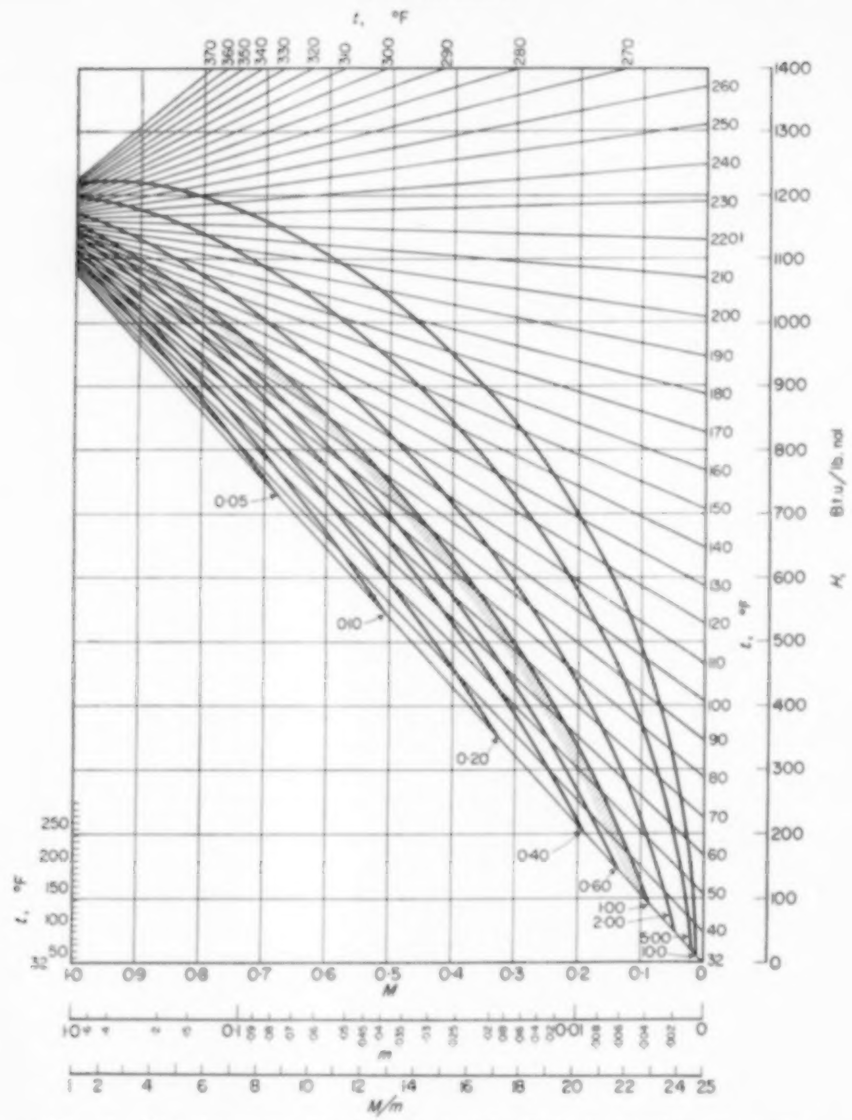

Fig. 10. Enthalpy-composition ($H-M$) chart for H_2O–air at various pressures.
1 nol H_2O = 1 lb_m H_2O 1 nol air = 25 lb_m air M = nol H_2O/nol mixture
H = enthalpy/nol mixture $M = m/[(1/25) + (24/25)\,m]$ $H = h/[(1/25) + (24/25)\,m]$
Numbers underlined at lower end of saturation lines represent total pressures in atm.

Number-of-transfer-units scale

On the base of the diagram is a scale for use in $N_{m,g}$ calculations, plotted in accordance with equation (23); j is on the line $M = 1$, g_1 on the line $M = 0$, and t on the line $M = 1/2$. The numbers give the value of $N_{m,g}$ when the final gas-phase point g_n lands on the corresponding graduation mark.

Applications of the chart

The extension of the low-m part of the diagram is valuable whenever the water content of air at moderate temperatures is in question, as in psychrometry and in drying. For example the composition of the air entering the cooling-tower in the next example is easily fixed, knowing the wet-bulb and dry-bulb temperatures.

3.2 *A Cooling-tower Example*

To illustrate the use of the chart, and of the calculation method of section 2.5 of this paper, we present an example of the determination of the number of transfer units (N.T.U.) of a cooling-tower. The complete construction is shown in Fig. 11.

Data

Water inlet temperature: 110°F

Water outlet temperature: 85°F

Air inlet condition: dry-bulb temperature: 85°F
wet-bulb temperature: 75°F

Total pressure: 1 atm

Air/water ratio:
1·5 times the minimum.

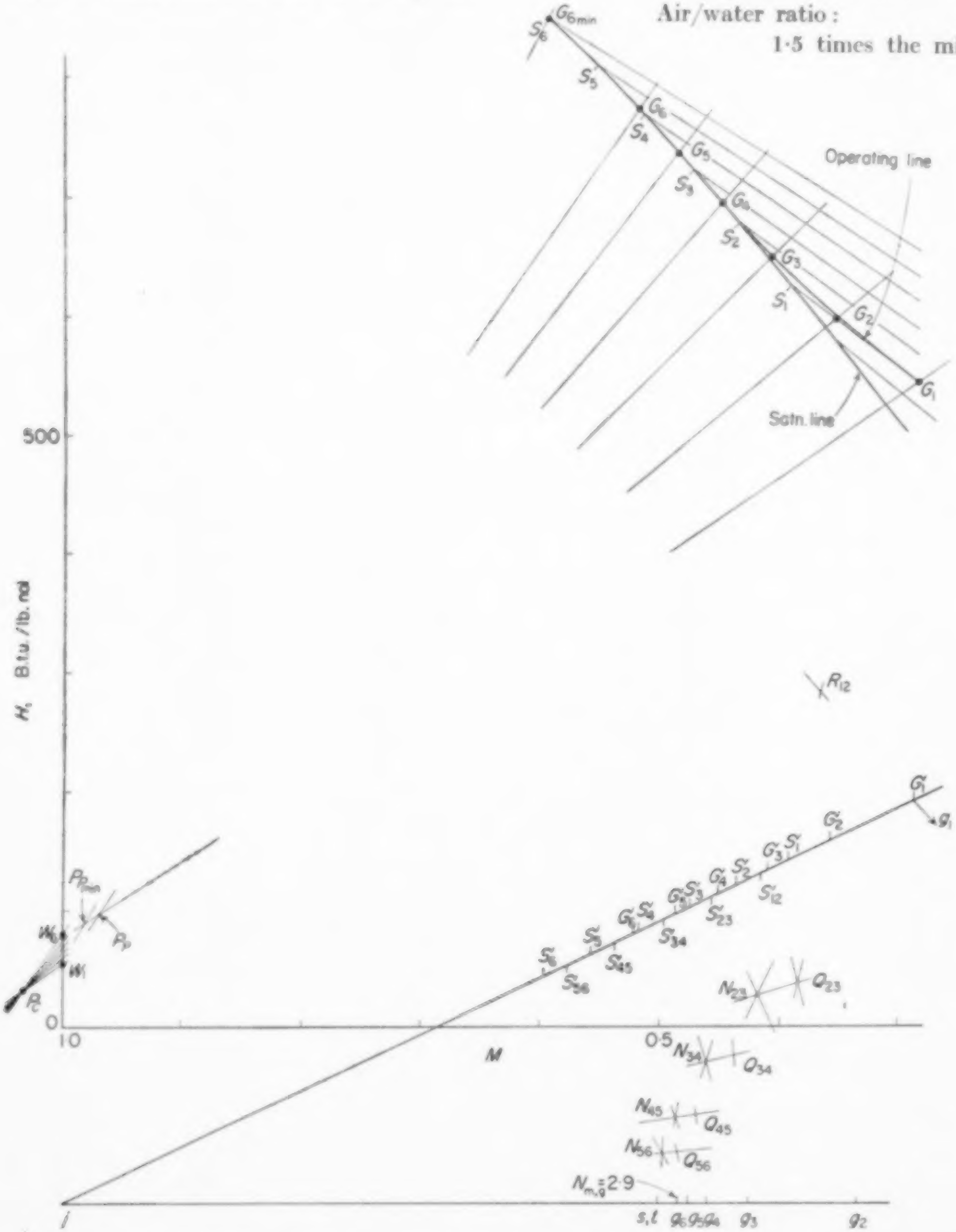

FIG. 11. Determination of number of gas-side mass transfer units for cooling-tower example.

Determination of corresponding water and gas stream states

The state-point of the water at inlet W_6, the water at outlet W_1 and the air at inlet, G_1, are marked on the chart (Fig. 11) directly from the data.

N.B. The suffix 6 to W at inlet is a consequence of deciding, in addition, to consider conditions at six levels in the tower, characterized by 5°F differences of water temperature.

The minimum permissible ratio of air rate to water rate is that causing the air to leave the tower in equilibrium with the incoming water: so $G_{6\,min}$ is on the 1 atm saturation line at 110°F. The corresponding "parallel-flow" pole, $P_{p\,min}$ is then drawn as the intersection of $W_1G_{6\,min}$ and W_6G_1. We have

$$\frac{\overline{W_6\,P_{p\,min}}}{\overline{P_{p\,min}\,G_1}} = \frac{\dot{m}_{G_1}}{\dot{m}_{W_6}} \cdot \frac{m_{G_1}}{M_{G_1}} \tag{29}$$

Since the air rate is to be 1·5 times the minimum, we find P_p, such that

$$\frac{\overline{W_6\,P_p}}{\overline{P_p\,G_1}} = 1{\cdot}5\,\frac{\overline{W_6\,P_{p\,min}}}{\overline{P_{p\,min}\,G_1}} \tag{30}$$

This is done by means of dividers. P_p is now the "parallel-flow" pole of the tower.

$W_1\,P_p$ is produced to the saturation line; its intersection is marked G_6 (for we know that the air will be practically saturated when it leaves the tower). $W_6\,G_6$ and $W_1\,G_1$ are now drawn to intersect at P_c. This is the counter-flow pole of the tower; it has the property that the state-points for the water and air streams at any level in the tower lie on lines passing through P_c.

Four more such lines are drawn: $P_c\,W_2\,G_2$, $P_c\,W_3\,G_3$, $P_c\,W_4\,G_4$ and $P_c\,W_5\,G_5$. The points W_2, W_3, W_4 and W_5 are on the liquid line at 90°F, 95°F, 100°F and 105°F. The points G_2, G_3, G_4, G_5 cannot yet be finally located, but we know that they lie on these lines.

(N.B. The part of the construction just described is actually less accurate when carried out on Fig. 11 than on a straightforward $h - m$ diagram, or an $H - M$ diagram with a smaller mass-unit ratio than 25 : 1 for the points P_p and P_c on Fig. 11 turn out to be rather near to the W's. Indeed there is nothing wrong with an $h - m$ chart for the whole of the N.T.U. construction, provided that the vertical scale is suitable. However it is easy to derive equivalent constructions which retain high accuracy on Fig. 11 as well).

Determination of the gas operating line

It will be assumed, as is common in cooling-tower design, that (i) $\sigma = 1$, (ii) the liquid-side heat-transfer resistance is very small. The consequences are that the gas-phase surface states S_1, S_2, ... S_6 can immediately be plotted at the other extremities of the mixed-phase isotherms through W_1, W_2, ... W_6, and that T is identical with S, so that G always moves towards S.

Now G_1S_1 is drawn to intersect P_cW_2 at G_2; G_2S_2 is drawn to intersect P_cW_c at G_3; etc. Joining up the G's gives the curve marked "operating line" in Fig. 11.

Determination of $N_{m,g}$

A sloping line is drawn through the point j where the $N_{m,g}$ scale intersects the line $M = 1$. Then the construction of section 2.5 is carried out, S replacing the T mentioned there, and the constructions of Fig. 9(a) or 9(b) being used as convenient. Details of the construction are shown in Fig. 11.

Finally, the point g_6 is obtained. A glance at the scale shows that $N_{m,g}$ is 2·9; so nearly three gas-side mass-transfer units of contact surface are needed to accomplish the required cooling of the water.

Comments on the calculation

The value of $N_{m,g}$ can only be taken as accurate to within about 5 per cent for the calculation as described; for higher accuracy a larger number of steps should have been taken. However, 5 per cent accuracy is often good enough for cooling-tower design.

No numerical work was needed in the construction.

The make-up water rate, $\dot{m}_{W_6} - \dot{m}_{W_1}$, is easily calculated from

$$\begin{aligned}\frac{\dot{m}_{W_6} - \dot{m}_{W_1}}{\dot{m}_{G_1}} &= \dot{m}_{G_6} - \dot{m}_{G_1}\\ &= 0{\cdot}0425 - 0{\cdot}0161\\ &= 0{\cdot}0264\end{aligned}$$

the numbers being read off quite easily from the horizontal m scale.

The ratio of inlet water to inlet air is given by

$$\frac{\dot{m}_{W_6}}{\dot{m}_{G_1}} = \frac{m_{P_p} - m_{G_1}}{1 - m_{P_p}}$$

$$= \frac{0{\cdot}585 - 0{\cdot}016}{1 - 0{\cdot}585}$$

$$= 1{\cdot}37$$

Here the accuracy is poorer because of the cramping of the m scale on the left.

Comparison with conventional calculation methods

The data of the above example were chosen to accord with those of a problem worked out in detail by Treybal [9], who used the Merkel method [10], also with five temperatures intervals.

Treybal's results, with those of the present paper in brackets for comparison, were

$N_{m,g}$	3·1	(2·9)
$\dot{m}_{W_6}/\dot{m}_{G_1}$	1·4	(1·37)
$(\dot{m}_{W_6} - \dot{m}_{W_1})/\dot{m}_{G_1}$	0·032	(0·026)

Discrepancies therefore exist. Since the Merkel method is in principle approximate, whereas the present one is so merely in practice, only a more detailed study would show which set of results is nearer the true answer; however Treybal's figure for the make-up water quantity is only an estimate.

The times taken to determine the N.T.U. by each method are probably about the same. The present method shows to advantage however when the moisture contents are sufficiently high to make the Merkel approximation too inaccurate.

4. Conclusions

(i) Enthalpy-composition charts for a single pair of substances employing a mass-of-mixture, a mole-of mixture or a mass-of-single-component basis, are all related to each other as shadow to image.

(ii) Such charts are particular members of a more general family of diagrams which are in homographic relation to each other.

(iii) In choosing a co-ordinate system for the plotting of a particular conserved-property charts, four constants may be arbitrarily chosen, apart from those governing scale changes. These may be chosen to give ease of drawing.

(iv) Particularly useful are $H - M$ charts which are like charts using the mole-of-mixture basis but in which the "molecular weight" ratio of the two components may be arbitrarily ascribed.

(v) Triangular diagrams and rectangular ones are also members of the same family.

(vi) Composition diagrams for ternary mixtures are similar in their projective properties to enthalpy-composition charts for binary mixtures.

(vii) The determination of the N.T.U. of a piece of transfer equipment may be carried out entirely graphically, apart from the final reading of a scale, by making use of the invariance of the cross-ratio of a range of four points under homographic transformation.

References

[1] Spalding D. B. *Chem. Engng. Sci.* 1959 **11** 183.

[2] Durell C. V. *Projective Geometry.* Macmillan, London 1938.

[3] Bošnjaković *Chem.-Ing.-Tech.* 1957 **29** 187.

[4] Bošnjaković *Technische Thermodynamik.* Steinkopf, Dresden 1937.

[5] Keenan J. H. *Thermodynamics.* John Wiley, New York 1941.

[6] W. Matz, *Thermodynamik des Waerme- und Stoffaustausches in der Verfahrenstechnik.* Steinkopf, Frankfurt 1949.

[7] Spalding D. B. *Proc. Inst. Mech. Engrs.* 1958 **172** No. 28.

[8] Spalding D. B. and Tyler R. D. *Int. Un. Pure Appl. Chem., Inst. Mech. Engrs. Joint Conf. 1957* Paper 1, Session 4.

[9] Treybal R. E. *Mass Transfer Operations.* McGraw Hill, New York 1955.

[10] Merkel, F. *Forsch-Arb. Ing. Verdunstungsk.* 1925 275.

Chemical Engineering Science, 1960, Vol. 11, pp. 242 to 251. Pergamon Press Ltd., London. Printed in Great Britain

Heat transfer in nozzles

W. C. Ragsdale* and J. M. Smith†
Purdue University, Lafayette, Indiana

(*Received* 3 *February* 1959)

Abstract—Local heat transfer rates and coefficients were measured between steam and the wall over the converging and diverging sections of a nozzle having a diameter of 0·400in. at the throat. The coefficients ranged from 43 to 290 B.t.u/(hr sq.ft/°F) over a Mach number interval from 0·46 to 1·80. Maximum coefficients were observed at the nozzle throat.

Correlations for well-developed turbulent flow in pipes could not be adapted to represent the observed results. A simple flat-plate equation based upon a length Reynolds number predicted Stanton numbers about 10 per cent lower than the experimental values. Bartz' method of modifying the flat plate concept to allow for gradients of bulk temperatures, velocities and pressures along the nozzle axis agreed well with the experimental data and represented an improvement over the flat plate equation.

Résumé—Les vitesses d'echange thermique local et les coefficients ont été mesurés entre la vapeur et la paroi sur les sections convergentes et divergentes d'un ajutage ayant un diamètre de 0,400in. au col.

Les coefficients s'étendent de 43 à 290 B.t.u/(hr sq.ft°F) sur un nombre de Mach variant de 0,46 à 1,80. Des coefficients maxima sont observés au col.

Des relations pour un écoulement turbulent bien établi, dans des conduits ne peuvent être adaptées à la représentation des résultats observés. Une équation linéaire basée sur plusieurs nombres de Reynolds prévoit des nombres de Stanton environ 10 fois plus petits que les valeurs expérimentales.

La méthode de Bartz modifiant le concept linéaire pour tenir compte des gradients des températures globales, des vitesses et des pressions le long de l'axe de l'ajutage, conduit à un accord avec les résultats expérimentaux et constitue une amélioration de l'équation linéaire.

Zusammenfassung—Örtliche Wärmeübergangskoeffizienten wurden zwischen Dampf und der Wand in konvergenten und divergenten Teil einer Düse gemessen, deren engster Durchmesser ca. 10 mm betrug. In einem Bereich der Machzahl von 0,46 bis 1,80 lagen die gemessenen Koeffizienten zwischen 244 und 1650 W/m^2 grd mit einem Maximum im engsten Querschnitt.

Die Beziehungen für voll entwickelte turbulente Rohrströmung konnten die gemessenen Werte nicht wiedergeben. Die Gleichung für die ebene Wand mit einer auf die Länge bezogenen Reynolds-Zahl ergaben Stanton-Zahlen, die ungefähr 10% niedriger als die gemessenen Werte waren. Dagegen erheilt man eine gute Übereinstimmung mit den gemessenen Werten, wenn man nach Bartz die Gleichung für die ebene Platte für Gradienten der Mischtemperatur, der Geschwindigkeiten und der Drücke längs der Düse verwendete; diese Methode stellt eine Verbesserung der Gleichung für die ebene Platte dar.

Interest in jet propulsion has directed increasing attention to the problem of predicting heat transfer rates in nozzles. Because of the large gradients of pressure, velocity and temperature in the direction of flow, the conventional correlations developed for flow in pipes or on flat plates would not be expected to be applicable. Flow in nozzles is also unlike pipe flow in that the flow length is usually too short to establish fully-developed velocity profiles. It appears more reasonable to describe the flow pattern in terms of a constant-velocity core surrounded by a boundary layer through which the velocity decreases to zero at the wall.

*Present address: Pratt & Whitney Aircraft Co., East Hartford, Conn.
†Present address: Northwestern University, Evanston, Illinois.

SAUNDERS and CALDER [1] measured heat transfer coefficients in the diverging section of a nozzle by passing hot combustion gases (at about 865 °C) through a nozzle made up of sections separated from each other by an air gap. It was concluded from the magnitude of the heat transfer coefficients obtained that the boundary layer must be turbulent. Substantiating evidence was available from velocity-profile measurements made at the exit of the nozzle.

The theoretical development of heat transfer coefficients for turbulent boundary layers is difficult and at present several assumptions have to be made to attain solutions of the momentum and energy equations. BARTZ [2] has solved the problem by assuming, among other things, that:

(1) A turbulent boundary layer exists throughout the nozzle.

(2) The velocity and temperature difference (stagnation temperature – wall temperature) variations in the boundary layer follow the 1/7 power law.

(3) The friction in the nozzle is the same as for a flat plate with the same boundary layer thickness.

(4) Reynolds analogy is valid for the boundary layer.

SIBULKIN [3] solved the momentum and energy equations by supposing, in addition, that the density in the boundary layer was constant (incompressible boundary layer). Other theoretical studies, for example that of KALIKHMAN [4] for the case of stream-wise pressure and velocity gradients, appear to be too complex to be useful in correlating heat transfer coefficients.

Sufficient experimental data are lacking for careful evaluation of the theories of heat transfer in nozzles. SAUNDERS and CALDER's results do not include the critical region of the throat where the heat transfer coefficients are at a maximum. BODEN [5] measured heat fluxes in a rocket motor fired with a nitric acid and aniline–furfuryl system, but insufficient data were taken to obtain heat transfer coefficients. Similarly, ZURCROW and Beighley [6] measured rates, but not coefficients, in a rocket motor using a nitric acid–jet–engine–fuel combustion mixture. GREENFIELD [7] employed a transcient method based upon the temperature–time history of a rocket motor made from copper. The results scattered considerably so that only an approximate, empirical correlation could be attempted.

The objective of the present work was to obtain reliable experimental data over the entire length of a nozzle, using a fluid whose physical properties were well established. Information was obtained for one nozzle design (throat diameter of 0·40 in.) at eleven positions between the entrance to the converging section and the exit of diverging region.

APPARATUS AND METHODS

Two stainless-steel, water-cooled nozzles of identical size and contour were used. Superheated stream was employed as the heat transfer medium because its Prandtl number is close to

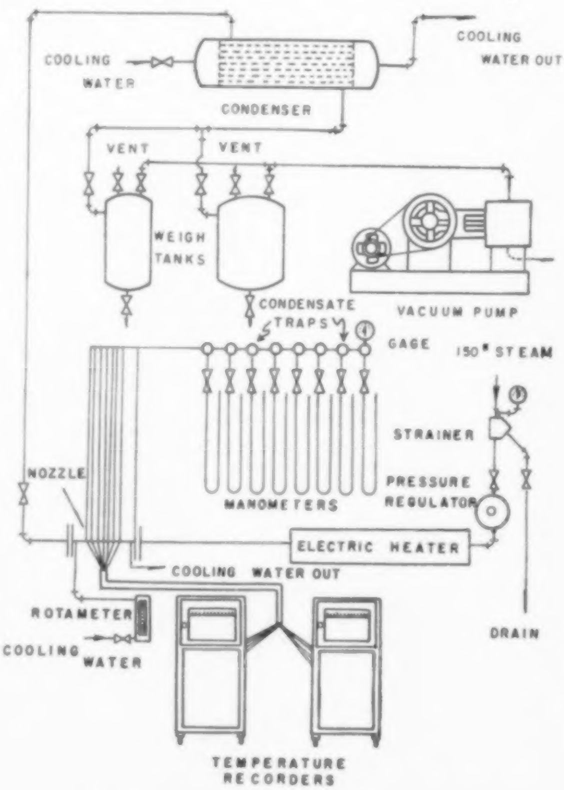

FIG. 1

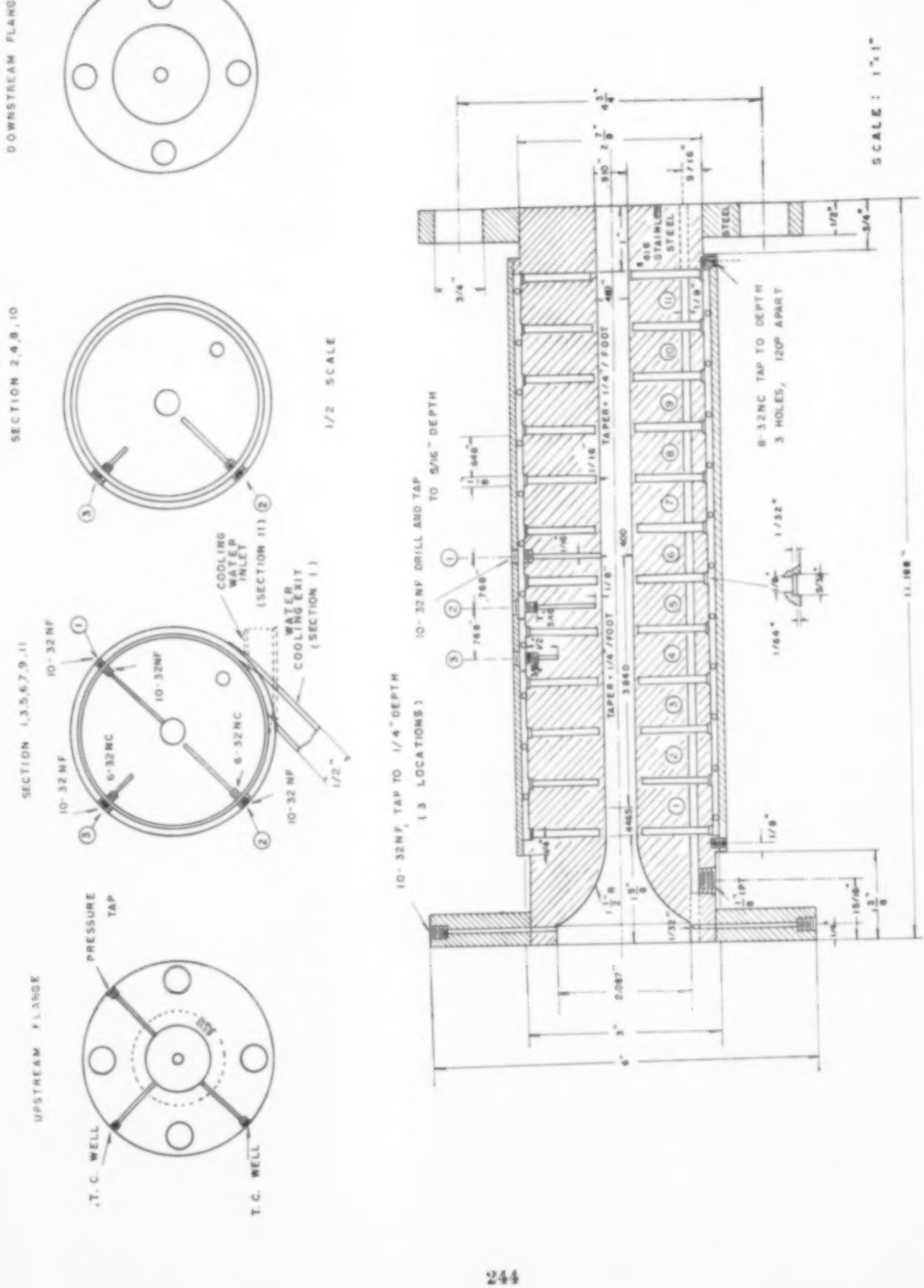
DOWNSTREAM FLANGE
SECTION 2,4,8,10
1/2 SCALE
SECTION 1,3,5,6,7,9,11
COOLING WATER INLET (SECTION 11)
WATER COOLING EXIT (SECTION 1)
UPSTREAM FLANGE
PRESSURE TAP
T.C. WELL
T.C. WELL
10-32 NF TAP TO 1/4" DEPTH (3 LOCATIONS)
10-32 NF DRILL AND TAP TO 5/16" DEPTH
8-32 NC TAP TO DEPTH 3 HOLES, 120° APART
TAPER = 1/4"/FOOT
TAPER = 1/4"/FOOT
STAINLESS STEEL
STEEL
SCALE: 1"=1"

Fig. 2

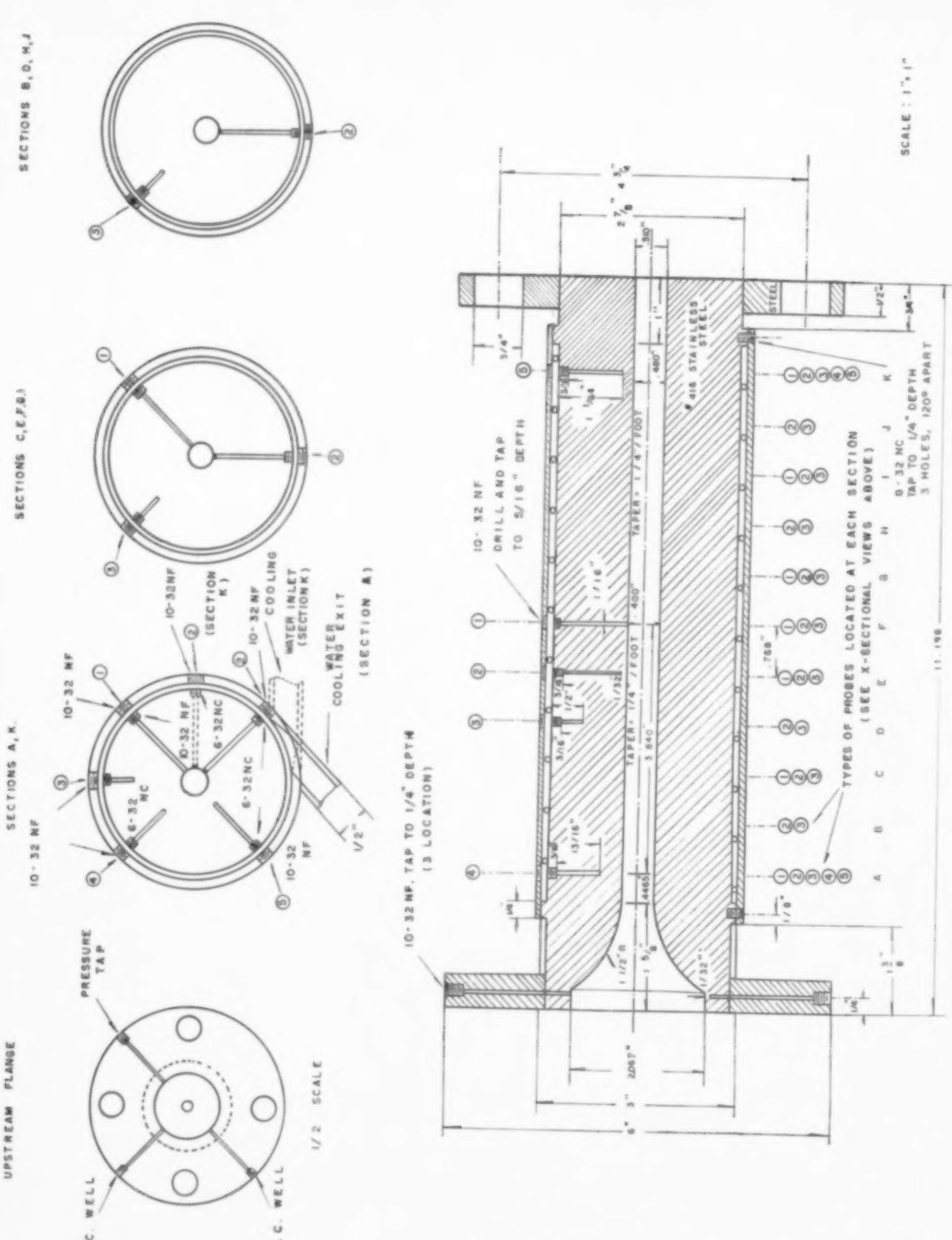
UPSTREAM FLANGE
1/2 SCALE
PRESSURE TAP
T. C. WELL
T. C. WELL
SECTIONS A, K
SECTIONS C, E, F, G, I
SECTIONS B, D, H, J
COOLING WATER INLET (SECTION K)
COOLING WATER EXIT (SECTION A)
10-32 NF DRILL AND TAP TO 5/16" DEPTH
10-32 NF, TAP TO 1/4" DEPTH (3 LOCATION)
416 STAINLESS STEEL
TYPES OF PROBES LOCATED AT EACH SECTION (SEE X-SECTIONAL VIEWS ABOVE)
8-32 NC TAP TO 1/4" DEPTH 3 HOLES, 120° APART
SCALE : 1" = 1"

FIG. 3

unity over a range of temperature. Since the recovery factor r has been found by a number of investigators [8–10] to be approximately equal to $(\mathrm{Pr})^{1/3}$, this means that the adiabatic wall temperature is equal to the more easily established stagnation temperature.

The heat transfer rate at the wall, q_w, was determined in both nozzles by measuring temperatures in the walls. It is necessary that q_w represent the heat transfer rate normal to the nozzle wall. In the sectional nozzle this was approached by insulating various sections of the nozzle from each other so that energy could flow in each section only in the radical direction. In the solid nozzle temperatures were measured around the boundaries of a region inside the wall. Then the temperatures within this region were obtained by solving the pertinent boundary value problem. In this manner radial temperature profiles, and hence the radial heat transfer rate, could be determined at any position along the nozzle length.

The apparatus as a whole is schematically pictured in Fig. 1. Saturated steam passed through a strainer, was throttled to 5–20 p.s.i.g., and heated to the desired temperature level by an electric heater. The superheated steam then flowed through a straight, insulated, standard 2 in. pipe to the nozzle entrance. In some runs, four 100-mesh screens were placed just upstream from the nozzle entrance to eliminate potential, thermal and momentum boundary layers at the beginning of the nozzle.

Both nozzles were machined from stainless steel (No. 416). Flanges and cooling jackets were made from ordinary steel and copper wire was wrapped around the nozzles, inside the cooling jacket, to provide helical passageways for the cooling water. The convergence and divergence of the nozzles was slight, as shown in Fig. 2 and 3, which give all the dimensions of the units.

In the sectional nozzle, circular grooves were cut in the walls (Fig. 2) so that there were eleven sections of equal width and two end sections. Two $\frac{1}{16}$ in. thermocouple wells (one long and one short) were drilled in each of the eleven central sections. The grooves were evacuated in order to reduce the heat transfer from one section to another.

In the solid nozzle (Fig. 3), temperatures were measured at the same eleven longitudinal positions. Two (one long and one short) $\frac{1}{16}$ in. thermocouple wells were drilled in the nozzle wall at positions B, C, D, E, F, G, H, I and J corresponding to sections Nos. 2–10 in the first nozzle. Four thermocouple wells were drilled (to four different depths) in the nozzle wall at positions A and K.

The thermocouple probe used to measure temperatures in the nozzle walls consisted of two 0·01 in. diameter wires, embedded in magnesium oxide insulation, inside a 0·062 in. O.D. stainless steel (No. 316) sheath. The short probes contained iron–constantan thermocouple wires and the long probes copper–constantan.

Range of Conditions

Runs were made at four steam flow rates ranging from 110 to 200 lb/hr. Inlet temperatures and pressures covered the range 516–617 °F and 5–20 p.s.i.g. The corresponding Reynolds numbers varied from 68,000 to 200,000. At each set of conditions four runs were made, two with screens at the nozzle inlet, and two without.

Calculation of Heat Transfer Coefficients

Sectional nozzle

From the temperature measurements, t_2 and t_1, at the two radial positions, the heat transfer rate for each section q_w was obtained from the equation

$$q_w = -\frac{2\pi k_s L (t_2 - t_1)}{\ln r_2/r_1} \tag{1}$$

where t refers to the temperature measured at a radius r from the centre line of the nozzle. An expression of the same form may be used to determine the wall temperature t_w, once q_w has been computed. The stagnation temperature $(T_0)_x$ was computed from the following heat balance:

$$(T_0)_x = (T_0)_{\text{inlet}} - \frac{\sum_0^x q_w}{w\, c_p} \tag{2}$$

In equation (2) the summation refers to the total energy transferred from the steam up to the axial position x. The inlet stagnation temperature

was measured with a half-shielded thermocouple. Since this is equal to the adiabatic wall temperature, T_{aw}, for steam at the conditions employed, the average heat transfer coefficient for the section is given by:

$$h = \frac{q_w}{(2\pi\, r_w\, L)\ (T_{aw} - t_w)} \tag{3}$$

Solid nozzle

The temperature distribution in the walls of the solid nozzle is described by the equation:

$$\frac{\partial^2 t}{\partial r^2} + \frac{1}{r}\frac{\partial t}{\partial r} + \frac{\partial^2 t}{\partial x^2} = 0 \tag{4}$$

for conditions of constant thermal conductivity. The boundary conditions, consisting of the measured temperatures indicated in Fig. 3, were such that equation (4) could not be solved analytically. Relaxation methods were employed to obtain the complete temperature distribution, using a Datatron digital computer (Electrodata Corporation). Illustrative results are shown in Fig. 4 for run no. 6. The letters identifying the radial profiles refer to the positions indicated in Fig. 3.

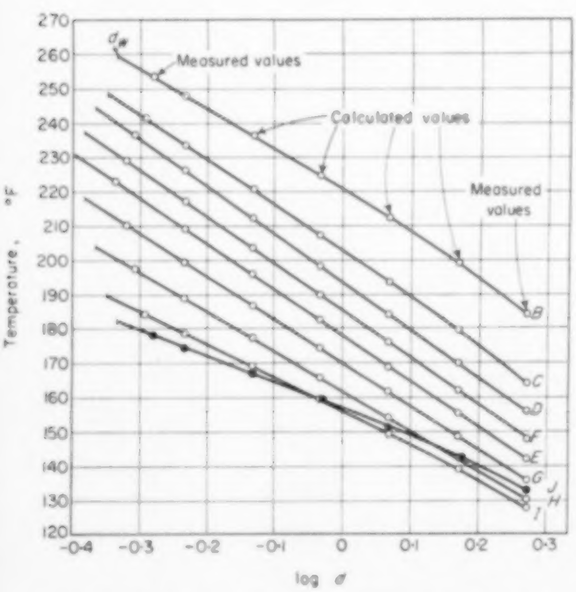

Fig. 4. Calculated radial temperature profiles at positions B through J for solid nozzle run 6.

Profiles, such as shown in Fig. 4, were extrapolated to the diameter at the nozzle wall (designated by d_w). The slope and temperature at the wall were then utilized in the following equation to determine the heat transfer rate:

$$\frac{q_w}{A} = k_s \left(\frac{\partial t}{\partial r}\right)_w \tag{5}$$

As in the sectional nozzle, the stagnation temperature at any location x was evaluated by an energy balance:

$$(T_0)_x = (T_0)_{\text{inlet}} - \frac{\int_0^x (q_w/A)\, dA}{w\, c_p} \tag{6}$$

Finally, the heat transfer coefficient was determined from equation (3).

Results

The heat transfer results are illustrated in Figs. 5 and 6*, where the local coefficient is

*Complete tabulation of the data and calculated results are given in Ref. [12].

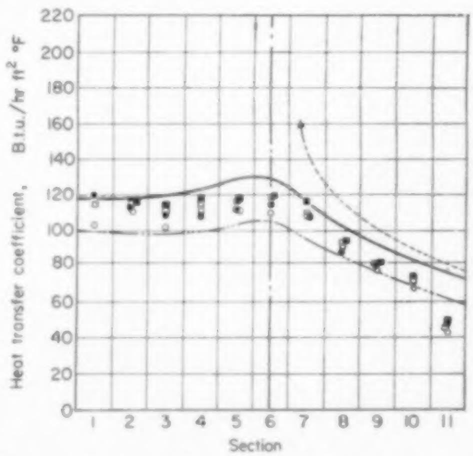

Fig. 5. Heat transfer coefficients for subsonic and supersonic flow of steam in a DeLaval nozzle. Sectional nozzle results.

Predicted values:
——— Bartz
- - - flat plate, equation (11)
— — flat plate, equation (10)
Average conditions:
$t_{\text{inlet}} = 617$ °F
$p_{\text{inlet}} = 5$ p.s.i.g
$w = 112$ lb/hr

Experimental values with screens:
○ run 25
● run 36
without screens:
□ run 29
■ run 40

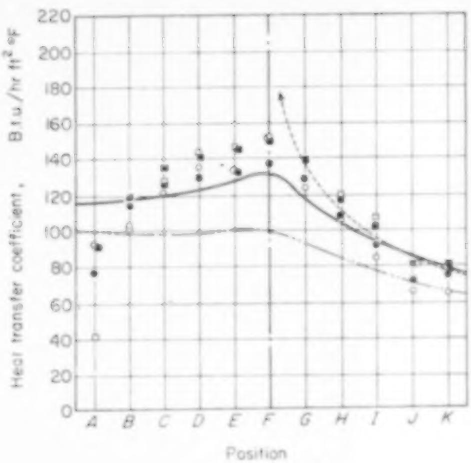

Fig. 6. Heat transfer coefficients for subsonic and supersonic flow of steam in a DeLaval nozzle. Solid nozzle results.

Predicted values:
—— BARTZ
– – – flat plate, equation (11)
— — —flat plate, equation (10)

Average conditions:
$t_{\text{inlet}} = 610$ °F
$p_{\text{inlet}} = 5$ p.s.i.g.
$w = 111$ lb/hr

Experimental values with screens:
○ run 5
● run 16

Without screens:
□ run 9
■ run 20

plotted versus the axial position in the nozzle. On each graph are shown the two sets of duplicate runs, one with entrance screens and one without. The coefficients range from 43 to 290 B.t.u/(hr ft² °F) over a Mach number variation from 0·46 to 1·8. The corresponding heat flux ranged from about 20,000 to 65,000 B.t.u/(hr ft²).

Fig. 5 indicates that the heat transfer coefficient first decreases slightly and then increases in the converging section of the sectional nozzle. The maximum value is attained at the throat. In the supersonic region downstream from the throat, the coefficient rapidly decreases. Runs at higher flow rates indicate larger coefficients, but the variation with position is similar to that illustrated in Fig. 5. The average reproducibility of the data for the sectional nozzle as judged by the duplicate runs, using all the data, is 3·5% for the runs with screens and 4·0% without screens. The results for the solid nozzle (Fig. 6) were not as good. Omitting the terminal positions A and K, since these results were suspect because of end effects, the reproducibility is 7·0% with screens and 5·0% without.

In the sectional nozzle the heat transfer coefficients were approximately the same with and without entrance screens. In the solid nozzle, the results with screens are approximately 11% lower than those without screens. While this seems to be somewhat larger than the reproducibility of the runs, it is difficult to explain how eliminating the thermal and momentum boundary layers by inserting screens would reduce the heat transfer coefficient. It may be that the presence of the screens lead to erroneous measurements of the entrance steam temperature. This comparison, along with the poorer reproducibility of the solid nozzle data, suggests that the measurements and computations for the sectional nozzle are more reliable.

Comparision of the results for the two nozzles at the same flow rates (Figs. 5 and 6) shows that the coefficients in the solid nozzle were about 15 per cent higher than those in the sectional nozzle. An analysis of errors indicates that the data obtained for the sectional nozzle are the reliable. From the error analysis and reproducibility tests, it is believed that the sectional nozzle results are accurate within 10 per cent. The solid nozzle data showed more random variation and would be subject to larger constant errors.

PREDICTION OF HEAT TRANSFER COEFFICIENTS

Flat plate methods

A simple concept of heat transfer in a nozzle is to imagine that the circular wall surface is opened out, becoming a flat plate. Because of the high Reynolds numbers in nozzle flow, the boundary layer is expected to be turbulent. Heat transfer in this turbulent layer will be determined by the time-average values of the product of the fluctuating contributions of the temperature and velocity. Suppose, in an approximate fashion, the resultant effect is a velocity v' perpendicular to the direction of flow. Then the heat transfer rate per unit area through the boundary layer is

$$\frac{q}{A} = c_p \, \rho \, v' \, (T_{av} - t_w) \tag{7}$$

VOL. 11 1959/60

In terms of the heat transfer coefficient this may be written

$$h = c_p \, \rho \, v' \tag{8}$$

The effect of turbulence, as measured by v', would be dependent upon the bulk velocity of the fluid and the dimensionless ratio of the boundary layer thickness δ and the distance x from the leading edge of the plate. If v' is directly proportional to u and inversely proportional to δ/x, equation (8) becomes

$$h = a\left(c_p \, \rho \, u \frac{x}{\delta}\right)$$

or

$$\mathrm{St} = \frac{h}{c_p \, \rho \, u} = a\left(\frac{x}{\delta}\right) \tag{9}$$

The boundary layer thickness ratio is dependent upon the length Reynolds number Re_x. LATZKO [11] has developed an expression for this ratio and then combined it with equation (9) to yield the following equation:

$$\mathrm{St} = 0{\cdot}0292\,(\mathrm{Re}_x)^{-0{\cdot}2} \tag{10}$$

This expression along with the experimental data are shown in Fig. 7 for the sectional nozzle, and in Fig. 8 for the solid nozzle. In evaluating the Reynolds and Stanton numbers, bulk values of the properties and velocity were used. Omitting the data on Fig. 7 for the last section (No. 11) in the nozzle, which are suspect because of end effects, equation (10) follows the trend of the observed results, but predicts values about 10 per cent low. Though the results shown on Fig. 8 for the solid nozzle scatter more, the same conclusions apply.

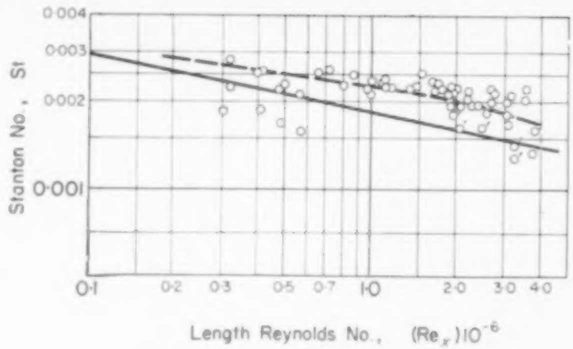

FIG. 8. Solid nozzle results (with screens).
– – – BARTZ method —— flat plate, equation (10)
′ end value

SAUNDERS and CALDER [1] used a modified form of equation (10) to correlate their data in the diverging section of a nozzle. The Reynolds number $\mathrm{Re}_{x''}$ was based upon the distance x'' from the throat. The data of this study are considerably lower than predicted by this means, as shown in Fig. 9. The SAUNDERS and CALDER expression may be written

$$\mathrm{St} = 0{\cdot}0285\,(\mathrm{Re}_{x''})^{-0{\cdot}2} \tag{11}$$

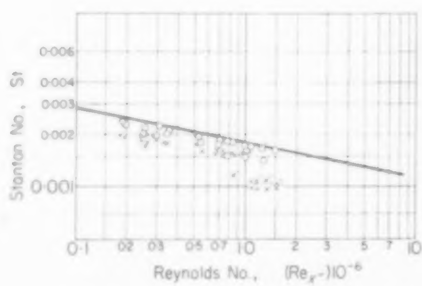

FIG. 9. Diverging region results.

$\mathrm{Re}_{x''} = \dfrac{x'' G}{\mu}$ ′ end section value

—— SAUNDERS and CALDER method, flat plate equation (11).

× experimental result, sectional nozzle

○ experimental result, solid nozzle (with screen)

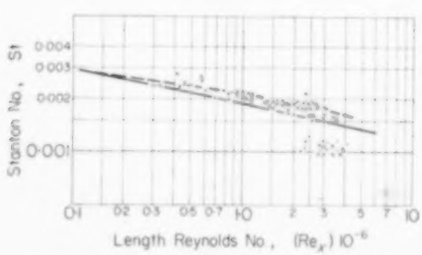

FIG. 7. Sectional results (with screens).
– – – BARTZ method —— flat plate, equation (10)
′ end section value

Nozzle equations

The use of the flat plate approach (equation 10) neglects the possible effects of pressure and velocity gradients, in the direction of flow, on the

heat transfer rate. BARTZ [2] and SIBULKIN [3] have taken these gradients into account by integrating the equations of motion, again supposing that a turbulent boundary layer exists throughout the nozzle.

BARTZ' solution, based upon the assumptions given earlier, is in the form of two equations, one (equation 12) for the momentum boundary layer thickness, θ, and one (equation 13) for the temperature boundary layer thickness, Δ. The heat transfer coefficient is then expressed in terms of ratios of θ and Δ to the velocity boundary layer thickness δ.

$$\frac{d\theta^{5/4}}{dx} + \frac{5}{8}\theta^{3/4}\left[\frac{M^2 - 2(\delta^*/\theta) - 3}{1 - M^2}\right]\frac{d}{dx}\left(\frac{A}{A_*}\right) = \left(\frac{5}{4}\right) 0{\cdot}0288\,\sigma\left[\left(\frac{\mu_0}{\rho_*\,\mu_*}\right)\frac{\theta}{\delta}\,\frac{A_*}{A_*}\right]^{1/4} \quad (12)$$

$$\frac{d}{dx}\frac{\Delta}{\delta} + \left(\frac{9}{8}\right)\left(\frac{\Delta}{\delta}\right)^{9/7}\frac{d}{dx}\left[\ln\frac{\lambda\,\theta\,c_p\,(T_0 - T_w)}{r}\right] = \frac{9}{8}(0{\cdot}0228\,\sigma)\,\frac{[(\mu_0/\rho_*\,\mu_*)(\theta/\delta)(A/A_*)]^{1/4}}{\theta^{5/4}\,\mathrm{Pr}^{0{\cdot}46}\,\lambda} \quad (13)$$

$$h = \left[\frac{0{\cdot}0228\,(\rho_*\,\mu_*)^{3/4}(\mu_0)^{1/4}\,c_p}{\mathrm{Pr}^{0{\cdot}46}}\right] \times \left[\sigma\left(\frac{\theta}{\delta}\right)^{1/4}\left(\frac{A}{A_*}\right)^{3/4}\right]\left[\left(\frac{\delta}{\Delta}\right)^{-1/7}\left(\frac{1}{\theta}\right)^{1/4}\right] \quad (14)$$

These three equations can be solved, numerically, for the heat transfer coefficient and the boundary layer thickness at any point, from a knowledge of the steam temperature entering the nozzle, the flow rate, wall temperature distribution and the nozzle geometry.

The BARTZ equations do not indicate a unique relationship between the Stanton number and length-Reynolds number, Re_x. However, for each nozzle, the results for different operating conditions correspond to a single such relationship. The results, shown on Figs. 7 and 8 as dotted lines, indicate good agreement with the experimental data.

SIBULKIN's method [3], based upon assuming the boundary layer is incompressible and somewhat different assumptions than BARTZ made, was also employed to calculate heat transfer coefficients for the nozzles. The results do not agree as well with the experimental data as the BARTZ or flat-plate prediction methods.

Application of pipe flow equations

The Colburn equation for well-developed turbulent flow in pipes

$$\mathrm{St} = 0{\cdot}023\,(\mathrm{Re}_d)^{-0{\cdot}2}\,(\mathrm{Pr})^{-2/3} \quad (15)$$

was adapted to nozzles by using the point value of the nozzle diameter and the bulk velocity in formulating the Reynolds number. The properties were evaluated at the bulk temperature of the steam. The Colburn equation is compared with the data for the sectional nozzle (with screens) in Fig. 10. The poor agreement in

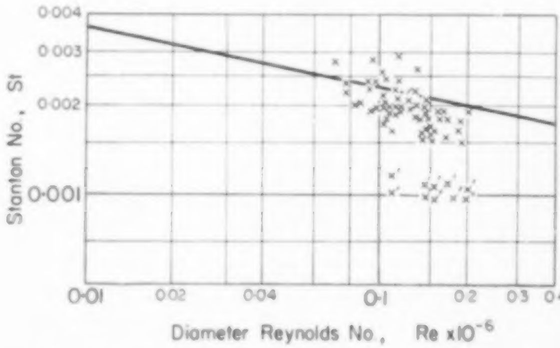

FIG. 10. Pipe flow equation (Colburn) correlation.
—— Colburn equation, equation (15)
x experimental data, sectional nozzle (with screens)
′ denotes end section result

comparison with Fig. 7 and 8 indicates that the boundary layer concept more appropriately describes heat transfer in nozzles. Other pipe-flow correlations [13, 14] were compared with the observed results, but no improvement was noted over the Colburn equation.

CONCLUSION

Experimental heat transfer coefficients in nozzles were found to decrease slightly at the entrance to the converging section and then increase to a maximum value at the throat. In the supersonic, diverging section the coefficients decreased sharply.

The data agree surprisingly well with a simple equation based upon a turbulent boundary layer

VOL. 11 1959/60

flowing along a flat plate. Better agreement is obtained with BARTZ' equations, which still presume a turbulent boundary layer but take into account velocity and pressure gradients in the direction of flow. Prediction methods based upon modifying correlations for turbulent flow in pipes are not as satisfactory.

NOMENCLATURE

A = area — ft^2

A_* = cross-sectional area of nozzle at throat — ft^2

c_p = specific heat at constant pressure — B.t.u/lb °F

d = diameter of pipe or nozzle — ft

G = mass velocity — lb/hr ft^2

h = heat transfer coefficient — B.t.u/hr ft^2 °F

k_s = thermal conductivity of stainless steel (#416) — (15·2 B.t.u/hr ft °F)

k = thermal conductivity of fluid in nozzle — B.t.u/hr ft °F

L = width of heat transfer area in a single section of the nozzle — ft

M = Mach number — dimensionless

p = static pressure — p.s.i.g.

Pr = Prandtl number — dimensionless

q = rate of heat transfer — B.t.u/hr

r = radius of any point in the nozzle. r_1 and r_2 corresponds to radii at which temperatures were measured — ft

The symbol r is also used to indicate the recovery factor, defined by the equation

$$r = \frac{T_{aw} - T}{T_0 - T}$$

Re_d = Reynolds number — dimensionless $\dfrac{du\rho}{\mu}$

Re_x = length Reynolds number — dimensionless $\dfrac{xu\rho}{\mu}$

T = static temperature of fluid — °F

T_{aw} = adiabatic wall temperature — °F

T_0 = stagnation temperature of fluid — °F

t = temperature within nozzle wall — °F

u = bulk or free-stream velocity — ft/sec

u' = velocity in boundary layer, in the x direction — ft/sec

u_* = velocity at nozzle throat — ft/sec

v' = velocity in y direction in boundary layer — ft/sec

w = flow rate of fluid — lb/hr

x = distance from entrance of nozzle measured in axial direction. In flat plate equation (equation 11) x'' represents distance measured from nozzle throat

y = distance, measured perpendicular to nozzle wall and into fluid

γ = ratio of specific heats

δ = thickness of velocity boundary layer

δ^* = displacement thickness of velocity boundary layer — ft

defined by equation

$$\delta^* = \int_0^\delta \left(1 - \frac{\rho' u'}{\rho u'}\right) dy$$

Δ = thickness of temperature boundary layer — ft

θ = thickness of momentum boundary layer — ft

defined by equation

$$\theta = \int_0^\delta \left(\frac{\rho' u'}{\rho u}\right)\left(1 - \frac{u'}{u}\right) dy$$

λ = dimensionless ratio of boundary layer thickness defined and computed by BARTZ [2]

μ = viscosity of fluid — lb/ft hr

ρ = density of fluid — lb/ft^3

ρ' = density of fluid in boundary layer — lb/ft^3

ρ_* = density of fluid in the free-stream at the nozzle throat — lb/ft^3

Subscripts

w = designates value at the nozzle wall

x = designates value at a distance x from nozzle inlet

REFERENCES

[1] SAUNDERS O. A. and CALDER P. H. *Heat Transfer and Fluid Mechanics Institute* 1951 p. 91.

[2] BARTZ D. R. *Trans. Amer. Soc. Mech. Engrs.* 1955 **77** 1235.

[3] SIBULKIN M. Heat Transfer and Fluid Mechanics Institute, Paper No. 6 1955.

[4] KALIKHMAN L. E., N.A.C.A. Tech. Memo. No. 1229 1949.

[5] BODEN R. H. *Trans. Amer. Soc. Mech. Engrs.* 1951 **73** 385.

[6] ZUCROW M. J. and BEIGHLEY C. M. *Jet Propulsion* 1952 **22** 323.

[7] GREENFIELD S. *J. Aero. Sci.* 1951 **18** 512.

[8] KAYE J., KEENAN J. H. and MCADAMS W. H. *Heat Transfer and Fluid Mechanics Institute* 1949 p. 147.

[9] KAYE J., KEENAN J. H., KLINGENSMITH K. K., KETCHUM G. M. and TOONG T. Y. *J. Appl. Mech.* 1952 **19** 77.

[10] KAYE J., TOONG T. Y. and SHOULBERG R. H. *J. Appl. Mech.* 1952 **19** 185.

[11] LATZKO H. *Z. Angew. Math. Mech.* 1921 **1** 268.

[12] RAGSDALE W. C. Ph.D. Thesis, Purdue University, August 1957.

[13] DEISSLER R. G., N.A.C.A. Technical Note No. 2242, 1950 ; No. 2529, 1952.

[14] HUMBLE L. V., LOWDERMILK W. H. and DESMOND L. G., N.A.C.A. Report No. 1020, 1951.

Chemical Engineering Science, 1960, Vol. 11, pp. 252 to 259. Pergamon Press Ltd., London. Printed in Great Britain

Helical flow of an annular mass of visco-elastic fluid

A. G. Fredrickson

Department of Chemical Engineering, University of Minnesota, Minneapolis 14, Minnesota

(*Received* 1 *May* 1959)

Abstract—An analytical solution of the equations of change is presented for the steady flow of an arbitrary visco-elastic fluid through a concentric cylinder annulus. It is assumed that motion is imparted to the fluid by an impressed pressure gradient and/or a gravitational acceleration and by the steady rotation of one or the other, or both, of the annulus cylinders. Under such conditions, the paths traced out by individual fluid particles will be circular helices.

The solution is presented in terms of definite integrals which contain an arbitrary function $F(Y)$; this function may be called an "apparent viscosity." It is shown how the function $F(Y)$ may be determined from standard experiments with capillary, or rotational, viscometers. Suggestions are advanced for performing the required integrations, and it is shown how the equations may be applied to other cases of interest.

Résumé—L'auteur présente une solution analytique des équations de la variation, pour l'écoulement permanent, d'un fluide arbitraire visco-élastique, à travers un anneau entre deux cylindres concentriques. Il est supposé que le mouvement est communiqué au fluide par l'application d'un gradient de pression ou par l'accélération de la pesanteur, ou par les deux actions simultanées, et par la rotation permanente de l'un ou l'autre, ou des deux cylindres constituant l'anneau.

Dans ces conditions, les trajectoires de chaque particule du fluide seront des hélices circulaires.

La solution est présentée en fonction d'intégrales définies qui renferment une fonction arbitraire $F(Y)$. Cette fonction peut être appelée "viscosité apparente." L'auteur montre comment la fonction $F(Y)$ peut être déterminée par des expériences standard avec viscosimètre capillaire ou rotatif.

Des suggestions sont présentées pour effectuer les intégrations nécessaires et il est montré comment les équations peuvent être appliquées à d'autres cas intéressants.

Zusammenfassung—Es wird eine analytische Lösung für die Verformungsgleichungen einer stationären Strömung einer beliebigen viskoelastischen Flüssigkeit durch einen konzentrischen zylindrischen Ringspalt mitgeteilt. Die Bewegung kann der Flüssigkeit entwerder durch einen angelegren Druckgradienten und/oder durch ein Beschleunigungsfeld und durch die stationäre Rotation des inneren, des äusseren oder beider Zylinder des Ringspalts aufgedrückt werden. Unter diesen Bedingungen sind die Stromlinien einzelner Flüssigkeitsteilchen Kreisspiralen.

Die Lösung wird in Form bestimmter Integrale mitgeteilt, die eine beliebige Funktion $F(Y)$ enthalten; diese Funktion sei " scheinbare Viskosität " genannt. Es wird gezeigt, wie die Funktion $F(Y)$ aus Standardversuchen mit Kapillar- oder Rotationsviskosimetern bestimmt werden kann. Zur Ausführung der verlangten Integrationen werden Vorschläge gemacht und es wird gezeigt, wie die Gleichungen auf andere interessierende Fälle angewandt werden können.

Introduction

In recent years, a number of articles concerning the flow of non-Newtonian fluids in annular spaces have appeared. Volarovich and Gutkin [1], Shchipanov [2] and van Olphen [3] published approximate solutions for axial flow of Bingham plastic materials in annuli, and Mori and Ototake [4] published a more general solution which unfortunately is in error. The exact solution for the flow of a Bingham plastic in an annulus was published by Laird [5] and by Fredrickson and Bird [6]. Fredrickson and Bird [6] also derived a solution for a so-called " power model " fluid; their results for both the Bingham plastic and the power model fluid were given in terms of dimensionless variables. The

tabulated solutions of FREDRICKSON and BIRD have been extended by MELROSE *et al.* [7] and by SAVINS [8].

FREDRICKSON [9] has derived a solution for the combined axial and tangential flow of an arbitrary, inelastic, non-Newtonian fluid in an annulus. His equations are actually a solution to a special case of the system of differential equations derived by RIVLIN [10] to describe the combined axial and tangential flow of an annular mass of visco-elastic fluid. It is the purpose of this paper to show how the equations of FREDRICKSON may be generalized to give the solution of the problem posed by RIVLIN; viz., for the helical flow of an annular mass of visco-elastic fluid.

VOL. 11 1959/60

CONSTITUTIVE EQUATIONS FOR VISCO-ELASTIC FLUIDS; THE THEORY OF RIVLIN AND ERICKSEN

RIVLIN and ERICKSEN [11] have published a phenomenological theory of stress-deformation relations for isotropic materials. On the basis of that theory, RIVLIN [12] has shown that if one assumes that in a visco-elastic fluid which is isotropic in its state of rest, the stress components, π_{ij}, at a point in the fluid are expressible as polynomials in the gradients of velocity, acceleration, second acceleration, ..., $(n-1)^{st}$ acceleration at that point and then the stress matrix, $\Pi\ (= \|\pi_{ij}\|)$ may be expressed as polynomial in n kinematic matrices $\mathbf{D}_1$, $\mathbf{D}_2$, ..., $\mathbf{D}_n$. The elements of the matrix $\mathbf{D}_1\ (= \|D_{ij}^{(1)}\|)$ are just twice the elements of the usual velocity-strain matrix:

$$D_{ij}^{(1)} = \frac{\partial v_i}{\partial x_j} + \frac{\partial v_j}{\partial x_i} \tag{1}$$

and the matrices $\mathbf{D}_r\ (= \|D_{ij}^{(r)}\|)$ with $r = 2, 3, \ldots, n$ are defined by the recursion formula

$$D_{ij}^{(r)} = \frac{\partial}{\partial t} D_{ij}^{(r-1)} + \sum_{l=1}^{3} v_l \frac{\partial}{\partial x_l} D_{ij}^{(r-1)} + \\ + \sum_{m=1}^{3} \left(D_{mi}^{(r-1)} \frac{\partial v_m}{\partial x_j} + D_{mj}^{(r-1)} \frac{\partial v_m}{\partial x_i} \right) \tag{2}$$

If the geometry of the flow situation is such that $\mathbf{D}_r = 0$ for $r > 2$, then RIVLIN [12] has shown that the relation between the stress matrix and the kinematic matrices is given by

$$\begin{aligned} \Pi = &- p\mathbf{I} + \alpha_1 \mathbf{D}_1 + \alpha_2 \mathbf{D}_2 + \alpha_3 \mathbf{D}_1^2 + \\ &+ \alpha_4 \mathbf{D}_2^2 + \\ &+ \alpha_5 (\mathbf{D}_1 \mathbf{D}_2 + \mathbf{D}_2 \mathbf{D}_1) + \alpha_6 (\mathbf{D}_1^2 \mathbf{D}_2 + \\ &+ \mathbf{D}_2 \mathbf{D}_1^2) + \\ &+ \alpha_7 (\mathbf{D}_1 \mathbf{D}_2^2 + \mathbf{D}_2^2 \mathbf{D}_1) + \\ &+ \alpha_8 (\mathbf{D}_1^2 \mathbf{D}_2^2 + \mathbf{D}_2^2 \mathbf{D}_1^2) \end{aligned} \tag{3}$$

for incompressible fluids. The coefficients α_k are not constants, but are expressible as polynomials in the ten* scalar invariants tr $\mathbf{D}_1$, tr $\mathbf{D}_1^2$, tr $\mathbf{D}_1^3$, tr $\mathbf{D}_2$, tr $\mathbf{D}_2^2$, tr $\mathbf{D}_2^3$, tr $\mathbf{D}_1 \mathbf{D}_2$, tr $\mathbf{D}_1^2 \mathbf{D}_2$, tr $\mathbf{D}_1 \mathbf{D}_2^2$, tr $\mathbf{D}_1^2 \mathbf{D}_2^2$. In the above expressions, it is to be understood that the usual rule [13] of matrix multipication is applied and that $\mathbf{D}_r^k = \mathbf{D}_r^{k-1} \mathbf{D}_r$. The trace ("tr") of a matrix is simply the sum of its diagonal elements.

For inelastic fluids, the stress is a function only of the velocity-strain (i.e., up to an arbitrary hydrostatic pressure, $-p$), so that the matrices $\mathbf{D}_r$ with $r > 1$ do not affect the stress. For such fluids, RIVLIN's equation becomes

$$\Pi = - p\mathbf{I} + \alpha_1 \mathbf{D}_1 + \alpha_3 \mathbf{D}_1^2. \tag{4}$$

Equation (4) is the equation derived by REINER [14, 15] and by RIVLIN [16] and applied by RIVLIN [16, 17] to explain the so-called "Weissenberg effect" [18]†. The coefficient α_1 may thus be called the "viscosity" and the coefficient $\frac{1}{2}\alpha_3$ has been called [19] the "normal stress coefficient." The derivations of FREDRICKSON cited above utilized the constitutive equation (4) with the further hypothesis that the coefficient α_3 could be set equal to zero.

OLDROYD [20] has formulated an alternate theory of visco-elasticity. The constitutive equation of OLDROYD contains terms not only in the gradients of velocity, acceleration, ..., $(n-1)^{st}$ acceleration, but also in the convective derivatives of the elements of Π. In this paper, however, it will be assumed that the rheological behaviour of the fluids in question is given by equation (3).

*For incompressible fluids, tr $\mathbf{D}_1 = 0$, so we need consider only nine scalar invariants.

†OLDROYD [20] has suggested that the Weissenberg effect may be due to fluid elasticity; this view seems to be borne out by the experimental work of ROBERTS [21].

Equations for Helical Flow in Annuli

Consider the steady, combined axial and tangential flow of a mass of visco–elastic fluid in a concentric cylinder annulus. Axial motion is imparted to the fluid by an impressed pressure gradient and/or a gravitational acceleration; tangential motion is imparted by causing one or the other or of both the annulus cylinders to rotate with constant angular velocity. By hypothesis, we are dealing with a region far enough removed from the entrance (or exit) of the annulus so that the angular velocity, ω, and the axial velocity, u, at any point of the region depend only on the radial distance of that point from the axis of the annulus.

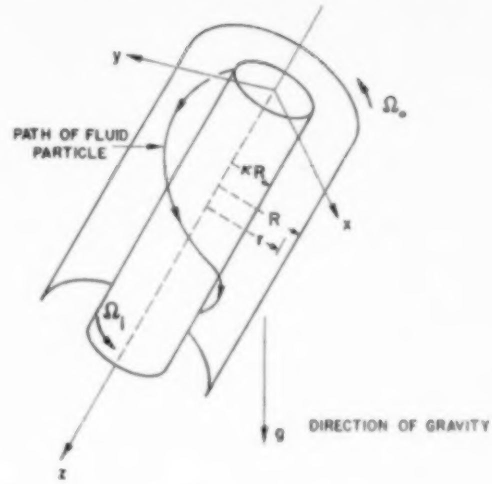

Fig. 1. Helical flow in an annulus.

Let the z-axis of a rectangular Cartesian co-ordinate system lie along the axis of the annulus, and point in the direction of axial flow (Fig. 1). Then, if one chooses the direction of the x-axis so that $y = 0$ at the point of fluid considered, the kinematic matrices $\mathbf{D}_r$ are given by [10]:

$$\mathbf{D}_1 = \begin{Vmatrix} 0 & r\omega' & u' \\ r\omega' & 0 & 0 \\ u' & 0 & 0 \end{Vmatrix}; \quad \mathbf{D}_2 = \begin{Vmatrix} 2\,(r^2\,\omega'^2 + u'^2) & 0 & 0 \\ 0 & 0 & 0 \\ 0 & 0 & 0 \end{Vmatrix};$$

$$\mathbf{D}_r = \mathbf{0}, \quad r > 2 \tag{5}$$

where primes denote differentiation with respect to r.

Let

$$Y = 2\,(r^2\,\omega'^2 + u'^2) \tag{6}$$

Then the invariants of $\mathbf{D}_1$ and $\mathbf{D}_2$ may be written as [10].

$$\left\| \begin{array}{l} \operatorname{tr} \mathbf{D}_1 = 0, \ \ \operatorname{tr} \mathbf{D}_1^2 = Y, \ \ \operatorname{tr} \mathbf{D}_1^3 = 0, \\ \operatorname{tr} \mathbf{D}_2 = Y, \operatorname{tr} \mathbf{D}_2^2 = Y^2, \ \ \operatorname{tr} \mathbf{D}_2^3 = Y^3, \\ \operatorname{tr} \mathbf{D}_1\,\mathbf{D}_2 = 0, \operatorname{tr} \mathbf{D}_1^2\,\mathbf{D}_2 = \tfrac{1}{2}\,Y^2, \\ \operatorname{tr} \mathbf{D}_1\,\mathbf{D}_2^2 = 0, \text{ and } \operatorname{tr} \mathbf{D}_1^2\,\mathbf{D}_2^2 = \tfrac{1}{2}\,Y^3. \end{array} \right\| \tag{7}$$

Hence, it appears that all coefficients α_k in equation (3) are functions only of Y. But Y is a function only of r so equations (7) show that the α_k are functions only of r.

Substitution of equations (5) into equation (3) yields the expressions for the stresses:

$$\begin{aligned} \pi_{11} &= -\,p + \tfrac{1}{2}\,(2\alpha_2 + \alpha_3)\,Y + (\alpha_4 + \alpha_6)\,Y^2 + \\ &\quad + \alpha_8\,Y^3, \\ \pi_{22} &= -\,p + \alpha_3\,r^2\,\omega'^2, \quad \pi_{33} = -\,p + \alpha_3\,u'^2, \\ \pi_{12} &= r\omega'\left[\alpha_1 + \alpha_5\,Y + \alpha_7\,Y^2\right], \\ \pi_{13} &= u'\left[\alpha_1 + \alpha_5\,Y + \alpha_7\,Y^2\right] \\ \pi_{23} &= \alpha_3\,r\omega'\,u'. \end{aligned} \tag{8}$$

However, by integration of the equations of motion, Rivlin [10] showed that

$$\pi_{12} = B/r^2; \quad \pi_{13} = \tfrac{1}{2}\,Pr + \frac{C}{r} \tag{9}$$

where B and C are constants of integration and P (another constant) is defined by

$$P = -\,\frac{\partial \pi_{33}}{\partial z} = \frac{\partial p}{\partial z} - \rho\,g_z. \tag{10}$$

In equation (10), ρ is the density of the fluid and g_z is the z-component of the gravitional acceleration g. (It is assumed that g_x and g_y may be neglected). The quantity P may be called the frictional pressure gradient.

Define the dimensionless radial co-ordinate ξ by

$$\xi = r/R \tag{11}$$

in which R is the radius of the outer annulus cylinder. Then combination of equations (8), (9) and (11) gives

$$\pi_{12} = \beta/\xi^2 = \xi \frac{d\omega}{d\xi} [\alpha_1 + \alpha_5 Y + \alpha_7 Y^2] \quad (12)$$

$$R\, \pi_{13} = \frac{PR^2}{2} \left(\frac{\xi^2 - \lambda^2}{\xi} \right) = \frac{du}{d\xi} [\alpha_1 + \alpha_5 Y + \alpha_7 Y^2] \quad (13)$$

where the constants β and λ may be derived from B, C and R. Equations (12) and (13) are identical to equations (4.9) of RIVLIN's paper [10].

Since the α_k are functions of Y, we can set

$$F(Y) = \alpha_1 + \alpha_5 Y + \alpha_7 Y^2 \quad (14)$$

so that (12) and (13) become

$$\frac{d\omega}{d\xi} = \frac{\beta}{\xi^3 F(Y)} \quad (15)$$

$$\frac{du}{d\xi} = \frac{PR^2}{2} \left(\frac{\xi^2 - \lambda^2}{\xi} \right) \frac{1}{F(Y)}. \quad (16)$$

The separation of variables represented by equations (15) and (16) is permissible, since Y, and therefore $F(Y)$, is a function of r (or ξ). The velocity distribution is then obtained by integration:

$$\omega = \Omega_0 - \beta \int_\xi^1 \frac{d\zeta}{\zeta^3 F(Y)} \quad (17)$$

$$u = -\frac{PR^2}{2} \int_\xi^1 \left(\frac{\zeta^2 - \lambda^2}{\zeta} \right) \frac{d\zeta}{F(Y)}. \quad (18)$$

In equations (17) and (18), we have used the boundary conditions that

$$\left.\begin{aligned} \omega &= \Omega_0 \\ u &= 0 \end{aligned}\right\} \text{ at } r = R\ (\xi = 1) \quad (19)$$

where Ω_0 is the angular velocity of the outer cylinder of the annulus. The boundary conditions at the inner cylinder of the annulus are

$$\left.\begin{aligned} \omega &= \Omega_i \\ u &= 0 \end{aligned}\right\} \text{ at } r = \kappa R\ (\xi = \kappa) \quad (20)$$

where κR is the radius and Ω_i is the angular velocity of the inner annulus cylinder. The conditions (19) and (20) are the statements that the fluid does not " slip " at the solid boundaries of the flow system.

From equations (17), (18) and (20), there result

$$\Omega_0 - \Omega_i = \beta \int_\kappa^1 \frac{d\zeta}{\zeta^3 F(Y)} \quad (17a)$$

$$0 = \int_\kappa^1 \left(\frac{\zeta^2 - \lambda^2}{\zeta} \right) \frac{d\zeta}{F(Y)} \quad (18a)$$

Equations (17a) and (18a) are the determining equations for β and λ. A method for performing the integrations called for by these equations will be presented below.

The volumetric flow rate, Q, is

$$Q = \int_0^{2\pi} \int_{\kappa R}^{R} u(r)\, r dr\, d\theta = 2\pi R^2 \int_\kappa^1 u(\xi)\, \xi\, d\xi \quad (21)$$

or, because of (18):

$$Q = -\pi P R^4 \int_\kappa^1 \xi\, d\xi \int_\xi^1 \left(\frac{\zeta^2 - \lambda^2}{\zeta} \right) \frac{d\zeta}{F(Y)} \quad (22)$$

Interchange of the order of integration and re-arrangement gives finally

$$\frac{4Q}{\pi R^3} = -4 \left(\frac{PR}{2} \right) \int_\kappa^1 \frac{(\kappa^2 - \zeta^2)}{F(Y)} \left(\frac{\zeta^2 - \lambda^2}{\zeta} \right) d\zeta \quad (23)^*$$

Equation (23) is the desired expression for the flow rate through the annulus.

The values of the torques required to maintain the cylinders of the annulus in steady rotation may now be computed. The torque on the inner cylinder (per unit length of cylinder) is given by the expression:

$$G_i = [\pi_{12}(\kappa R)] \cdot [2\pi\, \kappa^2 R^2]$$

*Equations (17a), (18a) and (23) show that for a given fluid, the relations between $4Q/\pi R^3$, $PR/2$, κ and $\Omega_0 - \Omega_i$ are independent of the *scale* of the apparatus upon which those relations are determined. This would be an important consideration in any experimental programme designed to test the validity of the theory developed herein.

or, because of (12),

$$G_i = 2\pi R^2 \beta, \tag{24}$$

Since in a steady state or rotation, the same couples must act on every lamina of the fluid, it follows that equation (24) also gives the torque acting on the outer cylinder (per unit length).

DETERMINATION OF CONSTANTS; INTEGRATION OF EQUATIONS (17a), (18a) and (23)

In general, the constants β and λ must be determined by trial-and-error numerical integration of equations (17a) and (18a). In order to perform these integrations, it is necessary to have a graph, table, or analytical expression describing the variation of $F(Y)$ with Y. It will be shown below how such a graph, table, etc. may be prepared by analysis of viscometric data. For "pseudoplastic" fluids, the graph of $F(Y)$ would have the general form of Fig. 4 in the article of JOBLING and ROBERTS [22] [for "η (apparent)"].*

At any rate, suppose viscometric experiments have established the dependence of $F(Y)$ on Y. Then to perform the integrations, the following procedure is suggested.

Reasonable values of β and λ are assumed. One then computes the values of π_{12} and π_{13} from equations (12) and (13) for a series of values of ξ between $\xi = \kappa$ and $\xi = 1$. At a given radius, ξ, a value of $F(Y)$ is assumed and $r\omega'$ and u' are computed from equations (8). The value of Y is then computed, and from the graph, table or equation for $F(Y)$ vs. Y the value of $F(Y)$ corresponding to the computed value of Y is found. If the assumed value of $F(Y)$ checks with the computed value of $F(Y)$, one then proceeds to the next value of ξ in the series and computes $F(Y)$ at that radius; otherwise, new values of $F(Y)$ must be assumed and the calculations repeated until assumed and calculated values of $F(Y)$ agree.

Once the variation of $F(Y)$ with ξ corresponding to the assumed values of β and λ has been established by the process described above, the integrations called for by equations (17a) and (18a) are performed by some numerical means. If the assumed values of β and λ satisfy equations (17a) and (18a), those values are correct and equations (17), (18) and (23) may be integrated (numerically) without difficulty. If the assumed values of β and λ do not satisfy equations (17a) and (18a), new values must be assumed and the entire process repeated. It is obvious that the amount of computational work necessary is rather formidable, and the method is best handled by a digital computer.

Finally, let it be noted that the values of β and λ so computed will hold for a particular set of values of $-PR/2$, κ and $\Omega_0 - \Omega_i$. If any of these quantities are changed, then β and λ will change also.

*In that article, the abscissa is $(\frac{1}{2} Y)^{1/2}$ = rate of shear

DETERMINATION OF $F(Y)$ FROM VISCOMETRIC DATA

The equations describing the flow of a viscoelastic fluid in a rotational ("Couette") type viscometer may be derived from the equations given in this paper by setting $u = 0$. Hence, for the Couette viscometer, the kinematic matrices become

$$\mathbf{D}_1 = \begin{Vmatrix} 0 & r\omega' & 0 \\ r\omega' & 0 & 0 \\ 0 & 0 & 0 \end{Vmatrix}; \; \mathbf{D}_2 = \begin{Vmatrix} 2r^2\omega'^2 & 0 & 0 \\ 0 & 0 & 0 \\ 0 & 0 & 0 \end{Vmatrix}; \; \mathbf{D}_r = \mathbf{0} \;\; r > 2 \tag{25}$$

The ten invariants of $\mathbf{D}_1$ and $\mathbf{D}_2$ are again given by equations (7), but the invariant Y assumes the simpler form

$$Y = 2r^2\,\omega'^2 \tag{6a}$$

For the stresses, we find

$$\pi_{11} = -p + \tfrac{1}{2}(2\alpha_2 + \alpha_3)\,Y + (\alpha_4 + \alpha_6)\,Y^2 + \alpha_8\,Y^3,$$

$$\pi_{22} = -p + \tfrac{1}{2}\alpha_3\,Y, \quad \pi_{33} = -p$$

$$\pi_{12} = r\omega'\left[\alpha_1 + \alpha_5\,Y + \alpha_7\,Y^2\right] = r\omega'\,F(Y)$$

$$\pi_{13} = \pi_{23} = 0 \tag{12a}$$

Hence, the function $F(Y)$ is simply

$$F(Y) = \frac{\pi_{12}}{r\omega'} \qquad \text{Couette.} \tag{26}$$

The stress π_{12} may be determined from the equations

$$\pi_{12} = \beta / \xi^2 \qquad (27)$$

$$G_i = G_0 = 2\pi\, R^2\, \beta \qquad (24a)$$

and the measured torques on the cylinders*. The quantity $r\omega'$ is the usual rate of shear, and may be determined from experimental data by the standard means [23].

Equation (26) shows that $F(Y)$ is nothing more than the *viscosity* (*apparent* viscosity, really, since the usual Couette viscometer does not distinguish between elastic and inelastic fluids) as determined by the Couette viscometer. Hence a plot of viscosity, as given by equation (26) against twice the rate of shear squared ($= Y$) gives the plot of $F(Y)$ vs. Y required in solving the problem of helical flow in an annulus.

The equations describing the flow of a visco-elastic fluid in a tube may be derived from the equations for helical flow in annuli by setting $\omega = 0$. Thus, the kinematic matrices may be written as

$$\mathbf{D}_1 = \begin{Vmatrix} 0 & 0 & u' \\ 0 & 0 & 0 \\ u' & 0 & 0 \end{Vmatrix}; \quad \mathbf{D}_2 = \begin{Vmatrix} 2u'^2 & 0 & 0 \\ 0 & 0 & 0 \\ 0 & 0 & 0 \end{Vmatrix};$$

$$\mathbf{D}_r = \mathbf{0}, \quad r > 2 \qquad (28)$$

for flow in a capillary tube. Because of equations (28), the ten invariants of $\mathbf{D}_1$ and $\mathbf{D}_2$ are again given by equations (7), but here, the invariant Y is

$$Y = 2u'^2 \qquad (6b)$$

For the stresses, we find

$$\pi_{11} = -p + \tfrac{1}{2}(2\alpha_2 + \alpha_3)\, Y + (\alpha_4 + \alpha_6)\, Y^2 + \alpha_8\, Y^3,$$

$$\pi_{22} = -p, \quad \pi_{33} = -p + \tfrac{1}{2}\alpha_3\, Y,$$

$$\pi_{12} = \pi_{23} = 0$$

$$\pi_{13} = u' \left[\alpha_1 + \alpha_5\, Y + \alpha_7\, Y^2\right] = u'\, F(Y). \qquad (12b)$$

Hence, the function $F(Y)$ is given by

$$F(Y) = \frac{\pi_{13}}{u'} \quad \text{Capillary} \qquad (29)$$

*The experimental data must of course be corrected for end effects, non-uniformity of shear rate, etc. The necessary corrections have been discussed by Toms [23].

In the capillary tube viscometer, the rate of shear is not uniform (as, to a first approximation, it is in a Couette viscometer with a small gap) but is a maximum at the wall of the tube and zero at the centre of the tube. However, the shear rate at the wall may be determined from the Rabinowitsch–Mooney equation [24, 25], and the corresponding shearing stress at the wall is given by

$$\pi_{13}\Big|_{\text{wall}} = \frac{PR}{2}. \qquad (30)$$

Hence, the function $F(Y)$ may be determined from capillary viscometer data by plotting $\pi_{13}/u'|_{\text{wall}}$ (again, an apparent viscosity) vs. twice the rate of shear at the wall squared ($= Y$). The data must be corrected for entrance and exit losses, kinetic energy effects, wall effects, etc. Methods of correction have been discussed by Oldroyd [26] and by Fredrickson [27].

Discussion and Conclusions

It was possible to solve Rivlin's equations for helical flow in annuli because of the relatively simple geometry of that type of flow. Thus, in helical flow, there are only two (u' and $r\omega'$) non-vanishing, independent elements of the velocity-strain matrix, and these are related to the stress (π_{12} and π_{13}) by the same relation. There is the further consideration that for the case considered, the coefficients α_k in the constitutive equation (3) are functions of only one invariant quantity, Y. As shown above, these two circumstances make it possible to separate the variables in Rivlin's equations and so to affect a solution.

In more complicated flow situations (such as, say, flow through a diffuser, development of flow in a pipe, etc.), the simplifications noted above would not result, and any attempt to arrive at an analytical solution would be faced with grave difficulties.

In this respect, let it be noted that the type of flow which prevails in the usual viscometric experiments (with capillary tubes or rotational viscometers) is not very general, in that the rheological coefficients α_k become functions of only *one* invariant quantity (Y). In a more

VOL. 11 1959/60

general flow situation, the coefficients α_k would appear as functions of other invariants. Hence, the usual data obtained from capillary tube or rotational viscometers may be inadequate to predict the rheological behaviour of non-Newtonian fluids in fairly general flow situations.

The method of solution adopted herein may also be used to solve the problem of combined axial and tangential flow of Bingham plastic materials in concentric cylinder annuli. According to Oldroyd [28], the Bingham plastic is described by the constitutive equation

$$\Pi = -p\mathbf{I} + \eta\,\mathbf{D}_1 \text{ if } \tau^2 > \tau_0^2,$$
$$\mathbf{D}_1 = \mathbf{0} \text{ if } \tau^2 \leqslant \tau_0^2 \qquad (31)$$

with

$$\eta = \frac{\mu_0}{1 - \tau_0/\sqrt{\tau^2}} \qquad (32)$$

In these equations, τ_0 is the yield stress, μ_0 is the (constant) plastic viscosity, and the invariant quantity τ^2 is defined by

$$\tau^2 = \tfrac{1}{2} \sum_{i=1}^{3} \sum_{j=1}^{3} (\pi_{ij} + p\delta_{ij})^2. \qquad (33)$$

For helical flow of a Bingham plastic material in an annulus, one can easily solve the equations of motion and so obtain expressions for the stresses (equation 9) and hence for the yield condition ($\tau^2 = \tau_0^2$); this will be a polynomial of sixth degree in the reduced radius ξ. The solution of this polynomial for the two roots lying between κ and 1 will give the boundaries of the "plug flow" region. The constitutive equations (31) may then be combined with the expression for the stresses and integrated to give the velocity distribution.

Notation

B, C = constants of integration
$\mathbf{D}_r$ = r^{th} kinematic matrix (elements $D_{ij}^{(r)}$)
G_i, G_0 = torques acting on unit lengths of inner and outer cylinders of annulus
$\mathbf{g}$ = acceleration due to gravity (components g_x, g_y, g_z)
$F(Y)$ = function of Y ("apparent viscosity") – defined by equation (14)
$\mathbf{I}$ = identity matrix (elements δ_{ij})
P = frictional pressure gradient – defined by equation (10)
p = hydrostatic pressure
Q = volumetric flow rate
R = radius of outer annulus cylinder
r = radial co-ordinate
u = axial velocity
v_i = i-component of velocity
x, y, z = cartesian co-ordinates
Y = invariant quantity – defined by equation (6)
α_k = k^{th} rheological coefficient in equation (3)
β, λ = constants of integration
δ_{ij} = Kronecker delta ($= 1$ if $i = j$; $= 0$ if $i \neq j$)
ζ = dummy variable of integration
η = "viscosity" of Bingham plastic material – defined by equation (32)
κ = ratio of radius of inner annulus cylinder to radius of outer annulus cylinder
μ_0 = plastic viscosity
Π = stress matrix (elements π_{ij})
ξ = dimensionless radial co-ordinate
ρ = density of fluid
τ^2 = defined by equation (33)
τ_0 = yield stress of Bingham plastic material
Ω_i = angular velocity of inner annulus cylinder
Ω_0 = angular velocity of outer annulus cylinder
ω = angular velocity of fluid at x, y, z.

References

[1] Volarovich M. P. and Gutkin A. M. *Zh. techn. Fiz.* 1946 **16** 321.
[2] Shchipanov, P. K. *Zh. techn. Fiz.* 1949 **19** 1211.
[3] van Olphen H. *J. Inst. Petrol.* 1950 **36** 223 (1950).
[4] Mori Y. and Ototake N. *Chem. Engng. (Japan)* 1953 **17** 224.
[5] Laird W. M. *Industr. Engng. Chem.* 1957 **49** 138.
[6] Fredrickson A. G. and R. B. Bird *Industr. Engng. Chem.* 1958 **50** 347.
[7] Melrose J. C., Savins J. G., Foster W. R. and Parish E. R. *Trans. AIME*, 1958 **213** 324.
[8] Savins J. G. *Trans. AIME* 1958 **213** 325.
[9] Fredrickson A. G. Ph.D. Thesis in Chemical Engineering, University of Wisconsin, Madison 1959.
[10] Rivlin R. S. *J. Rat. Mech. Anal.* 1956 **5** 179.

[11] RIVLIN R. S. and ERICKSEN J. L. *J. Rat. Mech. Anal.* 1955 **4** 329.

[12] RIVLIN R. S. *J. Rat. Mech. Anal.* 1955 **4** 681

[13] HILDEBRAND F. B. *Methods of Applied Mathematics.* p. 6. Prentice-Hall, New Jersey 1952.

[14] REINER M. *Amer. J. Math.* 1945 **67** 350.

[15] REINER M. *Quart. Appl. Math.* 1950-1951 **8** 341.

[16] RIVLIN R. S. *Proc. Roy. Soc.* 1948 A**193** 260.

[17] RIVLIN R. S. *Proc. Camb. Phil. Soc.* 1949 **45** 88.

[18] WEISSENBERG K. *Nature, Lond.* 1947 **159** 310.

[19] OLDROYD J. G. *Rheology* (Edited by Eirich F. R.) Vol. 1, Chap. 16, pp. 653-682, Academic Press, New York 1956.

[20] OLDROYD J. G. *Proc. Roy. Soc.* 1950 A**200** 523.

[21] ROBERTS J. E. *Proc. 2nd Int. Rheol. Congr. Oxford*, p. 91, 1953.

[22] JOBLING A. and ROBERTS J. E. *Rheology* (Edited by Eirich F. R.) Vol. 2, Chap. 13, pp. 503–535, Academic Press, New York 1958.

[23] TOMS B. A. *Rheology* (Edited by Eirich F. R.) Vol. 2, Chap. 12 pp. 475–501, Academic Press, New York 1958.

[24] MOONEY M. *J. Rheology* 1931 **2** 210.

[25] RABINOWITSCH B. *Z. Phys. Chem.* 1929 A**145** 1.

[26] OLDROYD J. G. *J. Colloid Sci.* 1949 **4** 333.

[27] FREDRICKSON A. G. to be published.

[28] OLDROYD J. G. *Proc. Camb. Phil. Soc.* 1948 **43** 100, 383, 396, 521; **44** 200, 214.

Chemical Engineering Science, 1960, Vol. 11, pp. 260 to 266. Pergamon Press Ltd., London. Printed in Great Britain

Unsteady state heat transfer in stationary packed beds

A. Klinkenberg and A. Harmens

Bataafse Internationale Petroleum Maatschappij N.V. (Royal Dutch/Shell Group) The Hague, Holland

(*Received* 26 *May* 1959)

Abstract—This paper deals with unsteady state heat transfer in fixed beds in the most general case of non-uniform initial bed temperature and varying gas inlet temperature. The gas and bed temperatures are described in terms of the solution to the more simple problem determined by uniform initial bed temperature and constant gas inlet temperature, which solution has already been evaluated in several different ways.

The treatment is kept general, leaving open the choice of the most practical form of the solution to the simpler problem. In applications this choice is made, taking into account the nature of the specific problem at hand. It will depend on the ranges of the independent variables encountered. Most fixed bed applications will be in a range where the error function solutions according to Klinkenberg are adequate.

Résumé—La communication traite de la transmission de chaleur à l'état non-stationnaire dans des lits fixes. Elle décrit le cas le plus général, celui d'une température initiale non-uniforme dans le solide et d'une température variable du gaz à l'entrée. Les températures du gaz et du solide sont dérivées de la solution du problème le plus simple, c'est à dire de celui à température initiale uniforme dans le solide et à température constante du gaz à l'entrée. Cette solution a déjà été évaluée de plusieurs façons différentes.

Le traitement est tout-à-fait général, laissant une liberté de choix dans le mode de solution du problème le plus simple. Pour les applications pratiques, ce choix se fait en tenant compte de leur nature spécifique. Il dépendra des régions des variables indépendantes qui se présentent. Pour la plupart des applications de lit fixe les solutions à fonction de probabilité selon Klinkenberg seront adéquates.

Zusammenfassung—Das Referat befasst sich mit der nicht-stationären Wärmeübertragung in Festbetten im allgemeinsten Falle der nicht gleichmässigen Anfangsbettemperatur und variabelen Gaseintrittemperatur. Gas- und Bettemperaturen werden dargestellt an Hand der Lösung des einfacheren Problems, das bestimmt wird durch gleichmässige Anfangsbettemperatur und konstante Gaseintrittemperatur, welche Lösung bereits in mehrerlei verschiedener Weise entwickelt worden ist.

Die Behandlung wird allgemein gehalten, wobei die Wahl der praktischsten Form der Lösung des einfacheren Problems offengelassen wird. Bei den Anwendungen wird diese Wahl getroffen unter Berücksichtigung der besonderen Art des jeweiligen Problems. Sie richtet sich nach dem Bereich der vorkommenden unabhängigen Variabelen. Die meisten Anwendungen von Festbetten werden in einem Bereich liegen, in welchem die Fehlerfunktionslösungen nach Klinkenberg ausreichen.

Introduction

Many authors working in the field of the heating or cooling of a packed bed by means of a flow of gas have considered a bed at initially uniform temperature being heated or cooled by a gas stream of constant inlet temperature*. We shall refer to the heat transfer problem with these simple initial and boundary conditions as "the elementary problem." A survey of the various forms of its solution, together with an examination of their convenience of application and, for approximate formulations, of their accuracy as well, has been given by one of the present authors [1].

*The usual assumptions include uniform gas and solid temperature over any bed cross-section, infinite thermal diffusivity in the solid and absence of longitudinal mixing and conduction.

VOL. 11 1959/60

A more complex case is that of a bed with an arbitrary initial temperature distribution, heated by a gas the inlet temperature of which is an arbitrary function of time. This problem has been treated by AMUNDSON [2] and, more recently, by REILLY [3]. AMUNDSON used Bessel functions; REILLY was the first to apply Fourier integrals or Fourier series. SAHLBERG [4] recently published a solution to the mathematically identical problem of the steady state behaviour of a cross-flow recuperator in which the temperatures of the entering gas streams vary along the widths of their entrances. He used the same approach as developed on a more general basis in the present article, and he employed the Bessel function solution to the elementary problem.

NUSSELT [5] and HAUSEN [6] have solved the problem of the regenerator with an arbitrary initial temperature distribution, cooled or heated by a gas of constant inlet temperature. NUSSELT gave the correct Bessel function solution. HAUSEN's "Wärmepolmethode," a heat source method, resembles the approach of the present paper. Because of the symmetry of the governing differential equations in terms of the two dependent and the two independent variables, the treatment by NUSSELT and by HAUSEN can easily be extended to include the case of variable inlet gas temperature as well.

We should like to point out that the analytical solution to the above general problem can easily be written in terms of any solution to the elementary problem, without it being necessary to specify the form of this solution. It has already been shown in [1] that the solution to the elementary problem can be expressed in a variety of formulations. Our treatment has therefore been kept general, in order to render possible the numerical solution of the general problem by way of any mathematical approach available for the elementary one, i.e. by any method yielding the response to a step-function input. The Bessel function solutions and our previous solutions employing error functions with corrected argument, for instance, may be employed. REILLY's method [3] is not suitable for this purpose, because the use of Fourier synthesis makes the evaluation of the step-function response superfluous. Although that response can easily be derived from his formulae, the use of it in the sense of the present article would be unnecessarily circuitous.

In the following sections the derivation is given of two pairs of solutions to the general problem, expressed in terms of a function F. This function represents the total exchange of heat in the elementary problem as a function of bed height and time. It need not be known explicitly for this derivation, but its properties, as they are required, are given. Finally various specific forms of F which, by substitution, enable direct numerical solution of a variety of practical problems are discussed.

DIFFERENTIAL EQUATIONS: THE ELEMENTARY PROBLEM

The mathematical treatment of transient heat transfer in packed beds as proposed in this paper is subject to a number of simplifying assumptions, a few of which were mentioned in the footnote on p. 260. Many previous articles, such as that by REILLY [3], give a full account of them.

The basic differential equations are :

$$-\frac{\partial T_1}{\partial Y} = \frac{\partial T_2}{\partial Z} \tag{1}$$

$$\frac{\partial T_2}{\partial Z} = T_1 - T_2 \tag{2}$$

in which

T_1 = gas temperature

T_2 = solid temperature

Y = dimensionless parameter proportional to length

Z = dimensionless parameter proportional to time*.

In the definition of Z the time the gas takes to pass through the bed has been ignored, this

*If U = heat transfer coefficient, a = surface area of packing per unit volume, d = density, c = specific heat, v = mean linear fluid velocity in the bed, F = fraction by volume, x = bed height, t = time, index f = fluid, index s = solid :

$$Y = \frac{Ua}{d_f c_f F_f} \cdot \frac{x}{v} \qquad Z = \frac{Ua}{d_s c_s F_s} \cdot t$$

time being very small in respect of the actual heating times.

Equations (1) and (2) were solved by most previous authors for the conditions:

$$\left.\begin{aligned} Y = 0 \rightarrow T_1 = 1\ (Z > 0) \\ Z = 0 \rightarrow T_2 = 0\ (Y > 0) \end{aligned}\right\} \qquad (3a)$$

These refer to "the elementary problem" of a bed initially at zero temperature, heated by a gas continuously entering at a temperature of unity.

The Total Amount of Heat Exchanged in the Bed

The heat balance requires the heat lost by the gas to be equal to the heat gained by the solid. When written in dimensionless form this becomes:

$$F(Y, Z) = Z - \int_0^Z (T_1)_{Y,\zeta}\, d\zeta = \int_0^Y (T_2)_{\eta, Z}\, d\eta \qquad (4)$$

The function F of Y and Z accordingly is the dimensionless representation of the amount of the amount of heat exchanged in the bed. It has been employed as such by Sahlberg [4].

It is important to note that F is a symmetrical function, viz.

$$F(Y, Z) = F(Z, Y) \qquad (5)$$

This can be demonstrated as follows. Equations (1), (2) and (3) remain unchanged if the following pairs of variables are interchanged:

Y and Z

T_1 and $1 - T_2$

If the same substitutions are made in (4) we obtain:

$$F(Z, Y) = Y - \int_0^Y (1 - T_2)_{\eta, Z}\, d\eta = \int_0^Z (1 - T_1)_{Y,\zeta}\, d\zeta$$

Since the 2nd and the 3rd member are identical with the 3rd and the 2nd member in (4), the symmetry of the function F, i.e. relation (5), has been proved.

According to (4) the derivatives of F are closely related to T_1 and T_2:

$$\frac{\partial F}{\partial Z} = 1 - T_1; \quad \frac{\partial F}{\partial Y} = T_2 \qquad (6a, b)$$

The relation between (6a, b) and (1) is obvious. As the conditions (3a) represent a unit step disturbance in gas inlet temperature, we may accordingly state:

$1 - \dfrac{\partial F}{\partial Z}$ = response of gas temperature to a unit step disturbance in inlet gas temperature.

$\dfrac{\partial F}{\partial Y}$ = response of solid temperature to a unit step disturbance in inlet gas temperature.

In order to examine the effect of a unit step disturbance in the initial solid temperature we must consider equations (1) and (2) with conditions

$$\left.\begin{aligned} Y = 0 \rightarrow T_1 = 0\ (Z > 0) \\ Z = 0 \rightarrow T_2 = 1\ (Y > 0) \end{aligned}\right\} \qquad (3b)$$

These conditions can be derived from (3a) by interchanging Y with Z and T_1 with T_2. The same transposition leaves the basic differential equations unaltered. Hence the solution to (1) and (2) with conditions (3b) can be derived from the solution to the previous case by making the above substitutions. F being invariant with respect to the transposition of Y and Z, this yields the following responses to unit step disturbances in inlet solid temperature:

$1 - \dfrac{\partial F}{\partial Y}$ = response of solid temperature to a unit step disturbance in initial solid temperature

$\dfrac{\partial F}{\partial Z}$ = response of gas temperature to a unit step disturbance in initial solid temperature.

All equations being linear, differentiation of a response to a step disturbance in gas or solid with respect to Z and Y, respectively, gives the response to a peak disturbance. Consequently

the following peak response functions can be tabulated:

function:	response of:	to peak disturbance in:
$-\partial^2 F/\partial Z^2$	gas temp.	gas
$\partial^2 F/\partial Y \partial Z$	solid temp.	gas
$-\partial^2 F/\partial Y^2$	solid temp.	solid
$\partial^2 F/\partial Y \partial Z$	gas temp.	solid

For most of the following discussion the type of the function F need not be specified, knowledge of the following of its properties being sufficient:

firstly:
$$\frac{\partial^2 F}{\partial Y\, \partial Z} + \frac{\partial F}{\partial Y} + \frac{\partial F}{\partial Z} = 1 \qquad (7)$$
(by substitution of 6a, b in 2)

secondly:
$$\left(\frac{\partial F}{\partial Z}\right)_{0,Z} = 0\,; \quad \left(\frac{\partial F}{\partial Y}\right)_{Y,0} = 0 \qquad (8a, b)$$
(by substitution of 6a, b in 3a)

thirdly:
$$\left(\frac{\partial F}{\partial Z}\right)_{Y,0} = 1 - e^{-Y}\,;$$
$$\left(\frac{\partial F}{\partial Y}\right)_{0,Z} = 1 - e^{-Z} \qquad (9a, b)$$

Equation (9a) is obtained by considering (7) along the boundary $Z = 0$ where, in view of (8b), (7) becomes a simple differential equation in $\partial F/\partial Z$. Equation (9b) is obtained in a similar manner.

Equation (9a) represents the well-known fact that the first gas which enters the bed cools down according to an exponential law because, during its passage, it constantly meets fresh solid at temperature $T_2 = 0$. Similarly, the solid material at the entrance to the bed is heated by the gas according to an exponential law, since the gas at that place is constantly at the temperature $T_1 = 1$. This is expressed by (9b).

Equations (7) to (9a, b) and their derivatives enable considerable simplifications of the final formulae to be derived in the following section.

Solution of the General Problem

The initial and boundary conditions (3a), representative of the elementary problem, having served to determine the properties of the function F, will now be replaced by conditions (10). These determine the more general heat transfer problem subject to arbitrary gas inlet temperature and initial solid temperature. These arbitrary functions are designated by θ. The new initial and boundary conditions are:

$$\left.\begin{aligned} Y = 0 &\rightarrow T_1 = \theta_1(Z) \\ Z = 0 &\rightarrow T_2 = \theta_2(Y) \end{aligned}\right\} \qquad (10)$$

The problem of integrating equations (1) and (2) with conditions (10) can readily be solved without any further knowledge of the function F, by superposition of responses to peaks (Hausen's method of "heat poles"). The gas, for instance, passing the place Y at the time Z has the temperature which it would have had if no other disturbances had entered the bed before — namely $e^{-Y}\theta_1(Z)$ — increased by the integrated contributions of all gas temperature peaks entering between the times 0 and Z and of all solid temperature peaks originally present between the places 0 and Y. The solid temperature is made up in a similar way. This yields the formulae:

$$T_1(Y, Z) = e^{-Y}\theta_1(Z) - \int_0^Z \theta_1(\zeta)\left(\frac{\partial^2 F}{\partial Z^2}\right)_{Y,(Z-\zeta)} d\zeta \;+$$
$$+ \int_0^Y \theta_2(\eta)\left(\frac{\partial^2 F}{\partial Y\, \partial Z}\right)_{(Y-\eta),Z} d\eta \qquad (11a)$$

$$T_2(Y, Z) = e^{-Z}\theta_2(Y) \;+$$
$$+ \int_0^Z \theta_1(\zeta)\left(\frac{\partial^2 F}{\partial Y\, \partial Z}\right)_{Y,(Z-\zeta)} d\zeta \;-$$
$$- \int_0^Y \theta_2(\eta)\left(\frac{\partial^2 F}{\partial Y^2}\right)_{(Y-\eta),Z} d\eta \qquad (11b)$$

The reader wishing to check the correctness of these solutions by substitution in (1), (2) and (10) will find that he needs only the properties of the function F expressed by equations (7), (8a, b) and (9a, b) (including some of the derivatives of these equations) and not its specific form.

In all previous work step functions rather than peak functions have been studied. Formulae (11a, b) may be adjusted accordingly by partial integration. This has the effect of replacing

integration over a series of successive peaks of magnitude θ by integration over a series of successive jumps equal to the first derivative θ'. If use is made of equations (7) to (9a, b) the resulting formulae become:

$$T_1(Y, Z) = \theta_1(Z) - \{\theta_1(0) - \theta_2(0)\}\left(\frac{\partial F}{\partial Z}\right)_{Y, Z} - \int_0^Z \theta_1'(\zeta)\left(\frac{\partial F}{\partial Z}\right)_{Y, (Z-\zeta)} d\zeta + \int_0^Y \theta_2'(\eta)\left(\frac{\partial F}{\partial Z}\right)_{(Y-\eta), Z} d\eta \qquad (12a)$$

$$T_2(Y, Z) = \theta_2(Y) + \{\theta_1(0) - \theta_2(0)\}\left(\frac{\partial F}{\partial Y}\right)_{Y, Z} + \int_0^Z \theta_1'(\zeta)\left(\frac{\partial F}{\partial Y}\right)_{Y, (Z-\zeta)} d\zeta - \int_0^Y \theta_2'(\eta)\left(\frac{\partial F}{\partial Y}\right)_{(Y-\eta), Z} d\eta \qquad (12b)$$

SPECIFIC FORMS OF F; DISCUSSION

For practical applications the function F may be written in, for instance, the following specific forms:

$$F = \int_0^Y \int_0^Z e^{-\eta-\zeta} I_0(2\sqrt{\eta\zeta})\, d\eta\, d\zeta \qquad (13)$$

$$F = \sum_{n=1}^{\infty} \sum_{m=1}^{\infty} (-1)^{m+n} \frac{(m+n-2)!\, mn}{(m!\, n!)^2} Y^m Z^n \qquad (14)$$

$$F = \sum_{n=0}^{\infty} \left(1 - e^{-Y} \cdot \sum_{k=0}^{n} \frac{Y^k}{k!}\right)\left(1 - e^{-Z} \cdot \sum_{k=0}^{n} \frac{Z^k}{k!}\right) \qquad (15)$$

It can easily be proved that these forms obey conditions (7) to (9a, b). The symmetry in Y and Z is obvious.

Substitution of (13) in (6a, b) yields the well-known elementary solutions for T_2 and T_2 first given by ANZELIUS [10] (see KLINKENBERG's survey [1]). Substitution of (13) in (11a, b) yields the Bessel function solutions which were derived by AMUNDSON ([2], his formulae 8 and 19). His solutions may be reduced to our simpler form by making use of the identity:

$$e^{-Y} \int_0^Z e^{-\zeta} I_0(2\sqrt{Y\zeta})\, d\zeta = 1 - e^{-Z} - e^{-Z} \int_0^Y e^{-\eta} I_1(2\sqrt{\eta Z}) \sqrt{(Z/\eta)}\, d\eta \qquad (16)$$

NUSSELT [5] obtained our solutions (11a, b), though only for one variable boundary condition, his gas inlet temperature being assumed to be constant ($\theta_1 = 0$).

Substitution of (14) in (6a, b) yields the elementary double power series solutions first published by SMITH [7].

Formula (15) in (6a, b) generates the solutions in exponentials and double power series given previously by one of the present authors [1].

The two sets of final formulae (11a, b) and (12a, b) do not contain the function F as such but only its derivatives. This allows of the utilization of some approximate solutions to the elementary problem which, by virtue of (6a, b), yield $\partial F/\partial Y$ and $\partial F/\partial Z$, although these forms cannot easily be integrated and do not exactly obey the conditions (7) to (9a, b).

For all except very low values of Y and Z the derivatives of F may be approximated by:

$$\frac{\partial F}{\partial Y} = \tfrac{1}{2} + \tfrac{1}{2}\operatorname{erf}\left(\sqrt{Z} - \sqrt{Y} - \frac{1}{8\sqrt{Z}} - \frac{1}{8\sqrt{Y}}\right) \qquad (17a)$$

$$\frac{\partial F}{\partial Z} = \tfrac{1}{2} - \tfrac{1}{2}\operatorname{erf}\left(\sqrt{Z} - \sqrt{Y} + \frac{1}{8\sqrt{Z}} + \frac{1}{8\sqrt{Y}}\right) \qquad (17b)$$

or, with only a slight loss of accuracy, by

$$\frac{\partial F}{\partial Y} = \tfrac{1}{2} + \tfrac{1}{2}\operatorname{erf}\left[\sqrt{(Z - \tfrac{1}{4})} - \sqrt{(Y + \tfrac{1}{4})}\right] \qquad (18a)$$

$$\frac{\partial F}{\partial Z} = \tfrac{1}{2} - \tfrac{1}{2}\operatorname{erf}\left[\sqrt{(Z + \tfrac{1}{4})} - \sqrt{(Y - \tfrac{1}{4})}\right], \qquad (18b)$$

as introduced by KLINKENBERG [1, 8]. It has been shown [1] that solutions (17a, b) are no longer of engineering accuracy for Y and/or Z below 2, but that they rapidly become more accurate for higher values of these variables. In the midpoint $Y = Z$ of an S-shaped break-through curve the error was determined at about $1/[48\, Y\sqrt{(\pi Y)}]$.

As a more accurate approximation, especially for low values of the variables, ONSAGER's

solutions [1] — without the added series — may serve. In the present notation these are:

$$\frac{\partial F}{\partial Y} = \tfrac{1}{2} + \tfrac{1}{2}\,\mathrm{erf}\,(\sqrt{Z} - \sqrt{Y}) - \frac{Z^{1/4}}{Y^{1/4} + Z^{1/4}}\,e^{-Y-Z}\,I_0\,(2\sqrt{YZ}) \qquad (19a)$$

$$\frac{\partial F}{\partial Z} = \tfrac{1}{2} - \tfrac{1}{2}\,\mathrm{erf}\,(\sqrt{Z} - \sqrt{Y}) - \frac{Y^{1/4}}{Y^{1/4} + Z^{1/4}}\,e^{-Y-Z}\,I_0\,(2\sqrt{YZ}) \qquad (19b)$$

A comparison of the preceding formulae leaves no doubt that (17a, b) and (18a, b) are the simplest ones for the calculation of the integrands for graphical or numerical integration of (11a, b) or (12a, b). They can be used for all except very low values of Y and/or Z which, however, in most cases imposes no practical limitation. The method can be applied in a much shorter time than REILLY's Fourier synthesis. For problems with low values of the variables (such as with cross-flow recuperators) the derivatives of functions (13), (14) or (15) or ONSAGER's solutions (19a, b) can be used for the evaluation of the integrands.

It may be recalled at this point that elaborate tabulations of $\partial F/\partial Y$ have been prepared by BRINKLEY [9] for values of Y and Z between 0 and 500. The other derivative, $\partial F/\partial Z$, can also be read from the tables since F is a symmetrical function. Accurate as these tables are (six figures behind the decimal point), their usefulness is greatly impaired by the fact that the increments in the values of the independent variables are too large. This calls for non-linear interpolation in intervals of four or five figures, which is both cumbersome and inaccurate.

DISCUSSION OF REILLY'S EXAMPLE

Returning once more to REILLY's paper [3] it must, unfortunately, be stated that his numerical example was illchosen to demonstrate the possibilities of his method. The initial disturbance in the solid temperature (his Fig. 1) can easily be described by superposition of two step-function disturbances. The problem may then be solved with the aid of the elementary solutions (6a, b) and the error functions with corrected argument (18a, b), without any numerical integration being required.

In REILLY's example the solid temperature T_2 at any place in the bed can be described as 1200°F plus the influence of a step disturbance of − 150°F plus the influence of a step disturbance of + 100°F which has travelled over a slightly shorter distance:

$$T_2 = 1200 - 150\left(\frac{\partial F}{\partial Y_1}\right) + 100\left(\frac{\partial F}{\partial Y_2}\right)\,{}^\circ\mathrm{F} \qquad (20)$$

Y_1 is the dimensionless distance between the measuring point and the beginning of the bed; Y_2 is the dimensionless notation of a distance which is 0·5 ft shorter. Formula (18a) for large values of Y and Z can be written in a slightly simplified form:

$$\frac{\partial F}{\partial Y} = \tfrac{1}{2} + \tfrac{1}{2}\,\mathrm{erf}\,[\sqrt{(Z - \tfrac{1}{2})} - \sqrt{Y}] \qquad (21)$$

In order to check REILLY's curve for T_2 after 25 min (this time being characterized by $Z = 97{\cdot}22$) a simple tabulation of $\partial F/\partial Y$ is prepared according to (21). For the sake of convenience the points are taken 0·5 ft apart. Their distance from the bed entrance is designated by x, in ft. The following values of $\partial F/\partial Y$ can easily be derived:

x (ft)	Y	$\partial F/\partial Y$
$x =$ 1·5 ft	$Y =$ 48·6	$= 1{\cdot}0000$
2	64·8	0·9942
2·5	81·0	0·8811
3	97·2	0·4864
3·5	113·4	0·1256
4	129·6	0·0142
4·5	145·8	0·0007

By proper substitution of $\partial F/\partial Y$ in (20) the following results are obtained:

$x = 2$ ft

$$T_2 = 1200 - (150 \times 0{\cdot}9942) + (100 \times 1{\cdot}0000) = 1150{\cdot}9\,{}^\circ\mathrm{F}$$

$x = 2{\cdot}5$ ft

$$T_2 = 1200 - (150 \times 0{\cdot}8811) + (100 \times 0{\cdot}9942) = 1167{\cdot}3\,{}^\circ\mathrm{F} \quad \text{etc.}$$

x	T_2
$x =$ 3ft	$T_2 =$ 1215·1°F
3·5	1229·8
4	1210·4
4·5	1201·3

VOL. 11 1959/60

These figures are considered accurate to within the last decimal given. They check very well with the curve in REILLY's Fig. 1.

REFERENCES

[1] KLINKENBERG A. *Industr. Engng. Chem.* 1954 **46** 2285.

[2] AMUNDSON N. R. *J. Phys. Chem.* 1950 **54** 812.

[3] REILLY P. M. *Amer. Inst. Chem. Engrs. J.* 1957 **3** 513.

[4] SAHLBERG P. H. *Trans. Swedish Ass. Engrs. Architects (Stockholm)* (Heat power group) 1957 **3** 8.

[5] NUSSELT W. *Z. Ver. Dtsch. Ing.* 1927 **71** 85.

[6] HAUSEN H. *Z. Angew. Math. Mech.* 1931 **11** 105.

[7] SMITH D. M. *Engineering* 1934 **138** 479 ; 606.

[8] KLINKENBERG A. *Industr. Engng. Chem.* 1948 **40** 1992.

[9] BRINKLEY S. R. *Tables of the Temperature-Distributing Function for Heat Exchange between Fluid amd Porous Solid.* Report U.S. Bureau of Mines, Pittsburgh, Febr, 2, 1957.

[10] ANZELIUS A. *Z. Angew. Math. Mech.* 1926 **6** 291.

Chemical Engineering Science, 1960, Vol. 11, pp. 267 to 273. Pergamon Press Ltd., London. Printed in Great Britain

The viscosity of liquids as a function of temperature

F. C. Eversteijn, J. M. Stevels and H. I. Waterman
Institute of Chemical Technology, Delft University, Delft, Netherlands

(*Received* 24 *August* 1959)

Abstract—In the past various formulae have been put forward as descriptions of the way in which the viscosity of liquids changes with temperature. Those proposed by Guzman and Andrade

$$\log \eta = A/T + B$$

and by Souders

$$\log \nu = A/T + B$$

do not appear to possess any general validity. Of the formulae that have been published since then, that of Cornelissen and Waterman

$$\log \nu = A/T^x + B$$

is a good description of viscosity as function of temperature. The derivation of this formula from that of Souders is discussed. The one is evolved from the other by way of viscosity values for alkenes and other hydrocarbons, the Cornelissen–Waterman formula also being applied to glass.

Résumé—Différentes formules ont déjà été établies pour représenter les variations de la viscosité des liquides avec la température.

Celles proposées par Gusman et Andrade :

$$\log \eta = A/T + B$$

et par Souders

$$\log \nu = A/T + B$$

ne paraissent pas posséder une validité générale. La formule publiée ultérieurement par Cornelissen et Waterman

$$\log \nu = A/T^x + B$$

donne une bonne représentation de la variation de la viscosité avec la température. L'établissement de cette formule à partir de celle de Souders est discutée. L'une est dégagée de l'autre au moyen des valeurs de la viscosité des alkènes et d'autres hydrocarbures ; la formule de Cornelissen–Waterman s'applique aussi au verre.

Zusammenfassung—In den letzten Jahren sind verschiedene Formeln für die Anderung der Viskosität von Flüssigkeiten und der Temperatur vorgeschlagen worden. Nach Vorschlägen von Guzman und Andrade gilt :

$$\log \eta = A/T + B$$

und nach Souders gilt :

$$\log \nu = A/T + B$$

Beide Gleichungen scheinen keine allgemeine Gültigkeit zu besitzen. Von den Formeln, die seitdem veröffentlicht wurden, stellt die von Cornelissen und Waterman

$$\log \nu = A/T^x + B$$

eine gute Beschreibung des funktionellen Zusammenhanges von Viskosität und Temperatur dar.

Die Abswichung dieser Formel von der von Souders wird diskutiert. Die eine wird aus der anderen aus Viskositätswerten für Alkene und andere Kohlenwasserstoffe entwickelt ; daneben wird die Cornelissen–Waterman-Formel auf Glas angewandt.

Introduction

Various writers have proposed relationships between the viscosity of liquids and their temperatures. In 1930 Andrade published one that had been proposed by Guzman as far back as 1913 [1]. The appropriate formula is

$$\log \eta = A/T + B \tag{1}$$

in which η is the dynamic viscosity, T the absolute temperature in degrees Kelvin and A and B constants.

In many cases this formula results in large discrepancies and for this reason Andrade revised the relationship in 1934, publishing the following formula:

$$\log (\eta\, v^{1/3}) = A/vT + B \tag{2}$$

in which v is the specific volume in g/ml. Where it is a matter of displaying viscosity changes with temperature in graphical form, formula (2) is difficult to work with. Souders [2] simplified it in 1937 into

$$\log \nu = A/T + B \tag{3}$$

where ν (kinematic viscosity) $= \eta/\rho$ and ρ is the density in g/ml.

This formula was stated by the author to be just as satisfactory as (2).

Since 1937 many other viscosity formulae have been proposed including that of Cornelissen and Waterman [3], which is

$$\log \nu = A/T^x + B \tag{4}$$

in which A, B and x are constants.

By quoting extensive numerical data, Cornelissen and Waterman demonstrated that their formula could be applied satisfactorily to very different systems, such as hydrocarbons and mixtures thereof, saturated and unsaturated mineral oils, and solutions of sugars and other substances.

We shall now go on to discuss the relation between this formula and that of Souders in greater detail. In order to give an impression of the magnitude of the errors arising when the

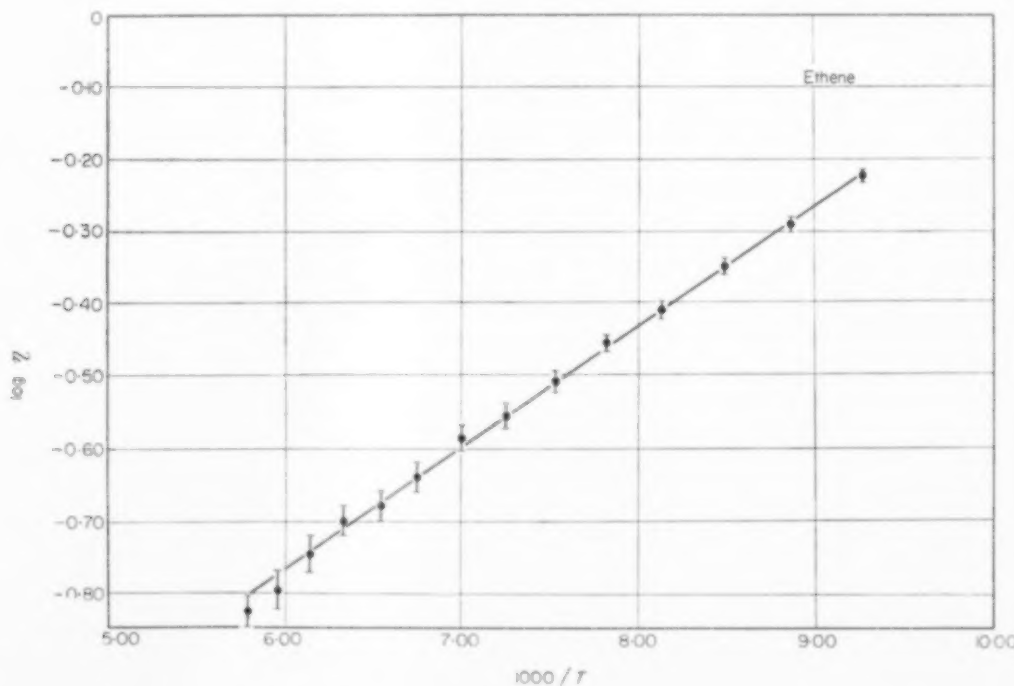

Fig. 1.

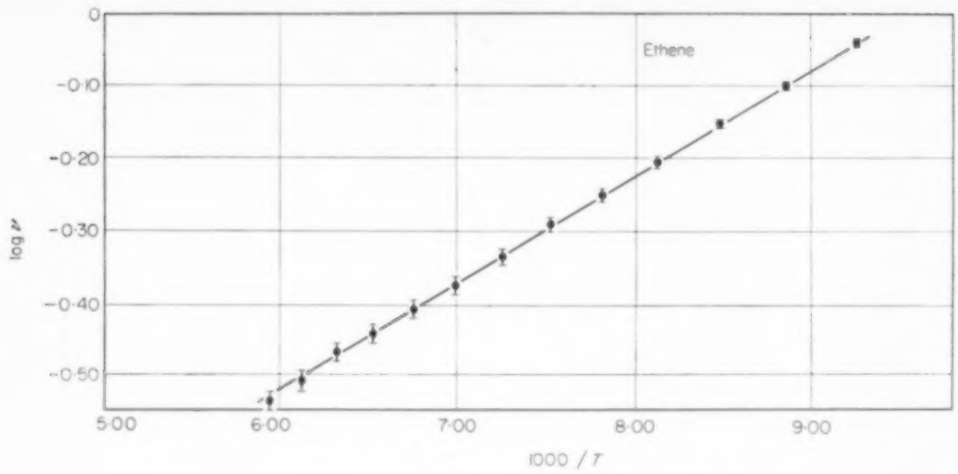

Fig. 2.

Cuzman–Andrade and Souders formula are employed, the viscosities of ethylene, 1–undecene and 1–eicosene have been plotted against temperature [4] in Figs. 1, 2, 3 and 4.

In Figs. 1 and 2 are represented not only the values of the logarithm of the viscosity but also the limits of the experimental accuracy by two horizontal lines.

In Figs. 3 and 4, however, the experiments are so accurate that the points sufficiently represent the experimental values.

The graphs in Figs. 1 and 2 show that the

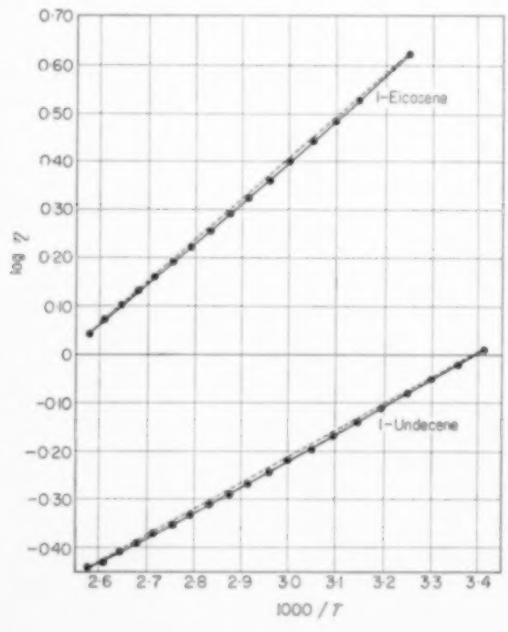

Fig. 3.

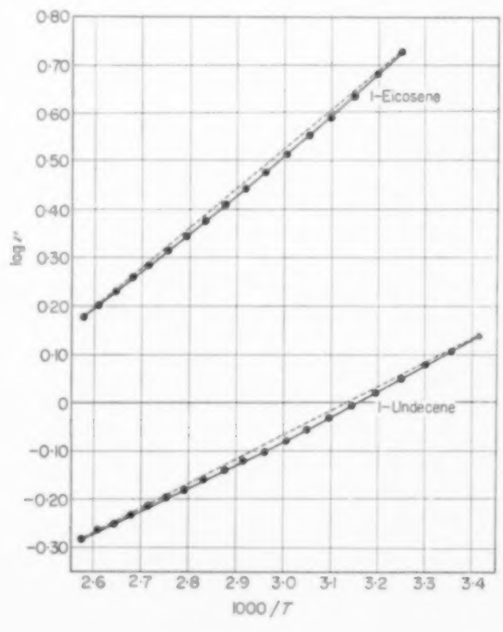

Fig. 4.

Table 1.

1–*undecene*			1–*eicosene*		
t (°C)	E_η (kcal/mol)	E_ν (kcal/mol)	t (°C)	E_η (kcal/mol)	E_ν (kcal/mol)
10	3·00	2·74	40	4·36	4·20
20	2·69	2·55	50	4·18	3·99
30	2·57	2·45	60	4·01	3·78
40	2·67	2·46	70	3·88	3·71
50	2·63	2·41	80	3·83	3·67
60	2·52	2·28	90	3·76	3·58
70	2·46	2·21	100	3·76	3·49
80	2·46	2·22			
90	2·44	2·15			
100	2·45	2·19			

GUZMAN–ANDRADE and SOUDERS formulae have a reasonable degree of validity for ethylene, if we take the experimental accuracy in consideration. For 1–undecene and 1–eicosene the discrepancies (see Figs. 3 and 4) are so great that it is quite impossible to apply the formulae (1) and (3) on these cases. Therefore straight dotted lines are drawn which show the deviations. Their failure is connected with the fact that $d(\log \eta)/d(1/T)$ and $d(\log \nu)/d(1/T)$ are not constant but are dependent on temperature. In various places in the literature [5] the term activation energy is used to indicate the value of this quantity multiplied by 2·30 R (R is the gas constant, whose value is 1·987 cal/mol). Henceforward we shall be using E_η and E_ν to stand for $2{\cdot}30\,Rd(\log \eta)/d(1/T)$ and $2{\cdot}30\,Rd(\log \nu)/d(1/T)$ respectively.

Table 1 contains figures showing how $E\eta$ and and $E\nu$ depend on temperature.

The Table reveals that E_η and E_ν decrease as temperature increases, the decrease being all the more rapid according as the molecular weight is greater. If the dependence on temperature is expressed in the form $E_\nu = C/T^{x-1}$, in which C and x are constants, the formula of CORNELISSEN and WATERMAN can be derived from it by integration.

The relationship $\log \eta = A/T^x + B$ can be deduced from the above in an analogous manner. The value of x for hydrocarbons does not seem to change very much if the dependence on temperature of $\log \eta$ is studied instead of that of $\log \nu$. However, this is not generally true of all substances.

It depends on the way in which the specific weights of various substances are affected by temperature. For example, in the case of mercury, [3] it is found that x is about 1·5 when the $\log \nu$ formula is employed and about unity when the $\log \eta$ one is employed. The authors prefer to use the $\log \nu$ formula for liquid hydrocarbons because this value is the one actually obtained from measurement.

Even so, the $\log \eta$ formula is sometimes useful when data given in the literature are being worked on. For example, the η of various types of glass is often known for different temperatures, while their specific gravity is not.

The formula of CORNELISSEN and WATERMAN is applicable to simple hydrocarbons whether of large or small molecular weight and also to mixtures of hydrocarbons. The value of x increases with molecular weight; it is about unity for ethylene and increases as the lengths of the chain does. x for 1–eicosene is about 2.

DEPENDENCE OF $E\eta$ AND $E\nu$ ON CHAIN LENGTH

Table 2 displays E_η and E_ν values for various alkenes as determined at two temperatures.

Table 2 shows that E_η and E_ν increase with the length of the chain. The same is found to be

Table 2

	$t = 10\ ^\circ C$		$t = 90\ ^\circ C$	
	E_η (kcal/mol)	E_ν (kcal/mol)	E_η (kcal/mol)	E_ν (kcal/mol)
1-heptene	1·82	1·58		
1-octene	2·10	1·94	1·87	1·53
1-nonene	2·40	2·24	2·08	1·77
1-decene	2·69	2·50	2·25	1·98
1-undecene	3·00	2·74	2·44	2·15
1-dodecene	3·22	2·93	2·59	2·38
1-tridecene	3·46	3·33	2·80	2·51
1-tetradecene	3·78	3·63	2·96	2·72
1-pentadecene	4·02	3·83	3·11	2·87
1-hexadecene			3·29	3·13
1-heptadecene			3·43	3·19
1-octadecene			3·59	3·23
1-nonadecene			3·65	3·43
1-eicosene			3·76	3·58

true of the alkylbenzenes, alkyl*cyclo*hexanes, alkyl*cyclo*pentanes and siloxanes [3, 6]. In general it may perhaps be said that E_η and E_ν decrease with increasing depolymerization, irrespective of whether this is brought about by chemical or physical means (temperature).

Application of Cornelissen and Waterman's Viscosity/temperature Formula to Glass

It has been investigated whether this formula can be applied to glass [7].

Generally the formula is used in the form

$$\log \nu = \log \eta/\rho = A/T^x + B$$

The density of glass varies with temperature to a much lesser extent than its viscosity does, and therefore the factor $1/\rho$ has but little influence on the variation in viscosity with temperature. Hence $\log \eta$ can be used instead of $\log \nu$. This will be clear from Table 3, which contains one or two examples extracted from the article by Shartsis *et al.* [8].

Table 3. Composition of glasses (in percentages by weight)

Na_2O	K_2O	Li_2O	SiO_2	$t\ ^\circ C$	$\log \eta$	$\log \nu$	$\log \rho$
20·0			80·0	1101	3·405	3·062	0·343
				1408	2·200	1·861	0·339
					1·205	1·201	0·004
	23·9		76·1	900	3·523	3·166	0·357
				1400	1·396	1·058	0·338
					2·127	2·108	0·019
		17·8	82·2	1000	2·933	2·594	0·339
				1391	1·430	1·104	0·326
					1·503	1·490	0·013

Table 4. Glass of composition $3\,SiO_2 \cdot Na_2O$* $\log \eta = 3{\cdot}528 \times 10^6 (1/T^{1{\cdot}913}) - 0{\cdot}4747$

Temperature (°K)	log η values		$10^6/_{T}\ 1{\cdot}913$	$\Delta\eta$ (%)
	Observed	*Calculated*		
1624·0	2·0576	2·0701	0·721	− 3·0
1608·3	2·1078	2·1180	0·735	− 2·4
1589·9	2·1688	2·1755	0·751	− 1·5
1574·6	2·2206	2·2253	0·765	− 1·1
1551·2	2·3006	2·3036	0·788	− 0·7
1534·0	2·3617	2·3636	0·805	− 0·5
1515·2	2·4297	2·4313	0·824	− 0·4
1494·6	2·5092	2·5082	0·846	+ 0·2
1472·9	2·5944	2·5925	0·869	+ 0·4
1453·9	2·6721	2·6698	0·891	+ 0·5
1434·8	2·7543	2·7506	0·914	+ 0·9
1417·5	2·8280	2·8264	0·936	+ 0·4
1399·2	2·9154	2·9094	0·959	+ 1·4
1378·3	3·0120	3·0082	0·987	+ 0·9
1352·0	3·1424	3·1390	1·024	+ 0·8
1331·2	3·2487	3·2477	1·055	+ 0·3
1309·4	3·3673	3·3673	1·089	0
1282·0	3·5198	3·5260	1·134	− 1·4
1261·8	3·6424	3·6495	1·169	− 1·7
1239·6	3·7803	3·7914	1·209	− 2·6
1221·9	3·8948	3·9124	1·244	− 4·1
1193·1	4·1030	4·1156	1·301	− 2·9
1175·9	4·2322	4·2440	1·338	− 2·8
1152·3	4·4133	4·4313	1·391	− 4·2
1127·0	4·6263	4·6444	1·451	− 4·2
1107·5	4·8007	4·8180	1·500	− 4·1
1088·8	4·9950	4·9926	1·550	+ 0·6
1063·8	5·2383	5·2414	1·620	− 0·7
1039·6	5·5065	5·4989	1·693	+ 1·8
1014·0	5·8149	5·7910	1·776	+ 5·7
985·2	6·2190	6·1463	1·877	+ 11·8
971·1	6·4200	6·3308	1·929	+ 12·3

*The viscosity values were obtained from the laboratories of Corning Glass Works.

In Table 4 the formula $\log \eta = A/T^x + B$ has been applied to a glass having the composition $3SiO_2 \cdot Na_2O$ in a range of viscosities between 10^2 and 10^6 p.

The results of applying the same formula to a silicate glass in a range of viscosities between 10^2 and 10^{13} p are shown in Table 5. It should be observed that these Tables are only provided by way of example, and that many more of the same kind could be given.

The question now arises as to why formula (4) has a better degree of validity than formulae (1) and (3) have. When we were dealing with hydrocarbons we concluded that the value of E_η decreases with increasing depolymerization and respectively increases with increasing polymerization. We shall now consider two cases.

(*a*) *Thermal depolymerization*

The fact that the viscosity of glass falls off as its temperature increases must be ascribed to the breakdown of the network (depolymerization). It may be expected, on the analogy of this, that the value of $E\eta$ will decrease at higher temperatures.

For glass, then, the quantity E_η is a function of temperature, decreasing as the temperature

Table 5. Composition of glass in percentages by weight:

SiO_2 : 67·2 Na_2O : 9·8 K_2O : 9·7
CaO : 7·2 MgO : 2·1 Al_2O_3 : 1·0
BaO : 2·0 ZnO : 1·0

$\log \eta = 5{\cdot}38{\cdot}10^8/(1/T)^{2{\cdot}63} + 0{\cdot}31$

Temperature (°K)	log η *values*		$10^8/T^{2{\cdot}63}$	*Discrepancy*	
	*Observed**	*Calculated*		*Absolute*	*Percentage*
798	13·13	12·84	2·330	+ 0·29	+ 2·2
848	11·00	11·00	1·987	0	0
898	9·37	9·50	1·709	− 0·13	− 1·4
948	8·17	8·28	1·483	− 0·11	− 1·3
998	7·15	7·27	1·295	− 0·12	− 1·7
1048	6·34	6·44	1·140	− 0·10	− 1·6
1098	5·68	5·71	1·004	− 0·03	− 0·5
1148	5·13	5·13	0·896	0	0
1198	4·65	4·62	0·801	+ 0·03	+ 0·6
1248	4·20	4·18	0·719	+ 0·02	+ 0·5
1298	3·85	3·80	0·648	+ 0·05	+ 1·3
1348	3·52	3·47	0·587	+ 0·05	+ 1·4
1398	3·20	3·17	0·533	+ 0·03	+ 1·0
1448	2·95	2·93	0·487	+ 0·02	+ 0·7
1498	2·70	2·70	0·445	0	0
1548	2·48	2·51	0·408	− 0·03	− 1·2
1598	2·25	2·33	0·375	− 0·08	− 3·5
1648	2·08	2·17	0·347	− 0·09	− 4·3

*The viscosity values were obtained from the Development Centre, Glass Division, N. V. Philips' Gloeilampenfabrieken. The accuracy of the log η values is ± 0·03.

increases. If its dependence on temperature is expressed by the relationship $E_\eta = 2{\cdot}30\,R.\, d(\log\eta)/d(1/T) = C/T^{x-1}$, where C and x are constants, the formula of Cornelissen and Waterman will be arrived at.

(*b*) *Chemical depolymerization*

Not only does E_η depend on temperature, as just noted, but we are faced with a phenomenon whereby it decreases with the degree of coherence (as it does in the hydrocarbons). In other words a decrease in E_η accompanies an increase in the number of ions modifying the network.

A similarity between chemical and thermal depolymerization is evident in the infra-red spectrum of glass: when the temperature is raised or the proportion of ions modifying the network is caused to increase, an analogous change in the intensity curves of the infra-red absorption is observed [9, 10].

References

[1] Andrade E. N. da C., *Endeavour* 1954 **13** 117.
[2] Souders M. *J. Amer. Chem. Soc.* 1937 **59** 1252.
[3] Cornelissen J. and Waterman H. I. *Chem. Engng. Sci.* 1955 **4** 238.
[4] *Selected Values of Properties of Hydrocarbons and Related Compounds.* American Petroleum Institute Research Project 44.
[5] Glasstone, Laidler and Eyring. *The Theory of Rate Processes* p. 493. McGraw Hill, New York 1941.
[6] Wilcock D. F. *J. Amer. Chem. Soc.* 1946 **68** 691.
[7] Cornelissen J., van Leeuwen J. and Waterman H. I. *Chim. et Ind.* 1957 **77** 69 ; 1958 **80** 398.
[8] Shartsis L., Spinner S. and Capps W. *J. Amer. Ceram. Soc.* 1952 **35** 155.
[9] Neuroth N. *Glastechn. Ber.* **28** 1955 411.
[10] Jellyman P. E. and Procter J. P. *J. Soc. Glass Tech.* 1955 **39** 173.

Vol. 11 1959/60

Chemical Engineering Science, 1960, Vol. 11, pp. 274 to 285. Pergamon Press Ltd., London. Printed in Great Britain

Heat transfer between a fluidized bed and a vertical tube

H. A. Vreedenberg

Koninklijke/Shell Laboratorium, Amsterdam
(Shell International Research Maatschappij N.V.)

(*Received 3 September 1958*)

Abstract—All the data available in the literature on heat transfer between a bed fluidized by means of a gas and an axially positioned tube are represented by two different correlations, one for the range of fine and light particles where the viscous forces on the particles are predominant and an analogy between the fluidized bed and a flowing gas or liquid is assumed, and another for the range of coarser and heavier particles where inertia effects prevail. The distinction between these two ranges has already been made in a previous article on heat transfer to a horizontal tube. The limitations of the applicability of the correlations are discussed and measures to be taken for maximizing the heat transfer under given conditions are considered. The correlations can also be used to obtain an estimate of the average coefficient of heat transfer between a fluidized bed and a set of vertical tubes which occupies a great part of the cross-section of the bed.

Résumé—L'auteur démontre que toutes les données qui se trouvent dans la littérature concernant l'échange de chaleur entre un lit fluidisé au moyen d'un gaz et un tube placé dans l'axe du lit, peuvent être représentées par deux corrélations qui s'appliquent à deux intervalles différents.

De ces intervalles, l'un est celui des grains fins et légers où prédomine l'effet des forces visqueuses sur les grains et où le lit fluidisé est considéré comme analogue à un courant de gaz ou de liquide. L'autre intervalle est celui des grains plus gros et plus lourds où prévalent les effets d'inertie. Dans un autre article, sur l'échange de chaleur avec un tube horizontal, ill a déjà été publié en quoi ces deux intervalles sont différents. L'auteur discute les limites d'appication des corrélations et considère les mesures nécessaires pour obtenir un échange de chaleur maximum sous des conditions données. Les corrélations aident aussi à évaluer le coefficient moyen d'échange de chaleur entre un lit fluidisé et une batterie de tubes verticaux qui occupe une large partie de la section transversale du lit.

Zusammenfassung—Alle in der Literatur verfügbaren Werte für den Wärmeübergang zwischen einem Fliessbett, das durch einen Gasstrom unterhalten wird und einem senkrecht stehenden Rohr, werden durch zwei verschiedene Beziehungen dargestellt; die eine gilt für das Gebiet der feinen und leichten Körnungen, wo die Adhäsionskräfte bei den Teilchen vorherrschen und eine Analogie zwischen dem Fliessbett und strömenden Gasen oder Flüssigkeiten angenommen wird, während die andere das Gebiet der gröberen und schwereren Körnungen, wo Trägheitswirkungen vorherrschen, erfasst. Der Unterschied zwischen diesen beiden Bereichen wurde schon in einer früheren Arbeit über den Wärmeübergang in einem horizontalen Rohr dargestellt. Die Grenzen der Anwendbarkeit dieser Beziehungen werden diskutiert und Massnahmen zur Erhöhung des Wärmeübergangs unter bestimmten Bedingungen erörtert. Die Beziehungen können ebenfalls zur Berechnung eines Durchschnittswertes für den Wärmeübergang zwischen einem Fliessbett und einem Bündel vertikaler Rohre dienen, das einen grossen Teil des Bettquerschnitts einnimmt.

1. Previous Work with Horizontal Tubes

In earlier publications, a comprehensive series of measurements of heat transfer from fluidized beds to horizontal single tubes has been reported [1, 2]. A simple correlation of the results of the measurements made before 1951 was first given [2], but it had to be revised when more data became available [1] and it proved useful to distinguish between two ranges.

The one range is that of fine and light particles. It is characterized by

$$\frac{G D_p \rho_s}{\rho \mu} < 2050$$

A new correlation for this range was derived from an assumed analogy between the fluidized bed and a flowing gas or liquid [1]. It contains the following dimensionless groups:

$$\frac{hD_t}{k}, \quad \frac{GD_t \rho_s (1-\epsilon)}{\rho\mu\epsilon}, \text{ and } \frac{c\mu}{k}$$

The range of coarse and heavy particles is characterized by

$$\frac{GD_p \rho_s}{\rho\mu} > 2550$$

The correlation for this range [1] contains the following dimensionless groups:

$$\frac{hD_t}{k}, \quad \frac{GD_t \rho_s}{\rho\mu}, \quad \frac{c\mu}{k} \quad \text{and} \quad \frac{\mu^2}{D_p{}^3 \rho_s{}^3 g}$$

In the intermediate range

$$2050 \leqslant \frac{GD_p \rho_s}{\rho\mu} \leqslant 2550$$

it was recommended that the average of the heat-transfer coefficients predicted by the two correlations be used.

Remark

The transition between the ranges can take place not only when D_p or ρ_s is varied, but also when gas properties like G, ρ, or μ are varied. Therefore is it incorrect to speak of ranges of fine and light materials on the one hand and of coarse and heavy materials on the other. But one may uphold this convenient fiction as long as one bears in minds the effect of the mass velocity and other gas properties.

2. Previous Work with Vertical Tubes

Table 1 enumerates all the investigations into heat transfer between beds fluidized by means of *gases* and vertically inserted cylinders. There is no uniformity in the methods used by the authors to determine the average particle diameter. It is impossible to account for these differences since the particle size distribution is not given. The appendix gives additional details.

A simple correlation of the experimental results up to 1951 [3, 4, 6, 8] has been presented elsewhere [8].

When, however, more and more experimental data became available [5, 7, 9, 10, 11, 12] some of these [7, 9, 11] necessitated a revision of the old correlation [8].

Table 1. Experiments with axial cylinders

Reference	*Particles*	*Gas*	*Average particle diameter*	*Diameter of axial cylinder*	*Diameter of fluidized bed*	*Ratio of diameters*	*Heated length of cylinder*	*Bed temperature*	*Mass velocity of gas*	*Heat-transfer coefficient*	*See Fig. nos.*	*Curves in Figs. 1–4*
				D_1	D_2	$\frac{D_2}{D_1}$			G	h		
			(μ)	(m)	(m)		(m)	(°C)	(kg/m^2 sec)	(J/m^{2}sec°C)		
[3]	Various	Air	60–879	0·0318	0·140	4·40	0·102	17–32	0·009–0·824	20–741	1; 3	B, C, . . . , T
[4]	Glass beads	Air	40–452	0·0125	0·073	5·85	0·219–0·876	57–111	0·518–2·03	175–652	3	U, V, W, X, Y
[5]	Glass beads	Air	900	0·0127	0·100	7·88	0·033	20	0·567–2·56	84–262	3	Z
[6]	SiC, Al_2O_3	Air, He, CO_2	97–249	0·0095	0·051	5·33	0·568	94–261	0·009–0·137	239–1060	2; 3	1, 2, . . . , 8
[7]	Sand, catalyst	Air	38–158	0·0095	0·102	10·7	0·572	29–345	0·022–0·250	273–597	2; 4	a, b, c, d, e
[8]	Sand	Air	215	0·0338	0·565	16·7	1·183	40–240	0·091–0·155	112–407	4	g, j
[9]	Various	Air, H_2, CO_2	65–900	0·0127–0·0133	0·100	7·51–7·88	0·033–0·037	20	0·009–1·54	35–1080	1; 3	k, l, . . . , r, t
[10]	Glass beads	Air	55–848	0·0127	0·120	9·46	0·127	93	0·032–2·10	184–868	2; 4	u, v, w, x, y
[11]	Microspheres, glass beads	Various	68–83	0·0064	0·102	16·0	0·152	−16–36	0·005–1·61	278–1000	1; 4	$\alpha, \beta, \ldots, \nu$
[12]	Sand	Air	450	0·0100	0·200	20·0	0·125	20	0·171–0·251	45–418	4	π, ρ, σ

VOL. 11 1959/60

3. Correlation Formulae for Heat Transfer from a Fluidized Bed to Vertical Tubes

It proved useful to distinguish between the same two ranges as in the case of horizontal tubes.

A new correlation for the range of *fine and light materials* can be derived from the assumed analogy with a gas or liquid flowing through the annular space between the cylindrical outer wall and the axial tube.

Walger [13] has published a critical survey of the literature on heat transfer between the walls of an annular space and a gas or liquid flowing turbulently through the annulus. He arrives at the conclusion that the coefficient of heat transfer at the inner wall can be represented by a simple relation between the Nusselt group, the Reynolds group, the Prandtl group of the fluid, the ratio between the diameters of the outer and inner cylinders, and the ratio between the viscosities of the fluid at the bulk temperature and at the temperature of the inner wall respectively; the difference between the diameters of the two cylinders has to be taken as the characteristic length in the Nusselt and Reynolds groups.

Consequently the assumed analogy leads to an attempt to represent the experimental results on heat transfer between fluidized beds of fine and light particles and vertically inserted cylinders by a relation between

$$\frac{h\,(D_2 - D_1)}{k},\ \frac{G\,(D_2 - D_1)\,\rho_s}{\rho\mu},\ \frac{c\mu}{k} \text{ and } \frac{D_2}{D_1}$$

The main difference between the first three of these groups and those occurring in the corresponding correlation for horizontal tubes (Section 1) is the absence of the factor $(1 - \epsilon)/\epsilon$ in the Reynolds group. It has to be omitted because the porosity is not given in most of the publications listed in Table 1. In view of the violent particle motion and consequent uniformity of temperature, there is no reason to introduce the viscosity of the gas at any other than the bed temperature.

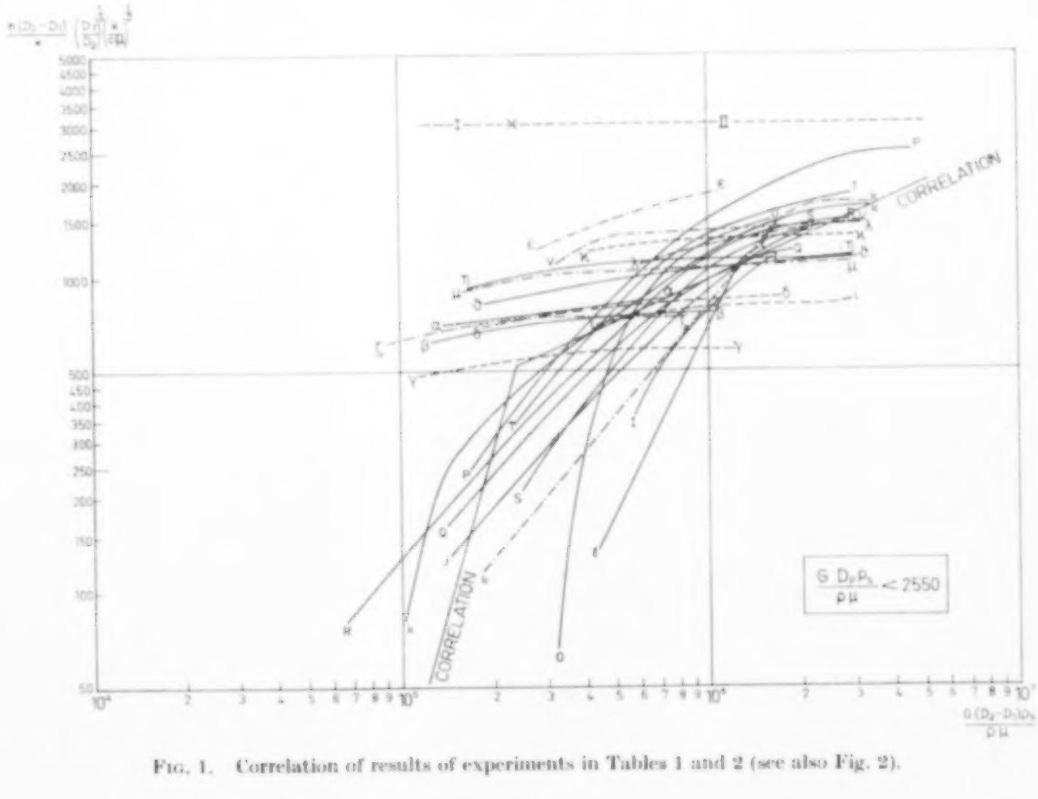

Fig. 1. Correlation of results of experiments in Tables 1 and 2 (see also Fig. 2).

The investigations enumerated in Table 1 comprise 110 series of measurements. In twenty-two of these the experimental conditions were entirely within the range

$$\frac{GD_p\,\rho_s}{\rho\mu} < 2050$$

which we qualified as the range of fine and light particles. In another twenty-four series the conditions were at least partly within the above range. It was found that a fair representation of the forty-six series or parts of series within the range can be given by plotting the composite group

$$\frac{h\,(D_2 - D_1)}{k}\left(\frac{D_1}{D_2}\right)^{1/3}\left(\frac{k}{c\mu}\right)^{1/2}$$

as a function of the Reynolds group

$$\frac{G\,(D_2 - D_1)\,\rho_s}{\rho\mu}$$

Figs. 1 and 2 show the forty-six experimental curves thus obtained ; they include the transition range

$$2050 \leqslant \frac{GD_p\,\rho_s}{\rho\mu} \leqslant 2550$$

where the correlation for fine and light particles has to be used in combination with the one for coarse and heavy materials. The broken line

$$\frac{h\,(D_2 - D_1)}{k}\left(\frac{D_1}{D_2}\right)^{1/3}\left(\frac{k}{c\mu}\right)^{1/2} = A\left\{\frac{G\,(D_2 - D_1)\,\rho_s}{\rho\mu}\right\}^B$$

where

$A = 0{\cdot}27 \times 10^{-15}$ and $B = 3{\cdot}4$ when

$$\frac{G\,(D_2 - D_1)\,\rho_s}{\rho\mu} \leqslant 0{\cdot}237 \times 10^6$$

and $A = 2{\cdot}2$ and $B = 0{\cdot}44$ when

$$\frac{G\,(D_2 - D_1)\,\rho_s}{\rho\mu} > 0{\cdot}237 \times 10^6$$

has been drawn through the set of experimental

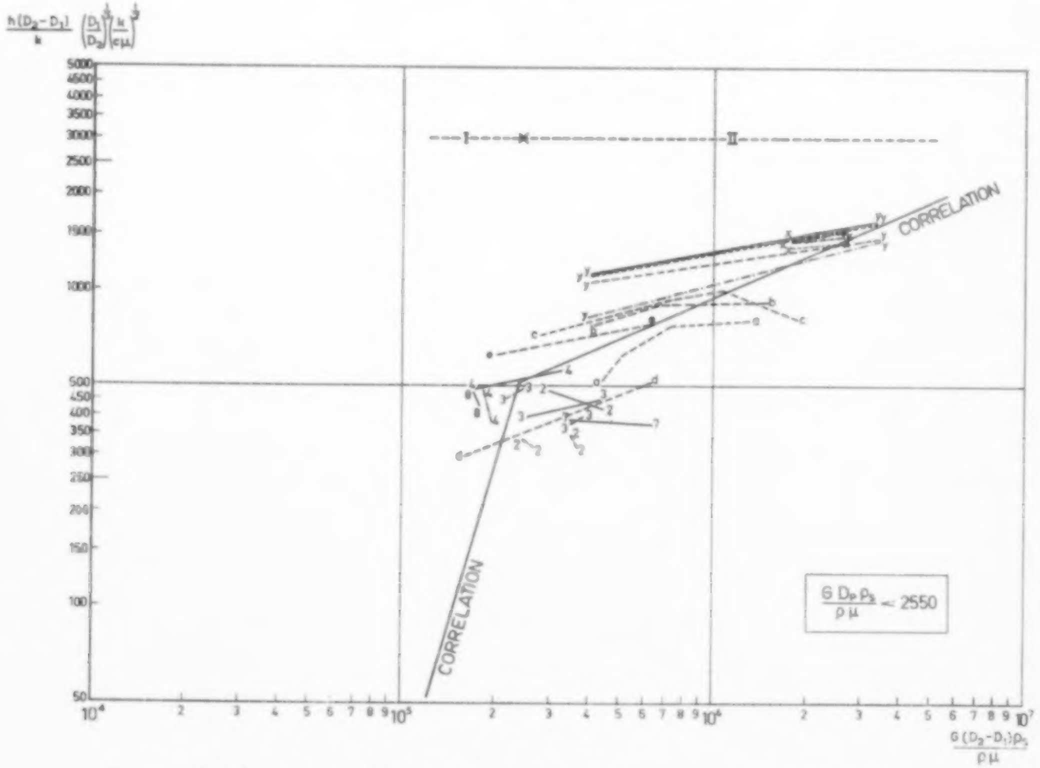

FIG. 2. Correlation of results of experiments in Tables 1 and 2 (see also Fig. 1).

VOL. 11 1959/60

curves; the co-ordinates of any point of these curves differ by no more than a factor 2·2 from those of the nearest point of the broken line.

A correlation for the range of *coarse and heavy particles* can be obtained by adding two dimensionless groups to the four occurring in the correlation of Figs. 1 and 2, namely

$$\frac{\mu^2}{D_p^3\, \rho_s^2\, g} \quad \text{and} \quad \frac{D_p}{D_2 - D_1}$$

It was found that a fair representation of the eighty-eight series or parts of series of measurements within this range and the transition range can be given by plotting

$$\frac{h\,(D_2 - D_1)}{k}\left(\frac{D_1}{D_2} \times \frac{D_p}{D_2 - D_1} \times \frac{k}{c\mu}\right)^{1/3}$$

as a function of

$$\frac{G\,(D_2 - D_1)\,\rho_s}{\rho\mu}\left(\frac{\mu^2}{D_p^3\,\rho_s^2\,g}\right)^{1/2}$$

The latter composite group may be written in the simpler form

$$\frac{G\,(D_2 - D_1)}{\rho\, D_p^{3/2}\, g^{1/2}}$$

and is thus found to be equal to the product of two other well-known groups, viz. the reciprocal of the group $D_p/(D_2 - D_1)$ introduced above, and the square root of the Froude group $G^2/D_p\,\rho^2\,g$ [1, 14].

Figs. 3 and 4 show the eighty-eight experimental curves. The broken line

$$\frac{h\,(D_2 - D_1)}{k}\left(\frac{D_1}{D_2} \times \frac{D_p}{D_2 - D_1} \times \frac{k}{c\mu}\right)^{1/3} = E\left\{\frac{G\,(D_2 - D_1)}{\rho\, D_p^{3/2}\, g^{1/2}}\right\}^F$$

where

$E = 0{\cdot}105 \times 10^{-3}$ and $F = 2{\cdot}0$ when

$$\frac{G\,(D_2 - D_1)}{\rho\, D_p^{3/2}\, g^{1/2}} < 1070$$

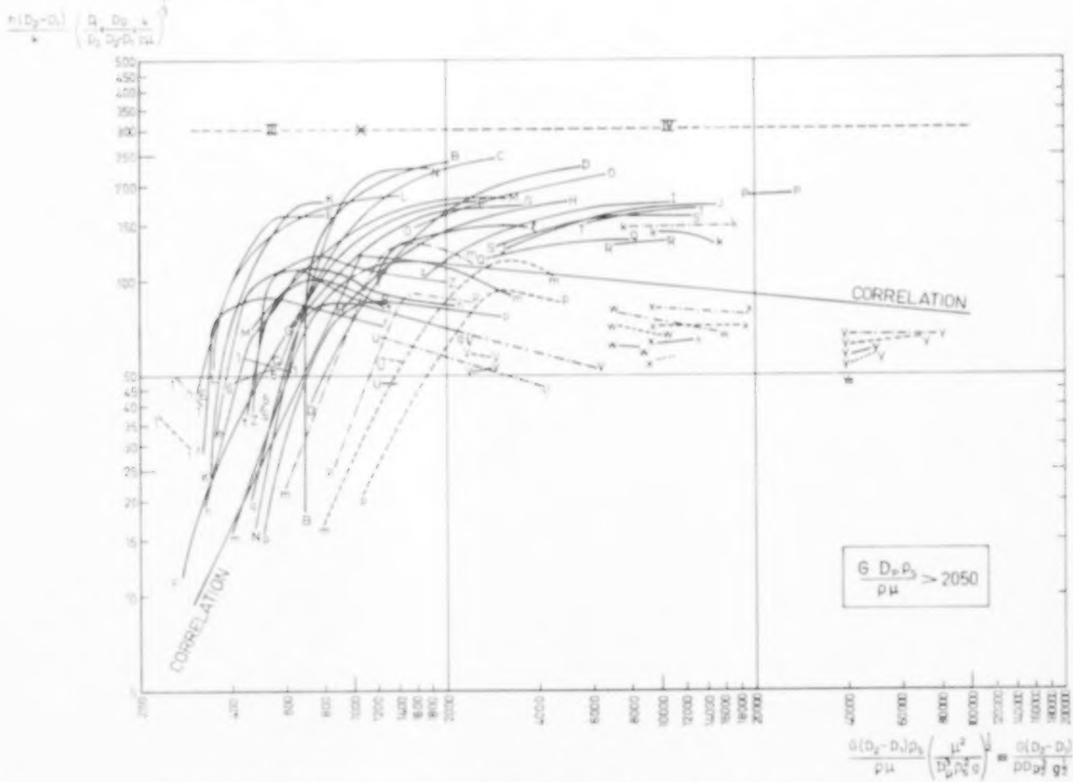

Fig. 3. Correlation of results of experiments in Tables 1 and 2 (see also Fig. 4).

VOL 11 1959

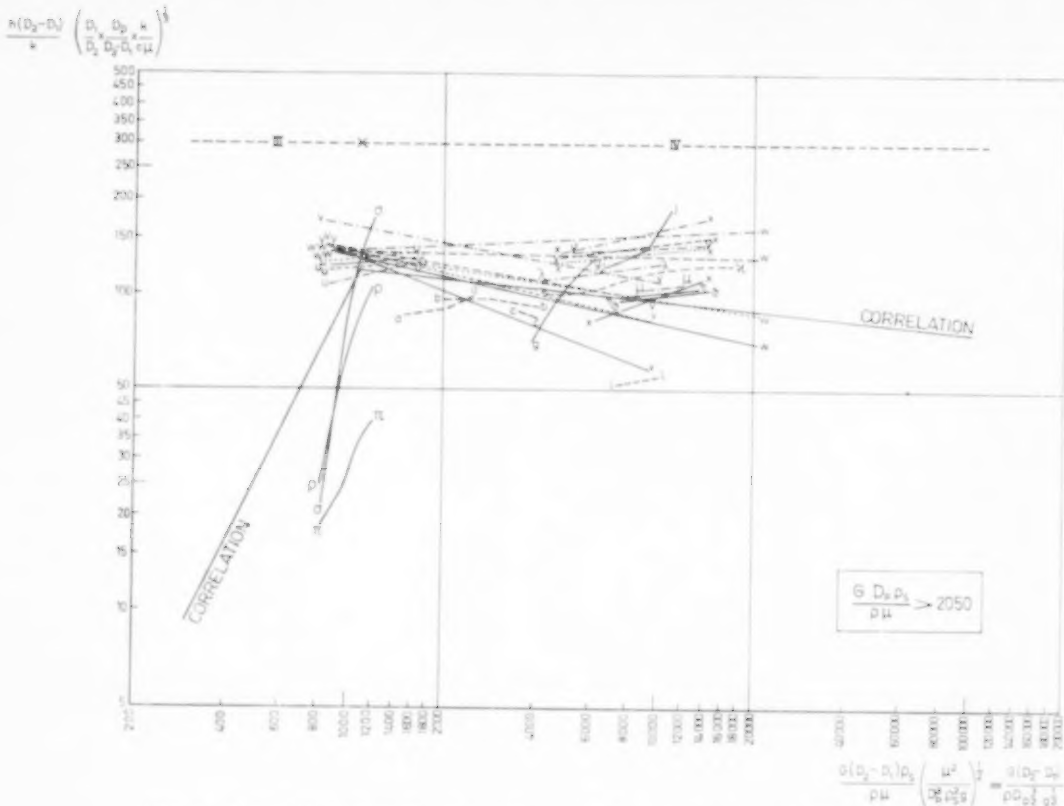

FIG. 4. Correlation of results of experiments in Tables 1 and 2 (see also Fig. 3).

VOL. 11 959/60

and $E = 240$ and $F = -0{\cdot}10$ when

$$\frac{G\,(D_2 - D_1)}{\rho\, D_p^{3/2}\, g^{1/2}} > 1070$$

has been drawn through the set of curves. Again, the co-ordinates of any point of these curves differ by no more than a factor 2·2 from those of the nearest point of the broken line.

The deviations between the experimental curves and the correlation lines in Figs. 1–4 are larger than those for horizontal tubes [1]. But then the latter were derived from our own experiments only, since there are no other data available in the literature, whereas the former are based on experiments by a great number of authors as specified in Table 1. There are wide differences between their experimental set-ups; the main dimensions are given in Table 1. It is known that the dimensions [11, 15] and configuration [4, 10] of the axial heating or cooling cylinders, as well as the method of introducing the fluidizing gas [12], greatly affect the experimental results. The greater part of the differences between the experimental curves in Figs. 1–4 may be ascribed to these influences, which cannot be described quantitatively in detail as is the case for the variables contained in the correlations, because the number of systematic experiments concerned is too small.

In their attempt to establish a general correlation WENDER and COOPER [16] included a restricted number of the experimental results of some of the authors listed in Table 1 [3, 4, 7, 10, 11]. The deviations between these experimental data and their correlation line are much larger than those in Figs. 1–4.

When the mass velocity G is increased at constant gas density and bed temperature, the correlations predict a rapid increase in h in Part I of Figs. 1 and 2 and in Part III of Figs. 3

and 4. The values of G involved there will not be much greater than the minimum value at which fluidization can occur. In Part II of Figs. 1 and 2 there will be a moderate increase in h. Owing to the higher values of G which correspond to this region, fluidization may be more pronounced than in Part I, but the bed is still assumed to behave like a flowing gas or liquid. In Part IV of Figs. 3 and 4, however, there will be a slight decrease in h. Here intense fluidization takes place with high bed porosities [2], and the paths of the particles differ essentially from those of the gas. A number of experimental curves obtained with increasing mass velocity clearly show the transition from a rapid increase in h via a moderate increase to a slight decrease [7, 9]; others do not cover more than one [4, 10, 12] or two [3, 11] of these stages. According to the correlations, h always attains its maximum value when G is increased to such an extent that the transition to Part IV of Figs. 3 and 4 just takes place. At lower values of G the conditions may be represented either by Part III or by some part of Figs. 1 and 2.

In the latter case the mass velocity at which h attains its maximum value follows from

$$\frac{G D_p \rho_s}{\rho \mu} = 2550$$

while, of course, at the same time the condition

$$\frac{G (D_2 - D_1)}{\rho\, D_p^{3/2}\, g^{1/2}} > 1070$$

has to be satisfied. Since any application of the correlations is subject to an uncertainty, it may be advised to take a mass velocity twice as high as the value corresponding to the maximum in h, in order to make certain that the transition to Part IV will already have taken place. Then the result will be a coefficient of heat transfer equal to $2^{-0.10} = 0.93$ times the maximum value according to the correlation; the difference is unimportant in view of the uncertainty in any application of the correlations.

When the diameter D_1 of the axial cylinder is increased while mass velocity, bed temperature, particle properties and bed diameter are kept constant, the correlations predict a decrease in h in Parts I and III, the same in Part II as long as $D_1 < D_2/2.68$, and also in Part IV as long as $D_1 < D_2/3.30$.

Since Table 1 shows that in all experiments on which the correlations are based the ratio $D_2/D_1 > 4.40$ [3], it is not permitted to apply them when the ratio is as low as 2·68 or 3·30 anyhow.

Therefore, for values of D_2/D_1 such that the correlations are applicable, they always predict decrease in h. It follows that the use of tubes of small diameter is always to be recommended when it is desired to obtain high heat-transfer coefficients.

Similar statements about the effects of other pertinent variables on h can easily be derived from the correlation formulae. In practical applications it will seldom be possible to vary a quantity such as G, D_p, D_2 and D_1 while keeping the others constant. If certain relations between these quantities are given it is, of course, possible to derive from the correlations the combined influence on h. An example will be worked out in the appendix.

4. RANGE OF VALIDITY OF THE CORRELATIONS

In view of the derivation of the correlation for *fine and light particles*, it is permissible to apply it when the relevant dimensionless groups are within or nearly within the range covered by the experiments. Therefore it is recommended that it be applied only in such cases where:

the Reynolds group $G D_p \rho_s / \rho\mu$ is smaller than 2050 [1];

the Reynolds group $G (D_2 - D_1) \rho_s / \rho\mu$ is between 0.1×10^6 and 5×10^6;

the Prandtl group $c\mu/k$ is between 0·06 and 1·5;

the ratio D_2/D_1 is between 4·0 and 25.

In the range of *coarse and heavy particles* the groups

$$\frac{\mu^2}{D_p^3\, \rho_s^2\, g} \quad \text{and} \quad \frac{D_p}{D_2 - D_1}$$

have been introduced only as a means of arriving at a useful correlation of the experimental data.

VOL.
11
959/60

Table 2. *Specification of experimental curves in Figs.* 1–4

Reference	Remarks	Particles	Gas	Average particle diameter (μ)	Diameter of axial cylinder D_1 (m)	Diameter of fluidized bed, D_2 (m)	Heated length of cylinder (m)	Bed temperature (°C)	Mass velocity of gas G (kg/m^2 sec)	Heat-transfer coefficient h (J/m^{2}sec°C)	See Fig. nos.	Curve in Figs. 1–4
[3]		Fe	air	375	0·0318	0·1397	0·1016	24–27	0·203–0·585	33–419	3	B —— B
		Fe		301				23–27	0·114–0·580	101–469	3	C —— C
		Fe		195				22–24	0·076–0·582	89–499	3	D —— D
		round sand		879				26–27	0·320–0·824	71–260	3	E —— E
		round sand		323				24–25	0·060–0·574	25–398	3	F —— F
		foundry sand		276				23–24	0·110–0·632	164–408	3	G —— G
		foundry sand		218				23–24	0·115–0·631	202–447	3	H —— H
		foundry sand		160				24–25	0·066–0·824	108–487	1 ; 3	I —— I
		foundry sand		128				24–31	0·015–0·824	38–509	1 ; 3	J —— J
		silica		738				19–21	0·269–0·621	39–288	3	K —— K
		silica		503				19–24	0·152–0·623	100–342	3	L —— L
		silica		314				25–27	0·105–0·731	156–404	3	M —— M
		glass beads		460				23–27	0·177–0·639	32–442	3	N —— N
		glass beads		158				21–32	0·030–0·527	20–596	1 ; 3	O —— O
		glass beads		60				25–27	0·016–0·481	72–741	1 ; 3	P —— P
		cracking catalyst		139				20–24	0·016–0·497	48–387	1 ; 3	Q —— Q
		cracking catalyst		98				24–27	0·009–0·410	24–435	1 ; 3	R —— R
		Al_2O_3		117				17–27	0·021–0·594	63–492	1 ; 3	S —— S
[3]		Al_2O_3	air	95	0·0318	0·1397	0·1016	18–22	0·021–0·438	93–554	1 ; 3	T —— T
[4]	Lowest section of heating element	glass beads	air	452	0·01248	0·0730	0·2191	57–82	0·650–2·03	175–262	3	U -·-· U
				284				63–94	0·628–1·55	235–329		V -·-· V
				155				74–101	0·716–1·60	376–466		W -·-· W
				101				93–103	0·518–1·00	509–564		X -·-· X
[4]		glass beads	air	40	0·01248	0·0730	0·2191	102–111	0·523–0·944	601–652	3	Y -·-· Y
[4]	Higher section of heating element	glass beads	air	452	0·01248	0·0730	0·2191	82	0·650	223	3	U - - - -
				284				89–94	0·628–0·706	256–287		V - - - - V
				155				92–101	0·716–0·977	388–422		W - - - - W
				101				96–103	0·518–0·923	444–497		X - - - - X
[4]		glass beads	air	40	0·01248	0·0730	0·2191	102–111	0·523–0·894	562–607	3	Y - - - - Y
[4]	Still higher section	glass beads	air	101	0·01248	0·0730	0·2191	103	0·518	379	3	X . . . .
[4]		glass beads	air	40	0·01248	0·0730	0·2191	104–111	0·523–0·606	503–542	3	Y . . . . Y
[4]	Highest section	glass beads	air	40	0·01248	0·0730	0·2191	104	0·541	447	3	Y
[4]	Average over whole height of heating element	glass beads	air	452	0·01248	0·0730	0·8763	82	0·650	185	3	U ——
				284				89–94	0·628–0·706	237–253		V —— V
				155				98–101	0·716–0·844	361–370		W —— W
				101				98–103	0·518–0·654	428–440		X —— X
[4]		glass beads	air	40	0·01248	0·0730	0·8763	104–111	0·523–0·606	532–568	3	Y —— Y
[5]		glass beads	air	900	0·0127	0·1000	0·0330	20	0·567–2·56	84–262	3	Z —— Z
[6]	Cooled tube	SiC	air	249	0·00953	0·0508	0·5683	133–261	0·119–0·137	332–403	3	1 —— 1
		SiC		178				123–219	0·052–0·075	485–527	2	2 —— 2
		SiC		124				103–221	0·042–0·072	445–516	2	3 —— 3
		SiC		97				146–241	0·029–0·056	494–715	2	4 —— 4
		Al_2O_3		249				193–201	0·126	274–284	3	5 —— 5
		Al_2O_3		178				147–173	0·067–0·093	356–384	3	6 —— 6
		Al_2O_3		124				117–228	0·049–0·083	406–491	2	7 —— 7
[6]	Cooled tube	Al_2O_3	air	97	0·00953	0·0508	0·5683	150–216	0·024	536–556	2	8 —— 8
[6]	Cooled tube	SiC	He	249	0·00953	0·0508	0·5683	94–190	0·010	659–699	3	1 - - - - 1
			He	178				141–178	0·009	880–909	2	2 - - - - 2
			He	124				143–174	0·009	971–1061	2	3 - - - - 3
			CO_2	249				209–235	0·101	239–252	3	1 -·-· 1
			CO_2	178				179–225	0·056	278–310	2	2 -·-· 2
			CO_2	124				165–209	0·052	354–432	2	3 -·-· 3
[6]	Cooled tube	SiC	CO_2	97	0·00953	0·0204	0·5683	154–239	0·042	392–415	2	4 -·-· 4
[7]		round sand	air	158	0·00953	0·1016	0·3715	29–242	0·038–0·214	375–488	2 ; 4	a - - - - a
		round sand		137				71–160	0·037–0·250	455–550	2 ; 4	b - - - - b
		round sand		118								

		round sand	air	158	0·00953	0·1016	0·5715	29–242	0·038–0·214	375–488	2 : 4	a - - - - a
		round sand		137				71–160	0·037–0·250	455–550	2 : 4	b - - - - b
		round sand		118				122–160	0·026–0·162	426–507	2 : 4	c - - - - c
		cracking catalyst		48				189–345	0·022–0·090	273–352	2	d - - - - d
[7]		regenerated catalyst	air	38	0·00953	0·1016	0·5715	71–112	0·033–0·100	329–460	2	e - - - - e
[8]	Cooled tube	sharp sand	air	215	0·0338	0·565	1·183	40–220	0·091	112–230	4	g —— g
[8]	Cooled tube	sharp sand	air	215	0·0338	0·565	1·183	40–240	0·155	176–407	4	j —— g
[9]		SiC	air	65	0·0127–0·0133	0·1000	0·0330–0·0366	20	0·009–0·35	35–710	1 : 3	k —— k
		SiC	air	150					0·037–0·31	58–570	1 : 3	l —— l
		sand	air	315					0·098–0·85	49–361	3	m —— m
		sand	air	450					0·136–0·90	54–291	3	n —— n
		sand	air	750					0·32–1·22	80–256	3	o —— o
		Al	air	310					0·123–0·76	51–285	3	p —— p
		Al	air	450					0·197–1·05	59–250	3	q —— q
		Al	air	750					0·295–1·14	71–221	3	r —— r
		glass beads	air	900					0·54–1·54	84–227	3	t —— t
		sand	H_2	315					0·197–1·12	157–1080	3	m - - - - m
		Al	H_2	310					0·258–1·12	206–908	3	p - - - - p
		SiC	CO_2	65					0·012–0·37	35–512	1 : 3	k - . - . k
		sand	CO_2	315					0·148–0·60	46–279	3	m - . - . m
[9]		Al	CO_2	310	0·0127–0·0133	0·1000	0·0330–0·0366	20	0·209–0·56	58–186	3	p - . - . p
[10]	Lowest section of heating element	glass beads	air	848	0·0127	0·1200	0·1270	93	0·661–1·25	266–317	4	u - . - . u
				376					0·192–2·10	366–562	4	v - . - . v
				219					0·090–2·07	539–627	4	w - . - . w
				106					0·140–0·471	657–868	2 : 4	x - . - . x
[10]		glass beads	air	55	0·0127	0·1200	0·1270	93	0·032–0·268	[illegible]	2	y - . - . y
[10]	Higher section of heating element	glass beads	air	848	0·0127	0·1200	0·1270	93	0·661–1·25	302–318	4	u - - - - u
				376					0·192–2·10	318–470	4	v - - - - v
				219					0·090–2·07	510–539	5	w - - - - w
				106					0·140–0·471	652–757	2 : 4	x - - - - x
[10]		glass beads	air	55	0·0127	0·1200	0·1270	93	0·032–0·268	488–674	2	y - - - - y
[10]	Still higher section of heating element	glass beads	air	848	0·0127	0·1200	0·1270	93	0·661–1·25	315–338	4	u . . . . u
				376					0·192–2·10	285–470	4	v v
				219					0·090–2·07	340–539	4	w . . . . w
				106					0·140–0·471	634–713	2 : 4	x x
[10]		glass beads	air	55	0·0127	0·1200	0·1270	93	0·032–0·268	504–752	2	y . . . . y
[10]	Highest section of heating element	glass beads	air	848	0·0127	0·1200	0·1270	93	0·661–1·25	310–324	4	u —— u
				376					0·192–2·10	184–470	4	v —— v
				219					0·090–2·07	274–539	4	w —— w
				106					0·140–0·471	419–560	4	x —— x
[10]		glass beads	air	55	0·0127	0·1200	0·1270	93	0·032–0·268	509–755	2	y —— y
[11]		microspheres	air	68	0·00635	0·1016	0·1524	34	0·039–0·187	358–437	1	α —— α
			air					34	0·035–0·284	323–392		β —— β
			He					13	0·005–0·049	580–687		γ - - - - γ
			CH_4					32	0·018–0·157	318–392		δ - - - - δ
			NH_3					−16	0·030–0·110	415–608		ϵ - . - . ϵ
[11]		microspheres	A	68	0·00635	0·1016	0·1524	32	0·044–0·386	278–340	1	ζ - . - . ζ
[11]		glass beads	air	83	0·00635	0·1016	0·1524	20	0·016–0·402	455–608	1 : 4	η —— η
			air					20	0·017–0·423	404–620		ϑ —— ϑ
			He					3	0·006–0·043	818–1004		ι - - - - ι
			CH_4					15	0·012–0·283	517–705		κ - - - - κ
			NH_3					0	0·020–0·196	386–574		λ - . - . λ
			A					21	0·025–0·456	415–516		μ - . - . μ
[11]		glass beads	CCl_2F_2	83	0·00635	0·1016	0·1524	36	0·084–1·61	289–403	1 : 4	ν - . - . ν
[12]	30 μ pores in ceramic bottom plate	sand	air	450	0·01000	0·200	0·1250	20	0·171–0·251	45–97	4	π —— π
[12]	90 μ pores									61–256		ρ —— ρ
[12]	150 μ pores	sand	air	450	0·01000	0·200	0·1250	20	0·171–0·251	52–418	4	σ —— σ

It follows that its application can be recommended only when ;

the Reynolds group $G D_p \rho_s/\rho\mu > 2550$;

all the variables are within or nearly within the range covered by the experiments as specified in the last column of Table 3 in the appendix.

For values of the Reynolds group $G D_p \rho_s/\rho\mu$ between 2050 and 2550 it is recommended that the average of the values given by the two correlations be considered as a good prediction of the heat-transfer coefficient h.

The correlations in Figs. 1–4 apply to heat transfer between fluidized beds and axially positioned cylinders only. Coefficients of heat transfer to vertical tubes in eccentric locations are about 1·6–1·8 times as high, when the distance between tube and axis is 0·35–0·71 times the bed radius [8]. Comparative measurements of coefficients of heat transfer at the wall of the bed and in the axis [4, 10] have shown that, depending on conditions of fluidization, the former may be either higher or lower than the latter, but both are lower than those in intermediate locations.

It is impossible to make a good estimate of the magnitude of these effects because the differences between the results of various experiments on heat transfer between fluidized beds and the wall [16, 17] are even larger than those for axial cylinders. In any case the influence of the eccentricity of an inserted tube seems to be smaller than the deviations between some experimental curves and the correlation lines in Figs. 1–4. Therefore, when a reasonable estimate of the average coefficient of heat transfer to a bank of vertical tubes which occupies a great part of the cross-section of the bed is to be made, it may be recommended that the correlations as given in Figs. 1–4 be applied.

Finally, it might be interesting to check how far the correlation established for cases where gas is the fluidizing agent is also valid if this function is performed by a *liquid*. Heat-transfer measurements in this type of system have been reported by WESSER and MARDUS [18], who used water as the fluidizing medium. However, in their case the Reynolds group $G(D_2 - D_1)\,\rho_s/\rho\mu$ was smaller than $0{\cdot}02 \times 10^6$ so that their data are outside the scope of our considerations. The production to the left of the straight line in Part II of Figs. 1 and 2 happens to be a reasonable representation of their experimental results.

5. APPENDIX

5.1 *Experimental data and conditions*

Table 2 specifies the experimental data pertaining to each curve in Figs. 1–4. Those experiments of MICKLEY and TRILLING [4] in which the bed porosity was higher than 0·70 have not been included, since they are outside the scope of the present investigation [8]. This limitation does not affect any of our conclusions. OLIN and DEAN [7] paid special attention to the influence of fouling of the particles on heat transfer. Only their results obtained with clean particles have been considered. The data obtained by WICKE and FETTING [9] with activated charcoal particles have not been included since the particle density is not reported. They state that in three other cases fluidization was disturbed by slugging phenomena. These cases have also been excluded, although the results obtained with SiC particles fluidized by hydrogen do agree with the correlation. Of course, data obtained at mass velocities so small that fluidization could not occur [3, 5, 9, 12] have not been considered either.

Electrical heating elements were inserted in the axis of the bed by the greater part of the authors ; in two investigations [6, 8] a water-cooled vertical tube was used instead.

Table 3 gives the extreme values of the most essential variables as applied in the experiments. Data for fine and light particles are given separately from those for coarse and heavy particles.

5.2 *Example of application of the formulae*

Suppose that, for a certain annular bed of sand which is to be fluidized the air mass flow rate be Φ_m, and that the pressure, the temperature and the degree of fluidization be given.

Then the mean diameter D_p of the sand particles and the diameters D_1 and D_2 of the cylindrical walls required for maximum coefficient of heat

VOL. 11 1959/60

Table 3. Range of variables in the experiments from which the correlations have been derived

Correlation			*Fine and light particles*	*Coarse and heavy particles*
Abscissa in Figs. 1–2	$\frac{G(D_2 - D_1)\rho_s}{\rho\mu}$		$0{\cdot}067 \times 10^6$ [3] – $3{\cdot}7 \times 10^6$ [3]	
Abscissa in Figs. 3–4	$\frac{G(D_2 - D_1)}{\rho D_p^{3/2} g^{\frac{1}{2}}}$			$0{\cdot}23 \times 10^3$ [6] – 76×10^3 [4]
Mass velocity of gas	G	kg/m² sec	0·005 [11] – 0·62 [11]	0·032 [11] – 2·6 [5]
Bed temperature		°C	– 16 [11] – 345 [7]	0 [11] – 261 [6]
Viscosity of gas at bed temperature	μ	kg/sec m	$9{\cdot}5 \times 10^{-6}$ [11] – $31{\cdot}5 \times 10^{-6}$ [7]	$9{\cdot}5 \times 10^{-6}$ [9] – $28{\cdot}2 \times 10^{-6}$ [6]
Thermal conductivity of gas at bed temperature	k	J/sec m °C	0·010 [11] – 0·20 [6]	0·010 [11] – 0·21 [6]
Density of gas at bed temperature	ρ	kg/m³	0·12 [6] – 4·8 [11]	0·08 [9] – 4·8 [11]
Density of particles	ρ_s	kg/m³	790 [11] – 3900 [6]	1910 [3] – 6950 [3]
Specific heat of particles at bed temperature	c	J/kg °C	675 [9] – 1060 [7]	470 [3] – 970 [7]
Prandtl group at bed temperature	$\frac{c\mu}{k}$		0·097 [11] – 1·00 [11]	0·039 [9] – 0·98 [11]
Mean volume–surface particle diameter [19]	D_p	m	38×10^{-6} [7] – 178×10^{-6} [6]	40×10^{-6} [4] – 900×10^{-6} [5, 9]
Diameter of fluidized bed	D_2	m	0·051 [6] – 0·140 [3]	0·051 [6] – 0·565 [8]
Outside diameter of vertical tube	D_1	m	0·006 [11] – 0·032 [3]	0·006 [11] – 0·034 [8]
Ratio of diameter D_2 to D_1	$\frac{D_2}{D_1}$		4·40 [3] – 16·0 [11]	4·40 [3] – 20·0 [12]
Equivalent diameter of annulus	$D_2 - D_1$	m	0·041 [6] – 0·108 [3]	0·041 [6] – 0·531 [8]
Ratio of particle diameter to equivalent diameter of annulus	$\frac{D_p}{D_2 - D_1}$		$0{\cdot}41 \times 10^{-3}$ [7] – $4{\cdot}3 \times 10^{-3}$ [6]	$0{\cdot}40 \times 10^{-3}$ [8] – $10{\cdot}3 \times 10^{-3}$ [5, 9]
Heated length of vertical tube		m	0·033 [9] – 0·572 [7]	0·033 [5, 9] – 1·18 [8]
Bed height in non-fluidized state		m	0·1 [9] – 1·0 [11]	0·1 [5, 9] – 1·7 [8]
Ratio of bed height to bed diameter			1·0 [9] – 13 [6]	0·7 [12] – 17 [4]
Coefficient of heat transfer between bed and tube	h	J/m² sec °C	20 [3] – 1060 [6]	25 [3] – 1080 [9]

transfer between the bed and the inner wall can be deduced using our correlations.

It follows from the data given for various kinds of sand [1, 2] that the minimum value of the product of mass velocity and kinematic viscosity at which fluidization of the sand could be observed, is approximately proportional to $D_p^{3/2}$, and that the proportionality constant β is equal to $0{\cdot}26\ \mathrm{kg/m^{3/2}\,sec^2}$. Therefore the specified degree of fluidization is conditioned by:

$$G\,\frac{\mu}{\rho} = \kappa\beta\, D_p^{3/2}$$

where κ is a given dimensionless number which is greater than unity. The given mass rate of flow is expressed by:

$$\frac{\pi}{4}(D_2^2 - D_1^2)\,G = \Phi_m$$

Elimination of the mass velocity G gives:

$$D_p^{3/2} = \frac{4\,\Phi_m\,\mu}{\pi\kappa\beta\,(D_2^2 - D_1^2)\,\rho}$$

When the expressions found for G and D_p are substituted in the correlation formulae, the result for the range of fine and light particles reads:

$$\frac{h\,(D_2 - D_1)}{k}\left(\frac{D_1}{D_2}\right)^{1/3}\left(\frac{k}{c\mu}\right)^{1/2} = A\left\{\frac{4\,\Phi_m\,\rho_s}{\pi\,(D_1 + D_2)\,\rho\mu}\right\}^{B}$$

or

$$h = \frac{H}{D_2 - D_1}\left(\frac{D_2}{D_1}\right)^{1/3}\frac{1}{(D_1 + D_2)^B}$$

For the range of coarse and heavy particles one has

$$\frac{h\,(D_2 - D_1)^{2/3}}{k}\left(\frac{D_1}{D_2}\times\frac{k}{c\mu}\right)^{1/3}\times$$
$$\left\{\frac{4\,\Phi_m\,\mu}{\pi\kappa\beta\,(D_2^2 - D_1^2)\,\rho}\right\}^{2/9} = E\left\{\frac{\kappa\beta\,(D_2 - D_1)}{\mu\, g^{1/2}}\right\}^{F}$$

or

$$h = J\,(D_2 - D_1)^{F-4/9}\left(\frac{D_2}{D_1}\right)^{1/3}(D_1 + D_2)^{2/9}$$

Here H and J are constant as long as D_1 and D_2 are the only variables considered.

If, in the first place, the effect of an increase in D_2 at a constant value of D_1 is considered, the formula for *fine and light particles* is found always to predict a decrease in h.

For *coarse and heavy particles* an increase in h is always obtained in Part III of the correlation graph where $F = 2{\cdot}0$, and a decrease is predicted in Part IV where $F = -0{\cdot}10$ as long as $D_2 < 69{\cdot}4\,D_1$; this mathematical condition is always fulfilled when it is permitted to apply the correlation, since the experimental basis covers the range $4{\cdot}0\,D_1 < D_2 < 30\,D_1$ only.

The increase in D_2 is, of course, coupled with a decrease in G which is proportional to $1/(D_2^2 - D_1^2)$, and a decrease in D_p which is proportional to $1/(D_2^2 - D_1^2)^{2/3}$. As long as the conditions remain within the range of fine and light particles, it is desirable to decrease the value of D_2 as far as possible, i.e. until the transition range is reached. At this limit we have

$$\frac{G D_p\,\rho_s}{\rho\mu} = \left\{\frac{4\Phi_m}{\pi\,(D_2^2 - D_1^2)\,\rho}\right\}^{5/3}\times\frac{\rho_s}{(\kappa^2\beta^2\mu)^{1/3}} = 2050$$

If there

$$\frac{\kappa\beta\,(D_2 - D_1)}{\mu\, g^{1/2}} < 1070$$

so that Part III of Figs. 3 and 4 comes into play, a further decrease in D_2 would have a negative effect, the maximum value of h having already been attained. In Part IV where

$$\frac{\kappa\beta\,(D_2 - D_1)}{\mu\, g^{1/2}} > 1070$$

higher values of h can still be obtained by means of a further decrease in D_2, until the maximum ordinate in Figs. 3 and 4 is reached; i.e.

$$\frac{\kappa\beta\,(D_2 - D_1)}{\mu\, g^{1/2}} = 1070$$

Summarizing, the most favourable value of D_2 at constant D_1 is determined by either

$$\left\{\frac{4\,\Phi_m}{\pi\,(D_2^2 - D_1^2)\,\rho}\right\}^{5/3}\times\frac{\rho_s}{(\kappa^2\beta^2\mu)^{1/3}} = 2050\,;$$

$$\frac{\kappa\beta\,(D_2 - D_1)}{\mu\, g^{1/2}} \leqslant 1070$$

or

$$\left\{\frac{4\,\Phi_m}{\pi\,(D_2^2 - D_1^2)\,\rho}\right\}^{5/3} \times \frac{\rho_s}{(\kappa^2\beta^2\mu)^{1/3}} > 2050\,;$$

$$\frac{\kappa\beta\,(D_2 - D_1)}{\mu\, g^{1/2}} = 1070$$

In practice, one will solve each of the equations

$$\left\{\frac{4\,\Phi_m}{\pi\,(D_2^2 - D_1^2)\,\rho}\right\}^{5/3} \times \frac{\rho_s}{(\kappa^2\beta^2\mu)^{1/3}} = 2050 \text{ and}$$

$$\frac{\kappa\beta\,(D_2 - D_1)}{\mu\, g^{1/2}} = 1070$$

for D_2; the smaller of the two values thus found is the correct solution.

In the second place, the effect of an increase in D_1 at a constant value of D_2 can be considered.

The formula for *fine and light particles* predicts a decrease in h as long as $D_1 < D_2/1{\cdot}61$ in Part I of the correlation graph where $B = 3{\cdot}4$, and as long as $D_1 < D_2/3{\cdot}29$ in Part II where $B = 0{\cdot}44$; these mathematical conditions are fulfilled when it is permitted to apply the correlation, i.e. when $4{\cdot}0\ D_1 < D_2 < 25\ D_1$.

For *coarse and heavy particles* a decrease in h is always obtained in Part III of the correlation graph where $F = 2{\cdot}0$, and also in Part IV where $F = -0{\cdot}10$ as long as $D_1 < D_2/2{\cdot}96$; this condition is again fulfilled when it is permitted to apply the correlation, i.e. $4{\cdot}0\ D_1 < D_2 < 30\ D_1$. The increase in D_1 involves an increase in G, and an increase in D_p. In all cases it is desirable to decrease D_1 as far as possible; a lower limit may be set for mechanical reasons or by the requirement that the inside of the vertical tube should be accessible for cleaning or maintenance.

The answer to the question of how to obtain the maximum value of h is, therefore, to choose the diameter D_1 of the inner cylinder as small as possible; then the diameter D_2 of the outer wall can be found as outlined above. The corresponding values of G and D_p can easily be determined. The solution thus obtained is valid only when $4{\cdot}0 < D_2/D_1 < 30$, and when D_p is within or nearly within the region covered by the experiments from which the value of β has been derived, in other words when the mean particle diameter is between 80 and 500 μ.

Numerical example

Let the following numerical data apply:

$\mu = 30 \times 10^{-6}$	kg/sec m
$k = 0{\cdot}0408$	J/sec m °C
$\rho = 0{\cdot}67$	kg/m³
$\rho_s = 2660$	kg/m³
$c = 1030$	J/kg °C
$\Phi_m = 0{\cdot}0010$	kg/sec
$\kappa = 6{\cdot}0$,	

while the minimum allowable tube diameter D_1 is 0·020 m. The maximum ordinate in Figs. 3 and 4 is then reached for $D_2 = 0{\cdot}0844$ m; for these values of D_1 and D_2

$$\left\{\frac{4\,\Phi_m}{\pi\,(D_2^2 - D_1^2)\,\rho}\right\}^{5/3} \times \frac{\rho_s}{(\kappa^2\beta^2\mu)^{1/3}} = 7710$$

$$\text{and} \quad \frac{\kappa\beta\,(D_2 - D_1)}{\mu\, g^{1/2}} = 1070$$

The corresponding values for mass velocity and mean particle diameter are $G = 0{\cdot}189$ kg/m² sec and $D_p = 304 \times 10^{-6}$ m. Since $D_2/D_1 = 4{\cdot}22$ is between 4·0 and 30, and the particle diameter is between 80 and 500 μ, this solution is correct. In this case h follows directly from the maximum value of the ordinate in Figs. 3 and 4:

$$\frac{h\,(D_2 - D_1)}{k}\left(\frac{D_1}{D_2} \times \frac{D_p}{D_2 - D_1} \times \frac{k}{c\mu}\right)^{1/3} = 120$$

whence $h = 668$ J/m² sec °C.

In the preceding discussion of the formulae it has been recommended that the value of the abscissa in Figs. 3 and 4 be chosen twice as high as the value corresponding with the maximum ordinate; the reasons were the uncertainty in the actual position of the maximum and the fact that the ensuing decrease in the calculated value of h was as low as 7 per cent. Although in the present example the decrease in h would be 8·5 per cent because of variations in D_2 and D_p occurring in the ordinate of the graph, this might induce one to choose here also $\kappa\beta\,(D_2 - D_1)/\mu g^{1/2} = 2140$ instead of 1070. In that case, however, D_2 would become so large that the conditions would already be in the range of fine and light particles. It is

therefore certainly not advisable to increase D_2 beyond the value at which the range of fine and light particles is entered, this value being determined by

$$\left\{\frac{4\,\Phi_m}{\pi\,(D_2^2 - D_1^2)\,\rho}\right\}^{5/3} \times \frac{\rho_s}{(\kappa^2 \beta^2 \mu)^{1/3}} = 2050$$

Thus $D_2 = 0{\cdot}124$ m, $\kappa\beta\,(D_2 - D_1)/\mu g^{1/2} = 1730$, $G = 0{\cdot}086$ kg/m² sec, $D_p = 182 \times 10^{-6}$ m. For these values of D_2 and D_p the heat-transfer coefficient is 623 J/m² sec °C according to the correlation for coarse and heavy particles, and 647 J/m² sec °C according to that for fine and light particles. The recommended estimate in the transition range is the average of these two values; it amounts to 635 J/m² sec °C and is lower than the maximum value calculated above by 5 per cent only.

VOL. 11 1959/60

It may be concluded that, in view of the uncertainty in the correlations, it is indeed advisable to choose $D_2 = 0{\cdot}124$ m, $G = 0{\cdot}086$ kg/m² sec, $D_p = 182 \times 10^{-6}$ m instead of the values calculated above.

Notation

A	= proportionality constant	
B	= exponent	
c	= specific heat of particles at bed temperature	J/kg °C
D_p	= mean volume-surface particle diameter [19]	m
D_t	= outer diameter of diametrical tube	m
D_1	= outer diameter of axial cylinder	m
D_2	= diameter of fluidized bed	m
E	= proportionality constant	
F	= exponent	
G	= mass velocity of fluidizing gas	kg/m² sec
g	= acceleration of gravity	m/sec²
H	= proportionality constant	Jm^{B-1}/sec °C
h	= coefficient of heat transfer between bed and tube	J/m² sec °C
J	= proportionality constant	$\mathrm{J/m}^{F+16/9}$ sec °C
k	= thermal conductivity of gas at bed temperature	J/sec m °C
β	= proportionality constant	$\mathrm{kg/m}^{3/2}\,\mathrm{sec}^2$
ϵ	= fraction of voids	
κ	= measure of the intensity of fluidization	
μ	= dynamic viscosity of gas at bed temperature	kg/sec m
ρ	= density of gas at bed temperature	kg/m³
ρ_s	= density of particles	kg/m³
Φ_m	= mass rate of flow of fluidizing gas	kg/sec

References

[1] Vreedenberg H. A. *Chem. Engng. Sci.* 1958 **9** 52.

[2] Vreedenberg, H. A. Proc. General Discussion on Heat Transfer. London 1951 pp. 373 and 389. The Institution of Mechanical Engineers 1951.

[3] Baerg A., Klassen J. and Gishler P. E. *Canad. J. Res.* (F) 1950 **28** 287.

[4] Mickley H. S. and Trilling C. A. *Industr. Engng. Chem.* 1949 **41** 1135.

[5] Wicke E. and Hedden K. *Chem.-Ing.-Tech.* 1952 **24** 82.

[6] Logwinuk A. K. Thesis, Case Institute of Technology, Cleveland, Ohio 1948; Miller C. O. and Logwinuk A. K. *Industr. Engng. Chem.* 1951 **43** 1220.

[7] Olin H. L. and Dean O. C. *Petrol. Engr.* 1953 **25** C23.

[8] Vreedenberg H. A. *J. Appl. Chem.* 1952 **2** (Supplementary issue No. 1) 26.

[9] Wicke E. and Fetting F. *Chem.-Ing.-Tech.* 1954 **26** 301.
Fetting F. and Wicke E. *Dechema-Monogr.* 1955 **24** 146.

[10] Toomey R. D. and Johnstone H. F. *Chem. Engng. Progr.* Symposium Series No. 5 1953 **49** 51.

[11] Mickley H. S. and Fairbanks D. F. *Amer. Inst. Chem. Engrs. J.* 1955 **1** 374.

[12] Brötz W. *Chem.-Ing.-Tech.* 1956 **28** 165.

[13] Walger O. *Chem.-Ing.-Tech.* 1953 **25** 474.

[14] Wilhelm R. H. and Kwauk M. *Chem. Engng. Progr.* 1948 **44** 201.

[15] Kramers H. *Chem. Engng. Sci.* 1958 **8** 45.

[16] Wender L. and Cooper G. T. *Amer. Inst. Chem. Engrs. J.* 1958 **4** 15.

[17] Chin-Yung Wen and Leva M. *Amer. Inst. Chem. Engrs. J.* 1956 **2** 482.

[18] Wesser U. and Mardus G. *Chem.-Ing.-Tech.* 1957 **29** 332.

[19] Dallavalle J. M. *Micromeritics.* Pitmans, London 1948.

Chemical Engineering Science, 1960, Vol. 11, pp. 286 to 292. Pergamon Press Ltd., London. Printed in Great Britain

The motion of a rigid sphere in a frictionless cylinder

J. Happel and P. A. Ast

New York University, Department of Chemical Engineering New York 53, N.Y.

(*Received 5 November 1959*)

Abstract—This investigation was undertaken in order to develop a sphere and cylinder model which would serve as a basis for further theoretical studies of assemblages of particles. Stokes equations of viscous flow were assumed to apply to the steady motion of a rigid sphere along the axis of an infinitely long cylinder. Solution of the problem is carried out under the postulate that the fluid shear on the cylinder walls is everywhere equal to zero.

An exact solution is obtained in the form of an infinite set of linear simultaneous equations for the coefficients in the Stokes' stream function.

The above problem was solved for a sphere to cylinder diameter ratio of 0·1 to 0·7. Results are presented in the form of a plot of the stream lines from the solution of the Stokes' approximation in the viscous flow region. Applications to flow relative to assemblages of particles is discussed.

Résumé—Cette étude a été entreprise dans le but de développer un modèle de sphères et de cylindres, pouvant servir de base à une étude théorique des assemblages de particules. Les équations de Stokes relatives à des écoulements visqueux, sont supposées s'appliquer au mouvement permanent d'une sphère rigide le long d'un axe d'un cylindre infiniment long. La solution du problème est effectuée en supposant que le cisaillement d'un fluide sur les parois du cylindre est partout égal à zéro.

Une solution exacte est obtenue sous forme d'une série infinie d'équations linéaires simultanées pour les coefficients de la fonction d l'écoulement de Stokes.

Le problème ci-dessus a été résolu pour un rapport du diamètre de la sphère au diamètre du cylindre de 0,1 à 0,7. Les résultats sont presentés sous forme d'un diagramme des lignes de l'écoulement provenant de la solution de l'approximation de Stokes dans la région de l'écoulement visqueux. Les applications à un écoulement concernant les assemblages de particules sont discutées.

Zusammenfassung—Diese Untersuchung wurde zur Entwicklung eines Kugel- und Zylindermodells unternommen, das als Grundlage für weitere theoretische Studien über Teilchenansammlungen dienen soll. Die Stokes' schen Gleichungen des viskosen Fliessens wurden als anwendbar angenommen für die gleichförmige Bewegung einer starren Kugel entlang der Achse eines unendlich langen Zylinders. Die Lösung des Problems wird unter der Voraussetzung durchgeführt, dass die Fliess-Beanspruchung der Zylinderwände überall gleich Null ist.

Eine exakte Lösung wird erhalten in Form einer unendlichen Reihe linearer simultaner Gleichungen für die Koeffizienten des Stokes'schen Strömungsgesetzes.

Das erwähnte Problem wurde für ein Durchmesserverhältnis von Kugel und Zylinder von 0,1 bis 0,7 erhalten. Die Ergebnisse sind in Form eines Diagramms der Stromlinien der Stokes'-schen Näherungslösung in zähen Bereich angegeben. Anwendungen auf die Strömung relativ zu Teilchenansammlungen werden diskutiert.

1. Introduction

The development of a "model cell" arrangement which could be used as a basis for theoretical studies involving pressure drop, fluidizing velocity, etc., in packed beds has been the subject of several investigations in the past. Faxen [1] investigated the effect of a rigid sphere moving through a viscous fluid along the axis of a tube employing the Stokes–Oseen resistance law. Wakiya [2] treated the case of a stationary

sphere in the flow of a viscous fluid in Poiseuille flow. Both investigators gave an approximate expression of the sphere drag. HAPPEL and BYRNE [3] arrived at a solution for the case of a moving sphere in the path of a moving viscous fluid by the use of a method of "reflections." In this case the velocity field was decomposed into its components, each of which satisfied the wall boundary conditions exactly and the sphere boundary conditions approximately.

A recent paper by RICHARDSON and ZAKI [4] proposed a cell model derived from the assumption that the sphere was surrounded by a hexagonal envelope of fluid. They were then able to idealize this assumption for the case of a cylindrical envelope and thus give an expression for the approximate drag of the sphere.

HABERMAN [5, 6] presented a method of solution for the case of a stationary or moving sphere located axially in a cylinder through which a viscous fluid flowed. Cylindrical and spherical co-ordinate solutions to Stokes' equations of flow were used to satisfy the boundary conditions on the cylinder and sphere respectively. The cylindrical boundary in this case was a physical wall and hence was not frictionless. KAWAGUTI [7] investigated a similar case, using the method of "reflections" similar to HAPPEL and BYRNE [8]. An approximate expression for the drag of a sphere in a frictionless cylinder was obtained, applicable up to a sphere to cylinder diameter ratio of 0·2–0·3.

The problem discussed in this paper was solved using a modification of HABERMAN's approach. The results are then exactly applicable throughout the entire range of sphere to cylinder ratios, unlike solutions derived in the past where methods other than HABERMAN's were employed.

MOTION OF A SPHERE IN A FRICTIONLESS CYLINDER

The fluid system investigated here is assumed to have such characteristics that Stokes' equations of motion apply. The Stokes' stream function expressed in terms of cylindrical co-ordinates is used to satisfy the boundary conditions on the cylinder walls and at infinity. This expression is then expanded, using both co-ordinate systems for convenience and compared with the stream function expressed directly in spherical co-ordinates. To enable the above comparison to be made, part of the latter expression is transformed into the cylindrical co-ordinate system where necessary. Comparison of the terms then yields a relationship between the constants. The boundary conditions on the sphere yield relationships between the constants in the spherical co-ordinate solution. Substituting the previous relationships into the relationships obtained from the sphere boundary conditions then yields an infinite set of linear simultaneous equations for the solution of the constants.

Theoretical development

The co-ordinate origin is taken at the centre of the sphere and the cylinder is assumed to be moving at a constant velocity U in the negative x-direction (Fig. 1).

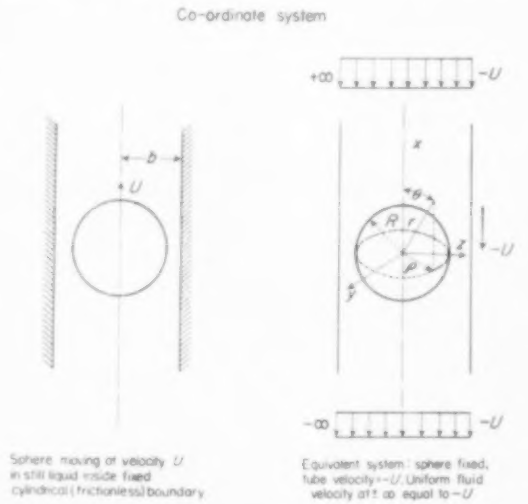

FIG. 1. Co-ordinate system.

The boundary conditions are:

On the surface of the sphere ($r = R$): $v_r = 0$, $v_\theta = 0$.

At infinity ($x = \pm\infty$): $v_x = -U$, $v\rho = 0$.

At the cylinder walls ($\rho = b$): $\dfrac{\partial v_x}{\partial \rho} = 0$, $v\rho = 0$.

The Stokes' stream function expressed in terms of cylindrical co-ordinates is [5]:

$$\psi = \int_0^\infty \left[\rho\, K_1(a\rho) f_1(a) + \rho^2 K_0(a\rho)\, F_1(a) + \right. \\ + \rho\, I_1(a\rho)\, g_1(a) + \\ \left. + \rho\,^2 I_0(a\rho)\, G_1(a)\right] \cos axda \quad (1)$$

The velocity components are:

$$v_x = -\frac{1}{\rho}\frac{\partial\psi}{\partial\rho}, \quad v_\rho = \frac{1}{\rho}\frac{\partial\psi}{\partial x}, \quad v_r = -\frac{1}{r^2 \sin\theta}\frac{\partial\psi}{\partial\theta}.$$

$$v_\theta = \frac{1}{r\sin\theta}\frac{\partial\psi}{\partial r}$$

Satisfaction of the boundary conditions on the cylinder walls yields the following two equations

$$-aK_1(ab)f_1(a) + \left[2K_1(ab) - abK_0(ab)\right]F_1(a) - \\ -aI_1(ab)g_1(a) - \left[2I_1(ab) + abI_0(ab)\right]G_1(a) = 0$$

$$K_1(ab)f_1(a) + bK_0(ab)\,F_m(a) + I_1(ab)g_1(a) + \\ + bI_0(ab)\,G_1(a) = 0 \quad (2)$$

We can therefore solve for $g_1(a)$ and $G_1(a)$ in terms of $f_1(a)$ and $F_1(a)$:

$$G_1(a)\frac{K_1(ab)}{I_1(ab)}F_1(a)$$

$$g_1(a) = -\frac{1}{a}\frac{1}{[I_1(ab)]^2}F_1(a) - \frac{K_1(ab)}{I_1(ab)}f_1(a) \quad (3)$$

Letting

$$S_1 = \frac{K_1(ab)}{I_1(ab)}, \quad S_2 = -\frac{1}{a}\frac{1}{[I_1(ab)]^2} \quad (4)$$

we obtain:

$$g_1(a) = S_2\, F_1(a) - S_1 f_1(a)$$

$$G_1(a) = S_1\, F_1(a) \quad (5)$$

Expansion of the cylindrical co-ordinate stream function yields:

$$\psi(x,\rho) = \int_0^\infty \rho K_1(a\rho)\left[a_0 + a_1 a + a_2 a^2 + \ldots\right]\times \\ \cos axda + \\ + \int_0^\infty \rho^2 K_0(a\rho)\left[b_0 + b_1 a + b_2 a^2 + \ldots\right]\times \\ \cos axda + \\ + \int_0^\infty \left[\rho\, I_1(a\rho)\, g_1(a) + \rho^2 I_0(a\rho)\, G_1(a)\right]\times \\ \cos axda + \frac{U\rho^2}{2} \quad (6)$$

Substituting for the K_0 and K_1 integrals and expanding the remainder of equation (6) in a Taylor series we obtain:

$$\psi = \frac{b_0\pi}{2} r\sin^2\theta + \frac{b_2\pi}{2}\frac{1}{r}\sin^2\theta\,(-3\cos^2\theta + 1) + \\ + \frac{b_4\pi}{2}\frac{1}{r^3}\sin^2\theta\,(-15\cos^2\theta + 9)\cos\theta + \ldots. \\ + \frac{a_1\pi}{2}\frac{1}{r}\sin^2\theta(945\cos^4\theta - 630\cos^2\theta + 45) + \\ + \ldots.. + \frac{1}{2}\rho^2\alpha_2 + \frac{1}{4}x^2\rho^2(-\alpha_4) + \\ + \frac{1}{24}\rho^4\left(\frac{3}{2}\alpha_4 + 3\beta_4\right) + \ldots.. + \frac{U\rho^2}{2} \quad (7)$$

where:

$$\alpha_n = \int_0^\infty \left[g_1(a)\,a + 2\,G_1(a)\right]a^{n-2}\,da$$

$$\beta_n = \int_0^\infty G_1(a)\,a^{n-2}\,da \quad (8)$$

The stream function obtained directly from spherical co-ordinates is ([5], p. 4):

$$\psi(r,\theta) = \sum_{n=2,4,\ldots}^{\infty} C_n^{-1/2}\times \\ \left[A_n r^n + B_n\frac{1}{r^{n-1}} + C_n r^{n+2} + D_n\frac{1}{r^{n-3}}\right] \quad (9)$$

Expansion of the above equation and term by term comparison with equation (7) yields:

$$B_2 = a_1\pi + \frac{2}{5}b_2\pi$$

$$B_n = (-1)^{n/2+1}\times \\ \left[\frac{n!}{2}a_{n-1} + \frac{n(n-1)n!}{2(2n+1)}b_n\right]\pi$$

$$D_2 = b_0\pi$$

$$D_n = (-1)^{n/2+1}\frac{n!}{2(2n-3)}b_{n-2}\pi \quad (10)$$

And since $r^2 = x^2 + \rho^2$ we obtain also:

$$A_2 = \alpha_2 + U$$

$$A_4 = -\frac{\alpha 4}{2} - \frac{\beta 4}{5}$$

$$A_n = (-1)^{n/2+1} \times \left[\frac{\alpha_n}{(n-2)!} + \frac{\beta_n}{(n-4)!\,(2n-3)}\right] \quad (11)$$

$$C_2 = \frac{1}{5}\,\beta_4$$

$$C_n = (-1)^{n/2+1}\,\frac{\beta_{n+2}}{(n-2)!\,(2n+1)} \quad (12)$$

Letting

$$S_1^{\,n} = \int_0^\infty S_1\,(ab)^n\,d\,(ab) \quad (13)$$

$$S_2^{\,n} = \int_0^\infty S_2\,(ab)^n\,\frac{d\,(ab)}{b} \quad (14)$$

VOL. 11 1959/60

and from the boundary conditions on the sphere we have:

$$v_r = 0 = -\sum_{n=2,4}^{\infty} P_{n-1} \times \left[A_n\,r^{n-2} + B_n\,\frac{1}{r^{n+1}} + C_n\,r^n + D_n\,\frac{1}{r^{n-1}}\right]$$

$$v_\theta = 0 = \sum_{2,4..}^{\infty} \frac{C_n^{-1/2}}{\sin\theta} \times \left[n\,A_n\,r^{n-2} - (n-1)\,B_n\,\frac{1}{r^{n+1}} + (n+2)\,C_n\,r^n - (n-3)\,D_n\,\frac{1}{r^{n-1}}\right] \quad (15)$$

Hence:

$$A_n = -\frac{2n+1}{2}\,B_n\,\frac{1}{R^{2n-1}} - \frac{2n-1}{2}\,D_n\,\frac{1}{R^{2n-3}} \quad (16)$$

$$C_n = \frac{2n-1}{2}\,B_n\,\frac{1}{R^{2n+1}} + \frac{2n-3}{2}\,D_n\,\frac{1}{R^{2n-1}} \quad (17)$$

and:

$$A_2 = \sum_{m=0,2\ldots}^{\infty} \frac{b_m}{R^{m+1}}\,(S_2^{\,m+1} + 2S_1^{\,m})\,\lambda^{m+1} - \sum_{m=1,3\ldots}^{\infty} \frac{a_m}{R^{m+2}}\,S_1^{\,m+1}\,\lambda^{m+2} + U \quad (18)$$

$$C_n = (-1)^{n/2+1}\,\frac{1}{R_n}\,\frac{1}{(n-2)!\,(2n+1)} \times \left[\sum_{m=0,2\ldots}^{\infty} \frac{b_m}{R^{m+1}}\,S_1^{\,n+m}\,\lambda^{n+m+1}\right] \quad (19)$$

etc.

From A_2, A_n, C_2, C_n we get the infinite set of linear simultaneous equations for b_0, $b_2 \ldots\ldots a_1$, $a_3 \ldots\ldots$

$$\frac{b_0}{R}\left[\frac{3\pi}{2} - 3{\cdot}52\,\lambda\right] + \frac{b_2}{R^3}\left[\pi - 2{\cdot}60\,\lambda^3\right] + \frac{a_1}{R^3}\left[\frac{5\pi}{2} - 2{\cdot}4\,\lambda^3\right] + \frac{a_3}{R^5}\left[-3{\cdot}225\,\lambda^5\right] + \ldots = -U$$

$$\frac{b_0}{R}\left[-0{\cdot}82\,\lambda^3\right] + \frac{b_2}{R^3}\left[\frac{42\pi}{5} - 4{\cdot}755\,\lambda^5\right] + \frac{a_1}{R^3}\left[-1{\cdot}6125\,\lambda^7\right] + \frac{a_3}{R^5}\left[54\pi - 9{\cdot}75\,\lambda^5\right] + \ldots = 0$$

$$\frac{b_0}{R}\left[\frac{5\pi}{2} - 2{\cdot}40\,\lambda^3\right] + \frac{b_2}{R^3}\left[3\pi - 3{\cdot}225\,\lambda^5\right] + \frac{a_1}{R^3}\left[\frac{15\pi}{2}\right] + \ldots = 0$$

$$\frac{b_0}{R}\left[-0{\cdot}17916\,\lambda^5\right] + \frac{b_2}{R^3}\left[6\pi - 1{\cdot}82\,\lambda^7\right] + \frac{a_3}{R^5}\left[42\pi\right] + \ldots = 0 \quad (20)$$

etc.

For the present purpose it was ascertained that the infinite series could be evaluated with sufficient accuracy to determine the drag coefficient by using eight simultaneous equations as shown in equation (20).

In order to test the applicability of the method numerical computations were carried out for a range of λ from 0·1 to 0·7 using an I.B.M. 650 computer.

For example:

for $\lambda = R/b = 0{\cdot}1$ and $R = 1$, the constants are:

$b_0 = -0{\cdot}57340\,U$
$b_2 = -0{\cdot}00021622\,U$
$a_1 = 0{\cdot}19116\,U$
$a_3 = 0{\cdot}000030881\,U$
etc. . . . .

The drag on the sphere has been shown to be [5],

$$d = -4\pi^2\,\mu\,b_0 \quad (21)$$

A wall correction factor can be defined on the basis of the drag on a sphere in an infinite medium (i.e. $D = 6\pi \mu RU$) as follows:

$$K = \frac{-4\pi^2 \mu b_0}{6\pi \mu RU} = \frac{-2\pi}{3} \frac{b_0}{UR} \tag{22}$$

Thus we have:

Table 1. *Correction factors to Stokes' drag*

Sphere to cylinder diameter ratio λ	(eq. 22) K	*Solids conc.* (eq. 26) ϕ	(eq. 27) K'
0·0	1·000	0·000	1·000
0·1	1·201	0·001	1·177
0·2	1·495	0·008	1·429
0·3	1·935	0·027	1·811
0·4	2·665	0·064	2·450
0·5	3·991	0·125	3·632
0·6	6·965	0·216	6·188
0·7	18·269	0·343	13·280

In the dilute range KAWAGUTI's [7] theoretical treatment is available for comparison with our result. He gives,

$$K = \frac{1}{1 - 1{\cdot}64931\,\lambda + 0{\cdot}79680\,\lambda^2}. \tag{23}$$

For $\lambda = 0{\cdot}1$, equation (23) gives a value for $K = 1{\cdot}198$, which is in excellent agreement with the value from Table 1, indicating the validity of the reflection technique in the dilute range.

No theoretical treatment or data are available for directly checking the value of K in the more concentrated region. It is difficult to see how a frictionless tube could be set up experimentally so HABERMAN's [6] result for a sphere in an actual cylindrical duct was checked experimentally. These data [9] not reported in detail here showed agreement to within several per cent of the theoretical result in the case of $\lambda = 0{\cdot}8$, for the drag on a sphere suspended in a viscous fluid.

It was also thought to be of interest to establish the nature of the fluid flow pattern for this model, since the rate of decay of velocity in an axial direction should represent the most extreme case encountered in sedimenting systems (i.e. the case for no spheres above or below the one we choose to consider). This evaluation was carried out numerically for the case of $\lambda = 0{\cdot}6$, using the values for the constants b_0, b_2, a_1 and a_3.

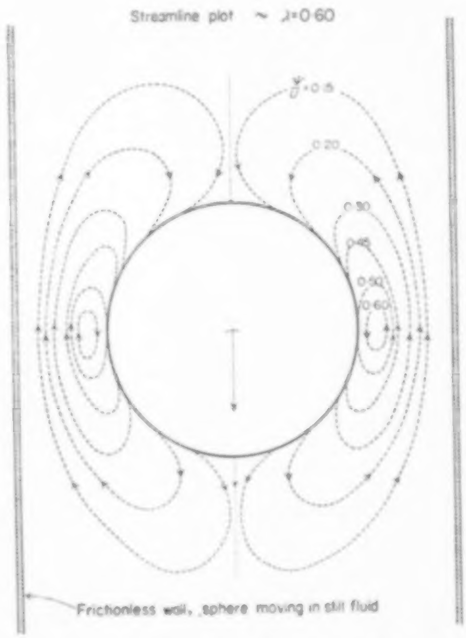

FIG. 2. Streamline plot $\sim \lambda = 0{\cdot}60$.

Thus we obtain:

$$A_2 = +\,7{\cdot}759\,U$$
$$A_4 = -\,0{\cdot}564\,U$$
$$B_2 = +\,3{\cdot}32\,U$$
$$B_4 = -\,1{\cdot}466\,U$$
$$C_2 = -\,0{\cdot}367\,U$$
$$C_4 = +\,0{\cdot}0486\,U$$
$$D_2 = -\,10{\cdot}750\,U$$
$$D_4 = +\,2{\cdot}087\,U$$

To check the accuracy of the constant evaluations we find the velocity forward of the sphere at $R = 1$:

VOL 11 1959/

$$v_r = - \cos\theta \left[B_2 \frac{1}{r^3} + A_2 + C_2 r^2 + D_2 \frac{1}{r} \right] - \frac{1}{2}(5\cos^3\theta - 3\cos\theta) \times \left[A_4 r^2 + C_4 r^4 + D_4 \frac{1}{r^3} + B_4 \frac{1}{r^5} \right] + \ldots\ldots + U\cos\theta \quad (24)$$

$v_r = 0{\cdot}95\ U = 95$ per cent of U, which is sufficiently close.

Substitution of the constants in $\psi(r, \theta)$:

$$\psi(r, \theta) = \sum_{n=2,4..}^{\infty} C_n^{-1/2} \left[A_n r^n + B_n \frac{1}{r^{n-1}} + C_n r^{n+2} + D_n \frac{1}{r^{n-3}} \right] \quad (25)$$

yields the streamline plot shown below ($\lambda = 0{\cdot}6$):

Of special interest is the axial velocity component v_r, forward of the sphere. For this case substitution in equation (24) yields the following:

r	*sphere diameters*	v_r
1	on sphere	$0{\cdot}95\ U \sim 1\ U$
2	0·5	$0{\cdot}93\ U$
3·5	1·25	$0{\cdot}30\ U$
3·6	1·30	$0{\cdot}020\ U$
3·605	1·302	$0{\cdot}005\ U$

Thus the velocity is negligible at a distance over 1·3 diameters from the sphere.

Application

The development above is applicable to the calculation of drag on an assemblage of particles based on the model of a cylindrical fluid envelope surrounding each particle, if an appropriate assumption can be made relating the model to the concentration of solids in the assemblage. The value of $R/b = \lambda$ only fixes the sphere diameter to cylinder diameter. In addition it is necessary in effect to establish the cylinder length of a unit cell to obtain a relationship between λ and the solids concentration ϕ of the form:

$$\phi = k\,\lambda^3 \quad (26)$$

Assumptions made by Richardson and Zaki and by Kawaguti give values of k ranging from 0·94 to 1·03 depending on the arrangement assumed in the assemblage. We have taken $k = 1$ here on the basis that the effect of the shape of the outside boundary is not important. This same relationship would apply in the case of a spherical outer cell boundary. Values of ϕ corresponding to $k = 1$ are tabulated in Table 1. The values of K in this Table then give the resistance experience by a sedimenting sphere in a suspension of solids concentration ϕ as compared with the drag on a sphere in an infinite medium. Thus, for example, at a solids concentration of $\phi = 0{\cdot}125$, $K = 3{\cdot}991$ so that the drag on each sphere in such as assemblage would be predicted equal to $3{\cdot}991 \times$ (Stokes' Law drag). Or in other words the spheres in such an assemblage would sediment at a rate equal to $1/(3{\cdot}991)$ as fast as if they were settling in an infinite medium.

It is interesting to compare the predictions of the sphere–cylinder model employed in this paper with a similar mathematical treatment [8], which has been shown to be in good agreement with a substantial amount of experimental data previously published. This latter model is based on the assumption that two concentric spheres can serve as the model for a random assemblage of spheres moving relative to a fluid. The inner sphere comprises one of the particles in the assemblage and the outer sphere consists of a fluid envelope with a "free surface." This treatment gives the following value for the correction factor K' to Stokes' Law:

$$K' = \frac{3 + 2\,\phi^{5/3}}{3 - \frac{9}{2}\phi^{1/3} + \frac{9}{2}\phi^{5/3} - 3\,\phi^2} \quad (27)$$

Values of K' obtained from equation (27) agree reasonably well with values of K predicted on the basis $\phi = \lambda^3$ by the sphere–cylinder model, up to $\phi = 0{\cdot}216$, where K is approximately 11 per cent below the corresponding value of K'.

Our results do not agree very well with those derived theoretically by Richardson and Zaki [4], who obtained substantially smaller values for the Stokes' law correction factor K. Their theoretical treatment assumes that the spheres in

an assemblage will be lined up directly one above the other and this may account for the smaller resistance to flow thus predicted. These authors also obtained experimental data on fluidization which is in agreement with their predicted relationships. Their results are discussed and compared with other data in reference [8]. Review of the large amount of data in this field [8] indicates a considerable spread, with values of K up to 100 per cent lower than predicted by our treatment. It appears that in range $\phi \simeq 0{\cdot}05$ to $0{\cdot}40$, the value of K may not be uniquely determined by ϕ alone, but that particle arrangement may also be an important variable.

The present result is considered to be of interest since it involves an exact solution of the boundary value problem proposed by various authors as a model of a sedimenting assemblage. It appears to be in good agreement with analogous theoretical treatments and throws light on the extent of disturbance of fluid motion near particles in sedimenting systems. It is demonstrated that in cell models for predicting sedimentation dynamics the shape of the outer fluid boundary assumed is not important up to substantial solids concentration.

Acknowledgements—This research was supported by a grant from the Petroleum Research Fund administered by the American Chemical Society. Grateful acknowledgement is hereby made to the donors. We would also like to thank Howard Brenner for his assistance and Herbert Setzer for his help in the computer programming.

Notation

a^2 = constant

a_n, b_n = constants in cylindrical co-ordinate solution

A_n, B_n, C_n, D_n = constants in spherical co-ordinates

b = radius of cylinder

c_n = constants

$C_n^{-1/2}(\cos\theta)$ = Gegenbauer polynomial

D = drag of sphere

$f_1(a), F_1(a), g_1(a), G_1(a)$ = constant functions

I_0 = modified Bessel function, first kind, zero order

I_1 = modified Bessel function, first kind, first order

K, K' = correction factors to drag as determined by Stokes' Law (equation 22 and equation 27)

K_0 = modified Bessel function, second kind, zero order

K_1 = modified Bessel function, second kind, first order

n = integer

$P_n(\cos\theta)$ = Legendre polynomial

r, θ = spherical co-ordinates

R = radius of sphere

S_1^n, S_2^{n+1} = integrals defined by equations (13), (14)

U = uniform velocity

$v_r, v_\theta, v_z, v_\rho$ = velocity components in direction indicated

λ = ratio of radii, R/b

μ = dynamic viscosity of external medium

ψ = stream function

References

[1] Faxen H. *Ark. Mat., Astron. Fys.* 1923 **17**; Dissertation, Uppsala University, 1921.

[2] Wakiya S. *J. Phys. Soc. Japan* 1953 **8** 254.

[3] Happel J. and Byrne B. J. *Industr. Engng. Chem.* 1954 **46** 1181.

[4] Richardson J. F. and Zaki W. N. *Chem. Engng. Sci.* 1954 **3** 65.

[5] Haberman W. *Wall effect for Rigid and fluid Spheres in Slow Motion*, p. 8 Ph.D. dissertation, University of Maryland 1956.

[6] Haberman W. and Sayre R. M. *Motions of Rigid and Fluid Spheres in Stationary and Moving Liquids Inside Cylindrical Tubes.* Report 1143. David Taylor Model Basin, U.S. Navy Dept., Washington, D.C. Oct., 1958.

[7] Kawaguti M. *J. Phys. Soc.* Japan 1958 **13** 209.

[8] Happel J. *Amer. Inst. Chem. Engrs. J.* 1958 **4** 197.

[9] Ast P. *The Motion of a Rigid Sphere in a Frictionless Cylinder.* M.S. Thesis, New York University, 1958.

Letters to the Editors

Note in connexion with the paper "Kinetics of watergas conversion reaction"*

In his discussion on the possibility of reduction of the catalyst (p. 137) the author calculated the oxidizing potential for the reaction $3FeO + \frac{1}{2} O_2 = Fe_3O_4$ at 500°C.

From the thermodynamic point of view, however, FeO is not stable below 565° [1]. The reduction of Fe_3O_4 should therefore proceed to Fe. If the author has extrapolated the iron–oxygen data to below the quadruple point of 565°C, the oxygen pressure for the FeO – Fe equilibrium should have been higher than that for the Fe_3O_4 – FeO equilibrium. However in Fig. 1 the two equilibrium pressures are in the natural order as would be the case only above the quadruple point. It is concluded therefore that the values for the two oxygen pressures as indicated in Fig. 1 cannot be both correct. Since the author's references to the sources of his thermodynamic data are incomplete, it is impossible to verify his calculations.

If a mixture of Fe_3O_4 and Fe is contacted with CO and H_2O under conditions where equilibrium is obtained, at 500°C no conversion of Fe_3O_4 in Fe or vice versa should occur for a H_2O/CO ratio of 0·614, using data by Emmett and Schultz [1]. The corresponding saturator temperature is 75°C.

The author's experimental value for the ratio at which no reaction occurs is 0·76, corresponding to 78°C saturator temperature. Although the author interpreted this experiment as a determination of the Fe_3O_4 – FeO equilibrium, it must have been the Fe_3O_4 – Fe equilibrium. The discrepancy in the H_2O/CO ratio might be caused by experimental errors (adjustment of saturator temperature, measurement of catalyst temperature) or by a diffusional resistance. However if these arguments do not offer a satisfactory explanation, the hypothesis that equilibrium is established, on which the author's further considerations are based, might be at fault.

G. van den Berg

N. V. Mekog, Ijmuiden, Netherlands

* P. Bortolini *Chem. Engng. Soc.* 1958 **9** 135.

Reference

[1] P. H. Emmett and J. F. Schultz *Amer. Chem. Soc.* 1933 **55** 1376.

Reply to the Letter from Dr. G. van den Berg, *concerning the article*

Kinetics of water-gas conversion reaction*

The scope of our work was that of examining if the mechanism determining the kinetics of water-gas conversion was that of the diffusion of the reagents and products between the gas phase and the surface of the catalyst. After having proved that this hypothesis was very reasonable, the chemical nature of the catylast was of secondary importance. The initial brief discussion on the possible reduced forms of the catalyst had the only object of establishing an H_2O/CO ratio range wherein we would be faced with an unchanged catalyst. The thermodynamic calculation has been worked out, as stated in the contents of the article, in accordance with the data given in Perry's *Chemical Engineer's Handbook* (1950 Edition) using the specific heats on p. 221, and the enthalpies and the free energies of formation on p. 239. We confirm that the numerical calculation is right and, if the results differ from those given by Emmet and Schultz, the fault is due to the inaccuracy of the thermodynamic data used. The casual coincidence of the conditions, thermodynamically foreseen by us, for the transformation Fe_3O_4–FeO, with the conditions experimentally detected for what Dr. van den Berg thinks rightly to be the Fe_3O_4–Fe transformation, has led us astray. We mention once more that we are only interested to settle the limit below which the value of the ratio H_2O/CO should *not* go. What happens below that limit is of no interest to us at all and thus we have not bothered to check the constitution of the catalyst under conditions different from the experimental ones. We wish, however, to kindly thank Dr. van den Berg for having clarified our misunderstanding.

P. Bortolini

Via Tolentino 19, Milan, Italy.

*P. Bortolini *Chem. Engng. Sci.* 1958 **9** 135.

Vol. 11 1959/60

SELECTION OF CURRENT PAPERS OF INTEREST TO CHEMICAL ENGINEERS

G. I. Taylor and P. G. Saffman: A note on the motion of bubbles in a Hele–Shaw cell (close parallel plates) and porous medium. *Quart. J. Mech. Appl. Math.* 1959 **12** 265–279.

St. I. Gheorghitza: Motions with an initial gradient (of dynamic pressure in incompressible fluid in a porous medium) *Quart. J. Mech. Appl. Math.* 1959 **12** 280–286.

H. Hasimoto: On the periodic fundamental solutions of the Stokes equations and their application to viscous flow past a cubic array of spheres. *J. Fluid Mech.* 1959 **5** 317–328.

G. J. Kynch: The slow motion of two or more spheres through a viscous fluid. *J. Fluid Mech.* 1959 **5** 193–208.

S. M. A. Haque: The effect of eddy viscosity on the velocity profile of steady flow in a uniform rough channel. *J. Fluid Mech.* 1959 **5** 310–316.

J. W. Elder: The dispersion of marked fluid in turbulent shear flow. *J. Fluid Mech.* 1959 **5** 544–560.

H. Brenner: Pressure drop due to viscous flow through cylinders (for various boundary conditions) *J. Fluid Mech.* 1959 **6** 542–546.

J. W. Miles: On the generation of surface waves by shear flows. Part 2. *J. Fluid Mech.* 1959 **6** 568–582. Part 3. Kelvin–Helmholtz instability. *Ibid.* 583–598. (See also *J. Fluid Mech.* 1957 **3** 185).

J. F. Cameron, I. S. Boyce and R. M. Glaister: Estimation of trace water-content in a halogenated oil by means of tritiated water. *Brit. J. Appl. Phys.* 1959 **10** 463–465.

A. F. Pyrah and R. S. Robertson: A method for the determination of trace amounts of water in hydrocarbons. *J. Inst. Petrol.* 1959 **45** 316–319.

T. Furman and H. Hampson: Experimental investigation into the effects of cross-flow with condensation of steam and steam–gas mixtures on a vertical tube. *Proc. Inst. Mech. Engrs.* 1959 **173** 147–169.

H. Fujita: Concentration-dependent sedimentation in two-component systems, with reference to differential boundaries. *J. Chem. Phys.* 1959 **31** 5–11.

A. E. Korvezee and J. L. Meijering: Validity and consequences of Schreinemaker's theorem on ternary distillation lines. (An equilibrium tie-line is tangent to a " no-reflux " distillation line). *J. Chem. Phys.* 1959 **31** 308–313.

P. C. Waterman and S. A. Stern: Separation of gas mixtures in a supersonic jet (large composition gradients are attained by expanding gas mixtures through a Laval nozzle). *J. Chem. Phys.* 1959 **31** 405–419.

F. Sebba: Concentration by ion flotation. *Nature, Lond.* 1959 **184** 1062–1063.

G. J. Kynch: Sedimentation and effective viscosity. *Nature, Lond.* 1959 **184** 1311.

SELECTION OF CURRENT SOVIET PAPERS OF INTEREST TO CHEMICAL ENGINEERS*

Ya. G. Goroshchenko: Extraction of tantalum and niobium by *cyclo*hexanone from sulphuric acid solutions. *Zh. prikl. Khim.* 1959 **32** 1904–1913.

R. Aberdyanskaya, S. M. Golyand and B. A. Chertkov: On partial pressure of SO_2 above ammonium sulphite–bisulphite solutions. *Zh. prikl. Khim.* 1959 **32** 1931–1936.

A. G. Bolshakov, A. V. Kortnev and G. N. Gasyuk: On vapour temperature of boiling solutions. *Zh. prikl. Khim.* 1959 **32** 1988–1992. Measurement of vapour (steam) temperature above boiling solutions of NaOH and KOH.

V. V. Kafarov and V. S. Muravev: Generalized equations for calculation of packed columns in different hydrodynamic regimes. *Zh. prikl. Khim.* 1959 **32** 1992–2001.

N. I. Gelperin and N. N. Zelenetski: Investigation of the process of rectification in packed columns at reduced pressure. *Zh. prikl. Khim.* 1959 **32** 2001–2005.

I. P. Mukhlenov and E. Ya. Tarat: On hydraulic resistance of the gas–liquid layer in sieve-type equipment. *Zh. prikl. Khim.* 1959 **32** 2006–2013.

N. P. Rudenko: Methods of separation of radioactive isotopes without carriers. *Khim. Nauka i Prom.* 1959 **4** 441–448.

V. I. Grebenshchikova: Co-crystallization of radioactive substances with various precipitates. *Khim. Nauka i Prom.* 1959 **4** 456–464.

N. M. Zhavoronkov, S. I. Babkov, V. Yu. Orlov, K. I. Sakodinski, N. N. Sevryogova, N. A. Sokolnitski and G. N. Chernikh: Production and application of stable isotopes. *Khim. Nauka i Prom.* 1959 **4** 487–498.

Ya. M. Varshavski and S. E. Vaisberg: Present methods of heavy water production. *Khim. Nauka i Prom.* 1959 **4** 498–509.

S. Ya. Pshezhetski: Effects of nuclear irradiation on gaseous reactions. *Khim. Nauka i Prom.* 1959 **4** 509–515.

M. A. Dalin, V. M. Mamedova and A. S. Kasparov: Vapour-phase catalytic hydration of propylene to *iso*propanol. *Khim. Prom.* 1959 (5) 385–387.

A. I. Brodvich, M. S. Zolotnitskaya and R. V. Krasnovskaya: Production of ethylene chlorohydrin from technical gases with low content of ethylene. *Khim. Prom.* 1959 (5) 394–397.

B. A. Chertkov: Purification of flue gases from SO_2 by a bubbling-type foam absorber. *Khim. Prom.* 1959 (5) 413–417.

A. I. Rychkov and V. K. Pospelov: Investigation of heat transfer in boiling of solutions of caustic soda in falling-film apparatus. *Khim. Prom.* 1959 (5) 426–429.

Ya. Beranek and D. Sokol: Velocity of fluidization of particles of irregular shape. *Khim. Prom.* 1959 (5) 430–435.

A. A. Erofeev and N. V. Tyabin: Mixing of visco-plastic dispersed systems with the aid of mixers. *Khim. Prom.* 1959 (5) 436–441.

L. N. Cherkasova: Effect of structure on thermal conductivity of polymers. *Zh. fiz. Khim.* 1959 **33** 1928–1932.

M. M. Shelechnik: Temperature distribution in a column in the presence of a first-order reaction. *Zh. fiz. Khim.* 1959 **33** 2073–2075. Reaction of gas with packing material.

Ya. N. Chernyak: On the expansion of gas bubbles in liquids of high viscosity. *Zh. tekh. Fiz.* 1959 **29** 1273–1276.

V. P. Frontasev and M. Ya. Gusakov: Thermal conductivity of some organic liquids. *Zh. tekh. Fiz.* 1959 **29** 1277–1284.

*To assist readers, translations of any article appearing in the above list can be obtained at a reasonable charge. All orders should be addressed to the Administrative Secretary of the Pergamon Institute at either Headington Hill Hall, Oxford or 1403 New York Avenue N.W., Washington 5, D.C. whichever is more convenient.

M. N. Kogan: On highly thermoconductive flows. *Dokl. Akad. Nauk SSSR* 1959 **128** 488–490.

S. R. Sergyenko, L. Nikuitkovski, Yu. T. Gordasa and A. A. Petrov: Adsorption properties of high-molecular hydrocarbons having a mixed structure. *Dokl. Akad. Nauk SSSR* 1959 **128** 769–772.

I. S. Avetisyan and G. I. Epifanov: Effects of surface-active lubricants on resistance to shear in friction. *Dokl. Akad. Nauk SSSR* 1959 **128** 977–978.

U. N. Pchelkin: Investigation into heat transfer from air in rectangular ducts. *Teploenergetika* 1959 **6** (9) 83–87.

F. P. Kazakevich, A. M. Krapivin, G. I. Anofryev and I. G. Vesely: Investigation into radiant heat transfer in the furnace of a steam boiler in burning of natural gas. *Teploenergetika* 1959 **6** (10) 34–38.

A. M. Sirota and E. P. Belyakova: On calorimetric properties of water under pressures up to 500 kg/cm^2 and temperatures up to 300 °C. *Teploenergetika* 1959 **6** (10) 67–70. Determination of c_p and calculation of enthalpies.

N. B. Vargaftik and O. N. Oleshchuk: Experimental investigation into heat conduction of water. *Teploenergetika* 1959 **6** (10) 70–74.

M. P. Vukalovich, V. N. Zubarev, A. A. Aleksandrov and Yu. Ya. Kalinin: Experimental determination of specific volume of water up to pressure of 120 kg/cm^2. *Teploenergetika* 1959 **6** (10) 74–77.

L. P. Gilyazetdinov: New method of structural analysis of hydrocarbon fuels and oils. *Khim. Tekh. Topl. Masel* 1959 **4** (8) 42–49.

6974-27-4

VOL.
11
959/60

END